Inventory of Shale Formations in the US, Including Geologic, Geochemical, Hydrological, Mechanical, and Thermal Characteristics

Fuel Cycle Research & Development

Prepared for

U.S. Department of Energy
Used Fuel Disposition

Patrick Dobson and
James Houseworth

Lawrence Berkeley National Laboratory

September, 2014

FCRD-UFD-2014-000512

Revision 2
12/20/2012

APPENDIX E

FCT DOCUMENT COVER SHEET [1]

Name/Title of Deliverable/Milestone/Revision No.	Inventory of Shale Formations in the US, Including Geologic, Geochemical, Hydrological, Mechanical, and Thermal Characteristics
Work Package Title and Number	Regional Geology R&D - LBNL FT-14LB081402
Work Package WBS Number	1.02.08.14
Responsible Work Package Manager	Patrick Dobson (signature on file) (Name/Signature)

Date Submitted 09/10/2014

Quality Rigor Level for Deliverable/Milestone[2]	☐ QRL-3	☐ QRL-2	☐ QRL-1 ☐ Nuclear Data	☒ Lab/Participant QA Program (no additional FCT QA requirements)

This deliverable was prepared in accordance with Lawrence Berkeley National Laboratory
(Participant/National Laboratory Name)

QA program which meets the requirements of
☒ DOE Order 414.1 ☐ NQA-1-2000 ☐ Other

This Deliverable was subjected to:

☐ Technical Review ☐ Peer Review

Technical Review (TR)

Review Documentation Provided

☐ Signed TR Report or,
☐ Signed TR Concurrence Sheet or,
☐ Signature of TR Reviewer(s) below

Peer Review (PR)

Review Documentation Provided

☐ Signed PR Report or,
☐ Signed PR Concurrence Sheet or,
☐ Signature of PR Reviewer(s) below

Name and Signature of Reviewers

_____ _____

_____ _____

_____ _____

NOTE 1: *Appendix E should be filled out and submitted with the deliverable. Or, if the PICS:NE system permits, completely enter all applicable information in the PICS:NE Deliverable Form. The requirement is to ensure that all applicable information is entered either in the PICS:NE system or by using the FCT Document Cover Sheet.*

NOTE 2: *In some cases there may be a milestone where an item is being fabricated, maintenance is being performed on a facility, or a document is being issued through a formal document control process where it specifically calls out a formal review of the document. In these cases, documentation (e.g., inspection report, maintenance request, work planning package documentation or the documented review of the issued document through the document control process) of the completion of the activity along with the Document Cover Sheet is sufficient to demonstrate achieving the milestone. If QRL 1, 2, or 3 is not assigned, then the Lab/Participant QA Program (no additional FCT QA requirements box must be checked, and the work is understood to be performed, and any deliverable developed, in conformance with the respective National Laboratory/Participant, DOE- or NNSA-approved QA Program.*

This page is intentionally blank.

SUMMARY

Inventory of Shale Formations in the US

This section provides a summary of the distribution, thickness, and depth of selected shale formations found within many of the sedimentary basins in the contiguous US. Clay-rich shale formations have a number of properties, such as low permeability, high cation exchange potential, and the ability to self seal, which make them candidates for a geologic repository for high-level radioactive waste. The United States has an abundance of thick shale deposits that span a wide range of geologic ages, mineralogic compositions, and geologic environments, some of which might be suitable for hosting repositories to safeguard radioactive waste. The objective of this report is to build upon previous compilations of shale formations within many of the major sedimentary basins in the US by developing GIS data delineating isopach and structural depth maps for many of these units. These data are being incorporated into the Los Alamos National Laboratory (LANL) digital GIS database being developed for determining host rock distribution and depth/thickness parameters consistent with repository design. Additional rock properties, such as total organic carbon (TOC) abundance and thermal maturity, are also included where available.

Rock Properties and In-Situ Conditions for Shale Estimated from Sonic Velocity Measurements

This section extends the development of methods to assess hydrological and geomechanical properties and conditions for shale formations based on sonic velocity measurements as reported in Dobson and Houseworth (2013). In that effort, publically available data sets were identified for shales under investigation for nuclear waste disposal in Europe and from shales of interest for oil exploration and production in the North Sea. These data were used in the development of several correlations which link properties to sonic compressional velocity. The advantage of using correlations based on sonic velocity is that properties can be estimated from geophysical logs. This information is often more readily available than direct property measurements on core that would otherwise be required. Furthermore, geophysical logs typically provide a continuous readout along wells that can be more readily used to characterize spatial variability in properties. In this report additional information is provided on the correlation between clay content and sonic velocity presented in Dobson and Houseworth (2013).

Additional correlations are developed here between the sonic velocity and thermal properties, i.e., thermal conductivity and specific heat. Correlations between sonic velocity and the van Genuchten capillary strength parameter and the van Genuchten pore-size-distribution index are also presented. These van Genuchten parameters can be used for the computation of two-phase capillary pressure and relative permeability parameter functions of saturation. The correlations developed were then used to assess properties and conditions in several shale formations of interest within the United States which have publically available data on sonic velocity. As in the previous study, some of the correlations were found to be weak or poorly defined, indicating that additional independent measurements are desirable to supplement such estimates. Further verification is also needed for many of the parameter estimates for the US shale formations analyzed; therefore, they should be viewed as initial estimates.

CONTENTS

FIGURES

TABLES

ACRONYMS

BRI	brittleness index
DEM	Digital Elevation Model
EIA	Energy Information Administration
GIS	Geographic Information Systems
LANL	Los Alamos National Laboratory
md	millidarcies
OCR	overconsolidation ratio
psi	pounds per square inch
RMSE	root-mean-square error
tcf	trillion cubic feet
TOC	total organic carbon
UCS	uniaxial compressive strength
USGS	U.S. Geological Survey

.

1. INTRODUCTION

This report documents FY14 progress for the work package entitled "Regional Geology R&D – LBNL". The major purpose of this work package is to augment the existing inventory of shale formations in the US in the LANL Geographic Information Systems (GIS) database and to examine physical properties associated with these rocks.

There are two main research tasks for this work package. The first (described in Section 2) is to build upon previous work conducted to obtain isopach and structural top data (either from published maps and figures or as GIS shape files) for selected shale units in the US through literature searches and personal contacts, and to include rock property characteristics, such as total organic carbon (TOC) and thermal maturity data, where available. The second task (described in Section 3) is to develop a methodology through the use of sonic velocity logs to estimate hydrologic and geomechanical properties of shales. Publically available field and laboratory data from shale samples have been used to develop correlations between measured sonic velocities and rock properties such as porosity, bulk density, clay content, permeability, uniaxial compressive strength, Young's modulus, and shear modulus.

2. INVENTORY OF SHALE FORMATIONS IN THE US

2.1 INTRODUCTION

Clay-rich shale formations have a number of properties, such as low permeability, high cation exchange potential, and the ability to self seal, which make them candidates for a geologic repository for high-level radioactive waste (e.g., Cuadros, 2008). The United States has an abundance of thick shale deposits that span a wide range of geologic ages, mineralogic compositions, and geologic environments, some of which might be suitable for hosting repositories to safeguard radioactive waste. The objective of this report is to build upon previous compilations of shale formations within many of the major sedimentary basins in the US (e.g., Merewether et al., 1973; Gonzales and Johnson, 1985; Dobson, 2011; 2012; Dobson and Houseworth, 2013; Perry et al., 2012; 2013; 2014) by developing GIS data delineating isopach and structural depth maps for many of these units. These data are being incorporated into the LANL digital GIS database being developed for determining host rock distribution and depth/thickness parameters consistent with repository design (Perry et al., 2011; 2013; 2014). Three main rock types are being incorporated into this database: salts, shales, and granitic basement rocks. This database can then be utilized for screening and comparison of potential repository sites (e.g., Rechard et al., 2011). This report represents an update of the Dobson and Houseworth (2013) report.

2.2 DATA SOURCES

Most of the shale data are from sedimentary basins where oil and gas deposits are present (Figure 2-1). The Energy Information Administration (EIA, 2011b) estimates that around 750 trillion cubic feet of undeveloped technically recoverable shale gas and 24 billion barrels of shale oil resources are in discovered shale plays in the lower 48 states. Formations that have been identified as having at least 20 trillion cubic feet (tcf) of shale gas include the Marcellus Shale (410 tcf), the Antrim Shale (20 tcf), the Haynesville Shale (75 tcf), the Eagle Ford Formation (21 tcf), the Fayetteville Shale (32 tcf), the Barnett and Woodford Shales (97 tcf), and the Mancos Shale (21 tcf). Many of these units are not shales in a strict sense, but may be better described as siliceous mudstones with reduced clay contents; these slightly brittle rocks can be subjected to successful hydrofracture treatment (Gale and Holder, 2010). While many areas within these sedimentary basins are sites of active and prospective oil and gas exploration and

development activities, there may be locations (such as within the shallower basin margins) that could be possible candidates for a repository.

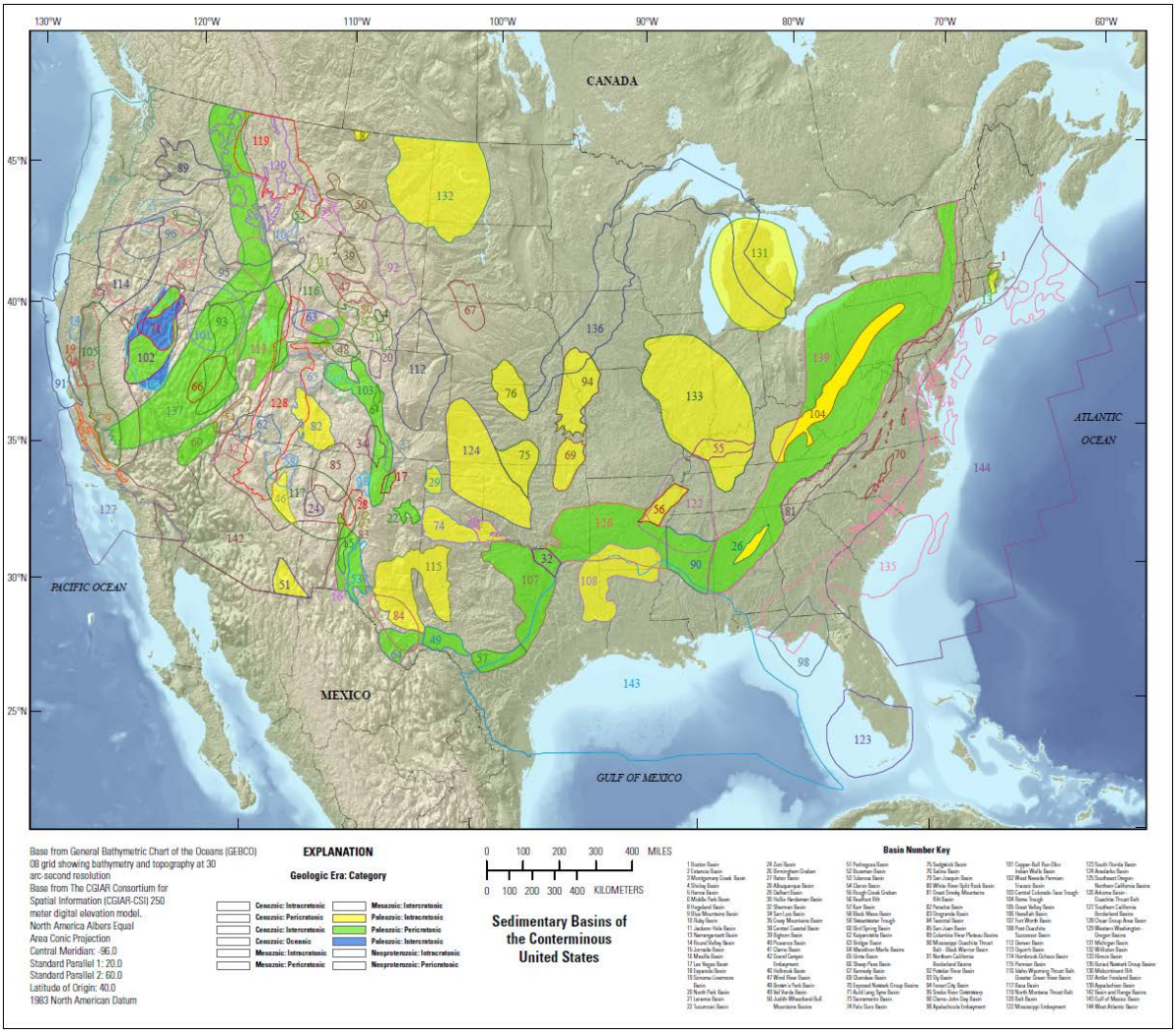

Figure 2-1. Sedimentary basins in the contiguous US. (Coleman and Cahan, 2012)

The data used for this report represent information that was either digitized using ArcGIS from published isopach and structure maps, or was available as GIS shape files that delineate formation isopachs and structural surfaces relative to a known datum, such as sea level or the ground surface. A number of data sources were obtained from the references listed in the discussions in Hovorka et al. (2003) of seal thickness and seal continuity for different saline formations in US sedimentary basins. The U.S. Geological Survey (USGS) Digital Data Series reports on petroleum systems and geologic assessment of oil and gas resources have been another helpful source of information. Numerous state geological survey reports have provided additional detailed information on local basin stratigraphy. Where maps were used to create GIS data layers, a jpeg version of the map was georectified using multiple geographic reference

points (such as country or state boundaries) and the thickness or structure contours were converted to vector format. Where depths are referenced to sea level instead of the ground surface, Digital Elevation Model (DEM) data are used. In the case of GIS data, metadata files were used to ascertain the geodetic reference datum used. In some cases, multiple data sources were used. More details on the methodology used to create the GIS structural top and isopach shape files can be found in Perry et al. (2012).

2.3 ISOPACH AND STRUCTURE MAPS

Maps of shale formation extents, thicknesses, and depths were obtained for the following units as organized by sedimentary basin. Table 2-1 summarizes formations for which isopach and/or structural data have been obtained. More comprehensive lists of shale formations can be found in Dobson (2011) and Gonzales and Johnson (1985). Units listed in ***bold italics*** represent formations for which GIS data have been obtained or generated. This report represents the current status of data collection: this is an ongoing process to populate the LANL GIS database.

Table 2-1. Identified data sources for isopach and structural data for shale formations within major sedimentary basins.

Appalachian Basin	
Utica Shale	Patchen et al., 2006 (Plates 1-28 & 2-6) (GIS data obtained from West Virginia Geological and Economic Survey)
Marcellus Shale	Erenpreiss et al., 2011 (GIS data obtained from Ohio Department of Natural Resources)
Olentangy Shale	Gray et al., 1982 (METC/EGSP Series 313, 314, 318, 320)
Ohio Shale	Gray et al., 1982 (METC/EGSP Series 310, 311, 312, 316, 317)
Black Warrior Basin	
Chattanooga Shale	Pashin, 2008 (Figure 6)
Illinois Basin	
Maquoketa Shale	Willman et al., 1975 (Figure O-26); Collinson et al., 1988 (Figure 22); Kolata and Noger, 1990 (Figure 5-13); Bristol and Buschbach, 1973 (Plate 1)
New Albany Shale	Hasenmueller and Comer, 2000 (GIS data obtained from Illinois State Geological Survey)
Michigan Basin	
Eau Claire Formation	Catacosinos and Daniels, 1991 (Figure 6)
Antrim Shale	Wylie and Wood, 2004; 2005; Matthews, 1993 (Figures 4 & 24)
Coldwater Shale	Merewether et al., 1973 (Figures 12 & 13); Gonzales and Johnson, 1985 (Figure 3-20)
Anadarko Basin	
Sylvan Shale	Amsden, 1975 (Plates 7 & 8); Amsden, 1980 (Panel 1)
Woodford Shale	Amsden, 1975 (Plates 3 & 4); Cardott and Lambert, 1985 (Figures 2 & 3); Rottmann, 2000
Kiowa Shale	Macfarlane et al., 1993 (Plates 7 & 8)
Graneros Shale	Macfarlane et al., 1993 (Plates 3 & 4)
Ardmore Basin	
Woodford Shale	Party et al., 2008 (Slides 41 & 43); Cardott, 2012 (Figure 10); Rottmann, 2000
Arkoma Basin	
Sylvan Shale	Amsden, 1980 (Panel 1)

Woodford Shale	Amsden, 1980 (Panel 3); Blackford, 2007 (Plates 12 & 13); Rottmann, 2000
Chattanooga Shale	Li et al., 2010 (Plates 4 & 6)
Fayetteville Shale	Ratchford et al., 2006 (Plates 2 & 3); Li et al., 2010 (Plates 3 & 5)
Gulf Coast Basin	
Wilcox Formation	Pitman, 2008
Eagle Ford Shale	Surles, 1987 (Figures 5, 8, 9, 12, & 14); Pitman, 2008; Harbor, 2011 (Figure 8) (GIS data obtained from US Energy Information Administration)
Haynesville Shale	Hammes et al., 2011 (Figures 7 & 8)
Smackover Formation	Pitman, 2008
Fort Worth Basin	
Barnett Shale	Pollastro et al., 2007 (Figures 6 & 15)
Permian Basin	
Woodford Shale	Broadhead, 2010 (Figures 4 & 12); Comer, 1991 (Plates 1 & 2); Ruppel et al., 2005 (GIS data obtained from University of Texas, Bureau of Economic Geology)
Barnett Shale	Broadhead and Gillard, 2007 (Plates V and VII) (GIS data obtained from New Mexico Bureau of Geology and Mineral Resources)
Williston Basin	
Bakken Shale	LeFever, 2008 (Sheets 1 & 5); LeFever et al., 2012 (GIS data obtained from North Dakota Geological Survey)
Big Snowy Group	Peterson, 1984 (Figure 12)
Pierre (Bearpaw) Shale	Schurr, 1977 (Figures 5 & 6); Carlson, 1982; Smith, 1999; Condon, 2000 (Plates 8 & 23)
Powder River Basin	
Pierre Shale	Schurr, 1977 (Figures 5 & 6); Denson et al., 1993a, b, c, d
Lebo shale member, Fort Union Formation	Lewis and Hotchkiss, 1981 (Plate 3)
Upper Hell Creek confining layer, Lance Formation	Lewis and Hotchkiss, 1981 (Plate 5)
Denver Basin	
Pierre Shale	Schurr, 1977 (Figures 5 & 6); Dechesne et al., 2011 (Plates 4 & 8)
San Juan Basin	
Mancos Shale	Ridgley et al., 2013 (Figures 6 & 10)
Green River Basin	
Green River Formation	Mercier et al., 2010c
Piceance Basin	
Green River Formation	Mercier et al., 2010a; Mercier and Johnson, 2012
Uinta Basin	
Green River Formation	Mercier et al., 2010b; Mercier and Johnson, 2012
Cuyama Basin	
Monterey Formation	Lagoe, 1982 (Plate VI); 1984 (Figure 11); Sweetkind et al., 2013 (GIS data obtained from US Geological Survey)
Santa Maria Basin	
Monterey Formation	Sweetkind et al., 2010 (GIS data obtained from US Geological Survey)

San Joaquin Basin	
Monterey Formation	Hosford Scheirer, 2013 (Figure 7.18)

2.3.1 Appalachian Basin

The Appalachian Basin is a composite foreland basin that contains a thick sequence of Paleozoic sedimentary rocks (Ettensohn, 2008). These rocks have been subjected to a number of orogenic events, resulting in faulting and folding. The Marcellus Shale has been the primary focus for numerous geologic studies (e.g., Lash and Engelder, 2011) because of its prolific shale gas resources.

GIS data were obtained for two major shale formations in this basin: the Ordovician Utica Shale and the Devonian Marcellus Shale, both major shale gas targets. The Utica Shale GIS dataset was developed as part of a comprehensive regional stratigraphic study conducted by the Trenton-Black River Research Consortium of the Ordovician Trenton-Black River carbonate system (Patchen et al., 2006). This study generated an interval-thickness map for the Utica Shale and a structural map for the top of the Trenton Limestone, which serves at the base of the Utica Shale. GIS data obtained from the West Virginia Geological and Economic Survey were used to generate isopach and structure maps for the Utica Shale (Figure 2-2).

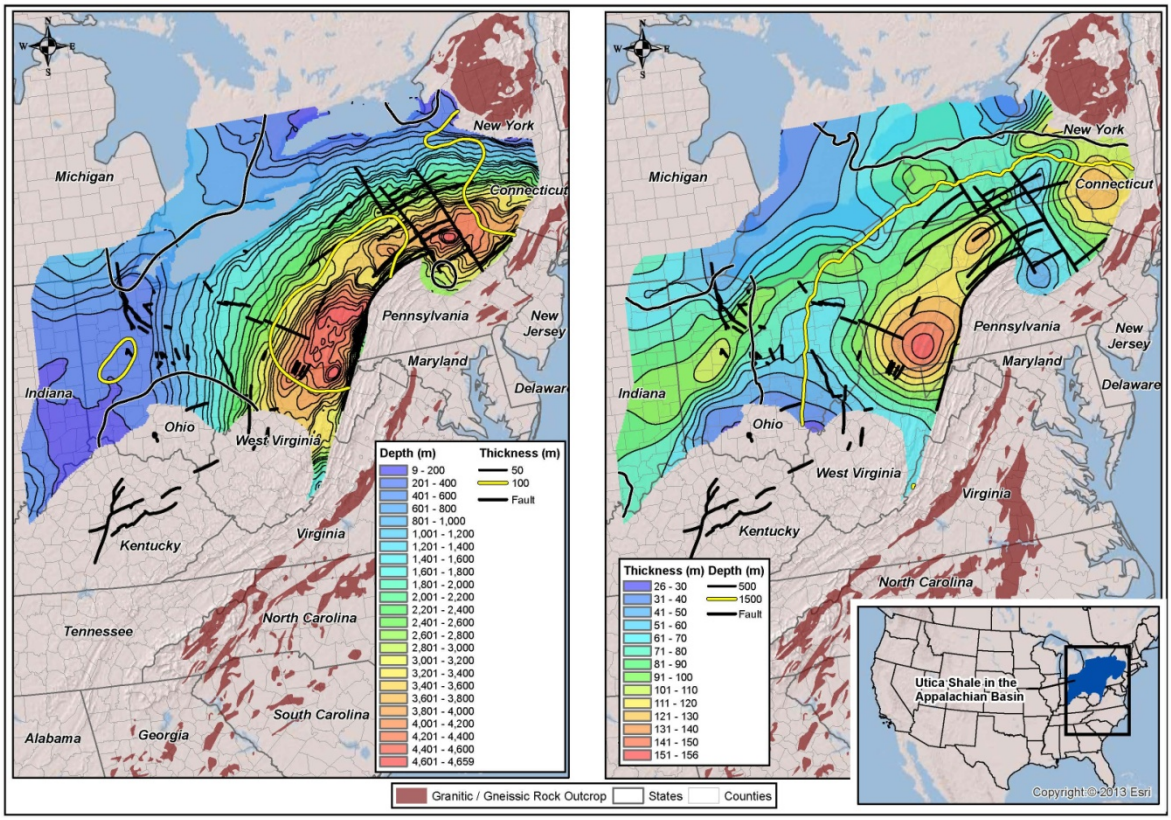

Figure 2-2. Depth and isopach maps of the Utica Shale, Appalachian Basin. Figure produced by LANL from shale data populated into the GIS database.

GIS data obtained from the Ohio Department of Natural Resources were used to generate isopach and structure maps for the Marcellus Shale (Figure 2-3). This unit has a total area of 95,000 square miles (EIA, 2011b). While this unit is very extensive, and is present in Ohio, Pennsylvania, West Virginia, Virginia, western Maryland and New York, there is only a limited area (in eastern Pennsylvania) where the shale thickness is at least 100 m at depths less than 1000 m.

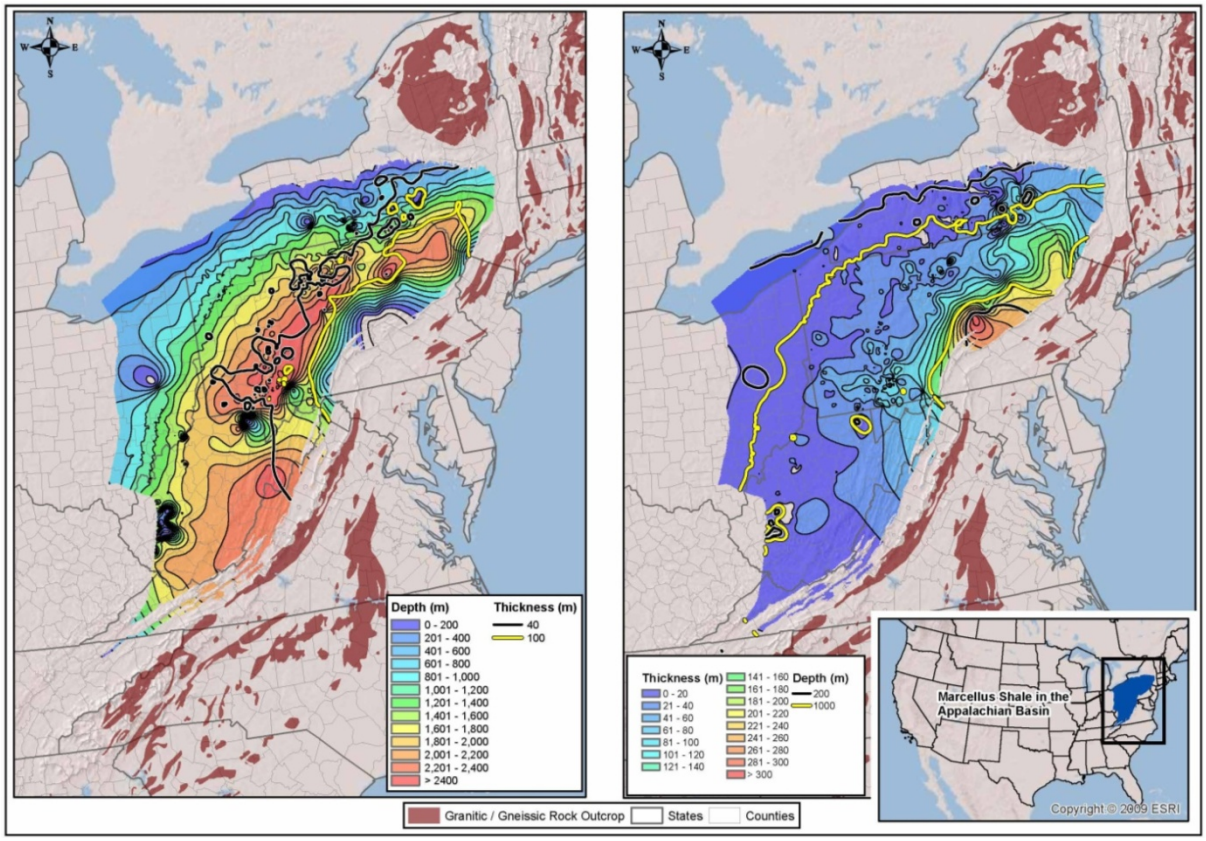

Figure 2-3. Depth and isopach maps of the Marcellus Shale, Appalachian Basin. Figure produced by LANL from shale data populated into the GIS database.

Structural top and isopach maps were also obtained for a number of additional Devonian black shale units in Ohio: the Chagrin, Cleveland and Huron members of the Ohio Shale and the Upper and Lower Olentangy Shales (Gray et al., 1982). The Ohio Shale is equivalent in age to the Chattanooga Shale, the New Albany Shale in the Illinois Basin and the Antrim Shale in the Michigan Basin (Gonzales and Johnson, 1985).

2.3.2 Black Warrior Basin

The Black Warrior Basin is a Paleozoic foreland basin located in Alabama and Mississippi (Thomas, 1988). It has three major shale formations: the Devonian Chattanooga Shale, the Mississippian Floyd Shale, and shale layers in the Pennsylvanian Pottsville Formation (Pawlewicz and Hatch, 2007). These shales have been identified as the source rocks for oil and gas deposits in the basin. Pashin (2008) has created an isopach map within the state of Alabama for the Chattanooga Shale (Figure 2-4). Almost all of the mapped section of the Chattanooga in this basin has a thickness less than 30 m.

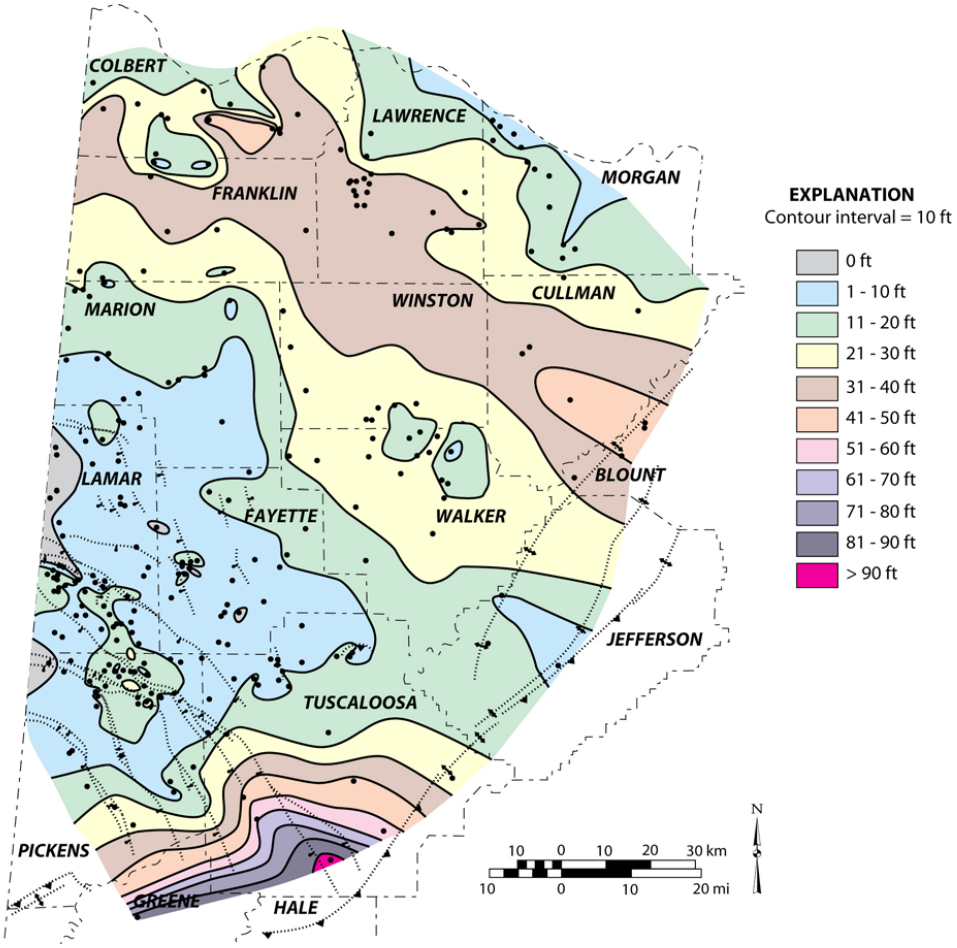

Figure 2-4. Isopach map of the Chattanooga Shale within the Alabama portion of the Black Warrior Basin (Pashin, 2008)

2.3.3 Illinois Basin

The Illinois Basin is filled primarily with Paleozoic age rocks, consisting of interbedded siliciclastic and carbonate sediments (Collinson et al., 1988; Swezey, 2009). The Devonian to Mississippian New Albany Shale is the most prominent shale unit in the Illinois Basin, with an areal extent of about 43,500 square miles and a thickness of 100 to 300 ft (Hasenmueller and Comer, 1994; EIA, 2011b). GIS data for this unit (Figure 2-5) is available over the entire basin (Hasenmueller and Comer, 2000). In the southern portion of the Illinois Basin, there is a small section of this unit with thicknesses greater than 100 m at a depth of less than 1000 m.

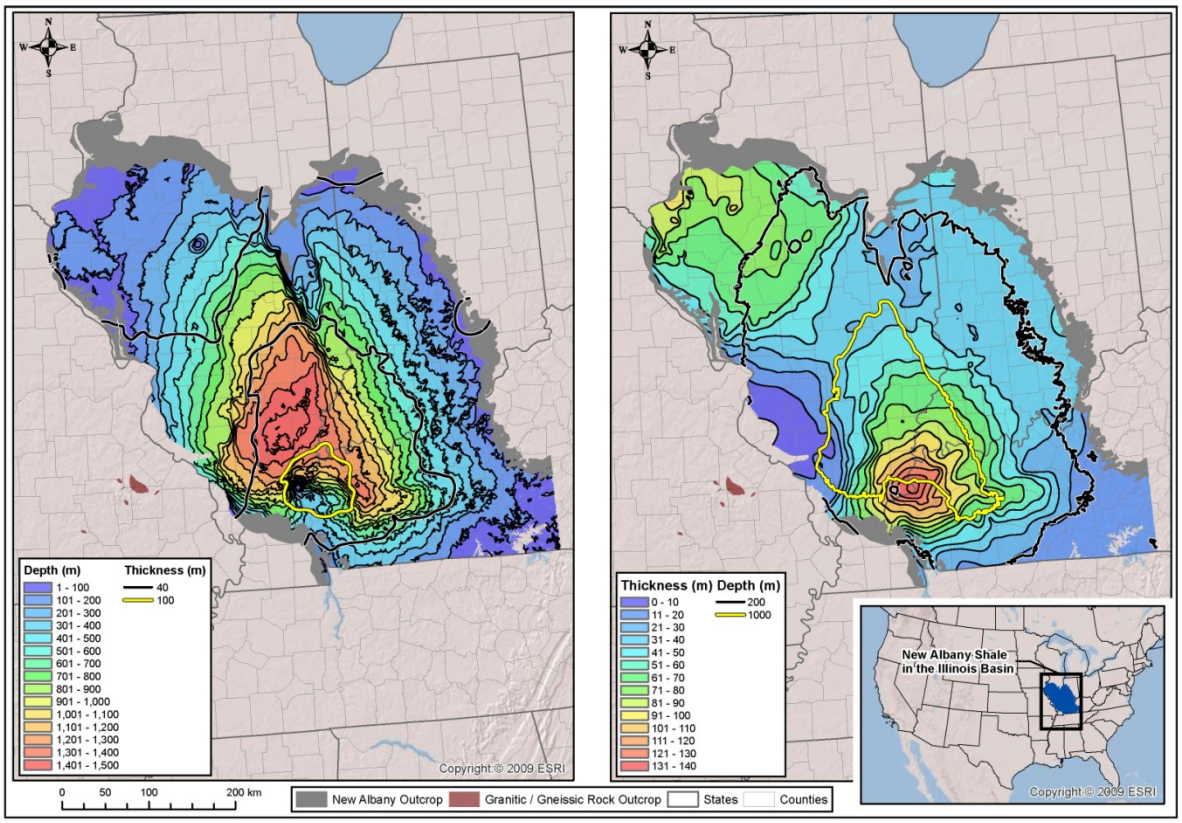

Figure 2-5. Depth and isopach maps of the New Albany Shale, Illinois Basin. Figure produced by LANL from shale data populated into the GIS database.

There are a number of studies with thickness and/or structural depth information on the Ordovician Maquoketa Shale. Bristol and Buschbach (1973) provide a plate depicting the top of the Galena Group, which represents the base of the Maquoketa Shale, for the state of Illinois. Willman et al. (1975) present a figure depicting the thickness of the Maquoketa Group, also restricted to Illinois. Collinson et al. (1988) and Kolata and Noger (1990) provide more regional depictions of the thickness of this unit. Given that this unit is older than the New Albany Shale, it is encountered at greater depths. The Illinois state data (Bristol and Buschbach (1973) and Willman et al. (1975)) were used to generate GIS maps of this unit (Figure 2-6).

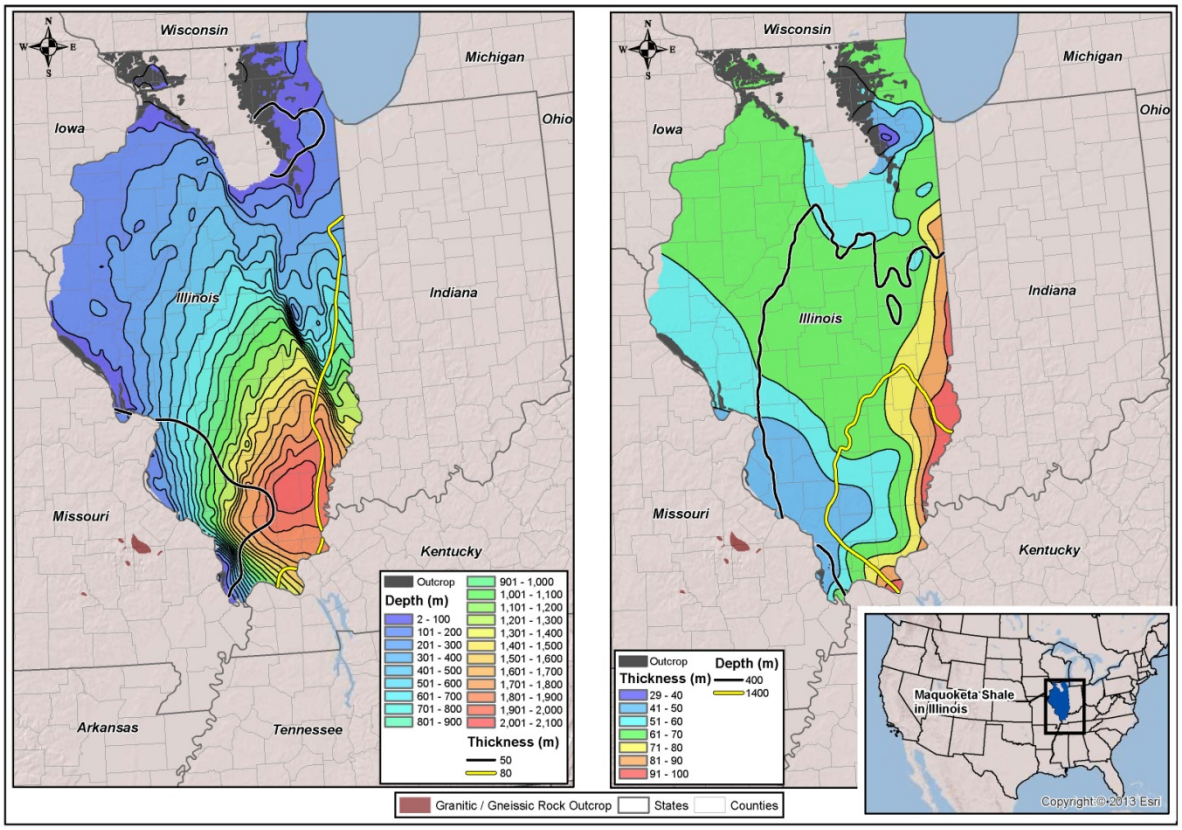

Figure 2-6. Depth and isopach maps of the Maquoketa Shale, Illinois Basin. Figure produced by LANL from shale data populated into the GIS database.

2.3.4 Michigan Basin

The Michigan Basin has a thick sequence of Paleozoic evaporites, carbonates, and siliciclastic sedimentary rocks (e.g., Merewether et al., 1973; Catacosinos et al., 1991; Swezey, 2008). Shale formations found in this basin include the Ordovician Utica and Collingwood Shales, the Silurian Cabot Head and Pointe aux Chenes Shales, the Devonian Antrim, Ellsworth, and Bedford Shales and the Mississippian Sunbury and Coldwater Shales. The predominant shale formation in the Michigan Basin is the Antrim Shale, a major producer of natural gas, with estimated recoverable shale gas resources of 20 trillion cubic feet (EIA, 2011b). Wylie and Wood (2004; 2005) and Matthews (1993) generated structure and isopach maps for a number of the hydrocarbon producing units in the Michigan Basin, including the Antrim Shale (Figure 2-7). Agrawal (2009) describes the depositional environment, mineralogy and TOC of the Antrim. GIS data were generated for the Coldwater Shale (Figure 2-8) using the isopach and structure map of Gonzales and Johnson (1985).

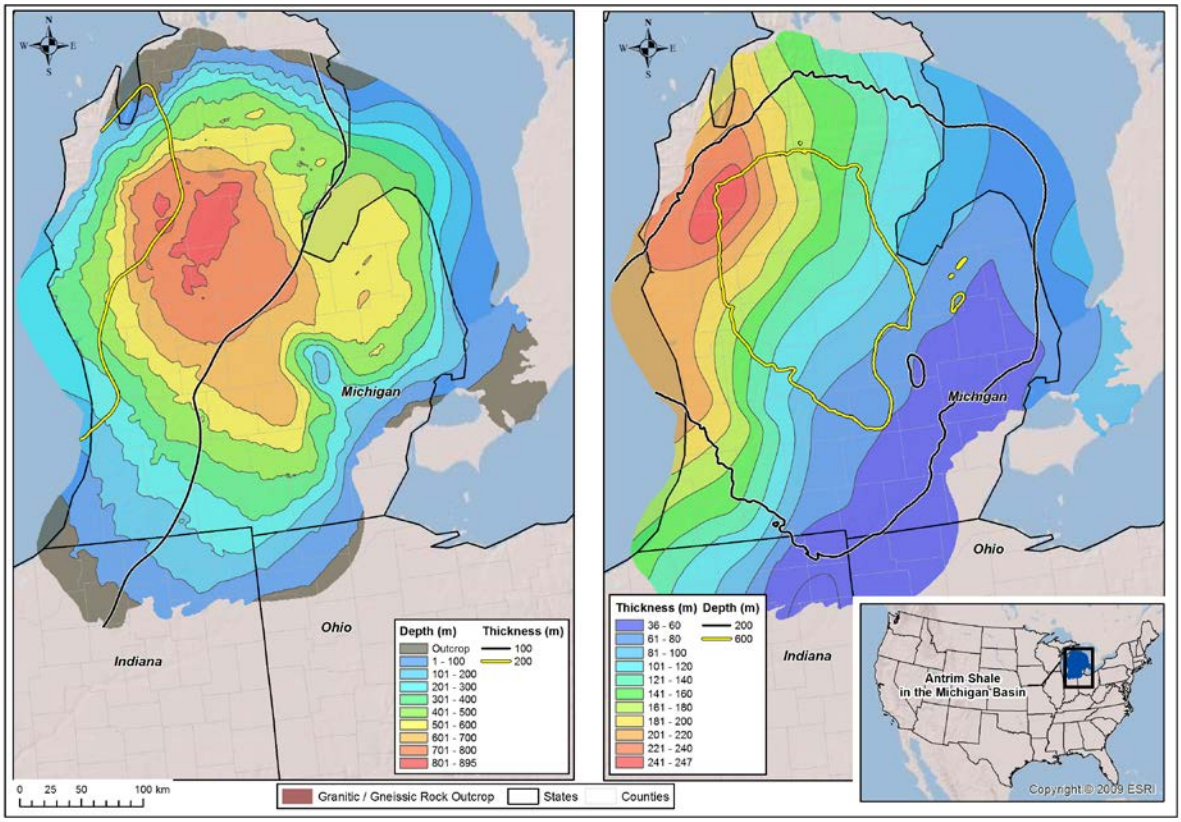

Figure 2-7. Depth and isopach maps of the Antrim Shale, Michigan Basin. Figure produced by LANL from shale data populated into the GIS database.

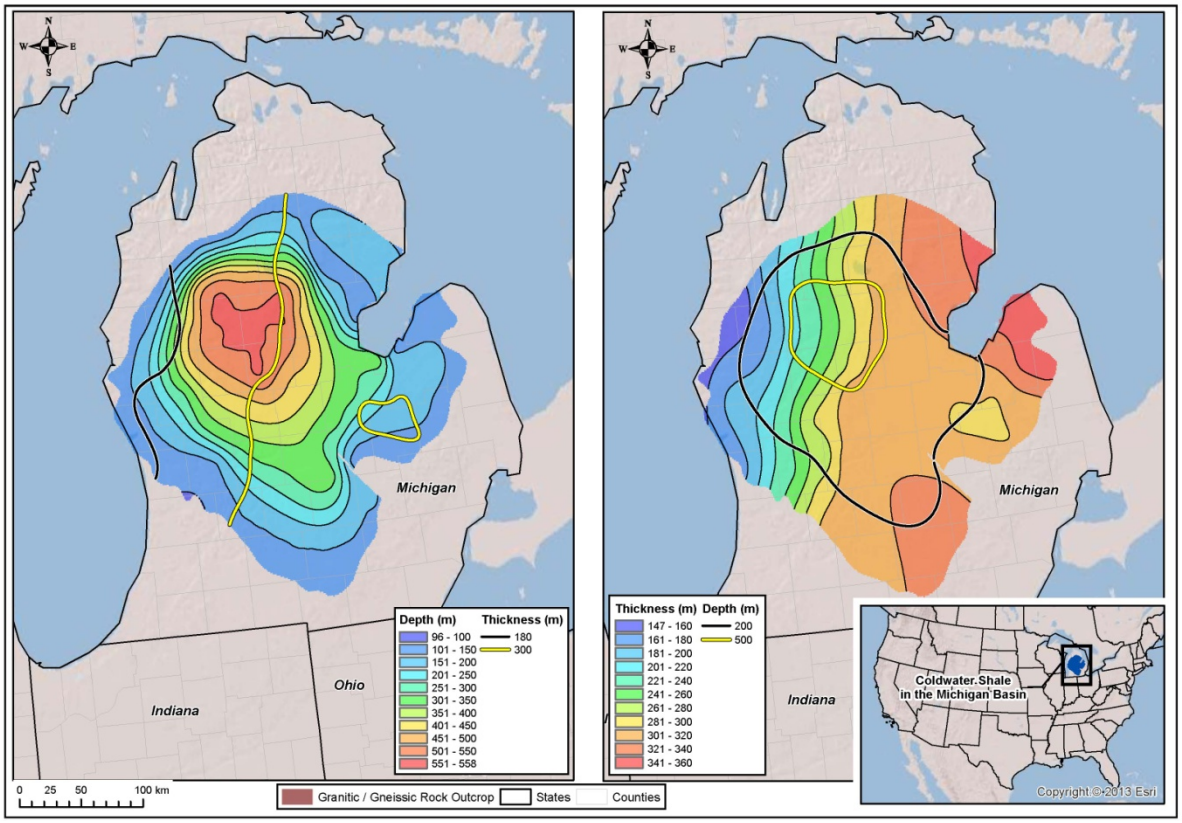

Figure 2-8. Depth and isopach maps of the Coldwater Shale, Michigan Basin. Figure produced by LANL from shale data populated into the GIS database.

2.3.5 Anadarko, Ardmore, and Arkoma Basins

The Anadarko, Ardmore, and Arkoma Basins, located in Oklahoma and neighboring states, are a series of fault-bounded sedimentary basins containing abundant hydrocarbon deposits. Detailed structure and isopach maps have been published for a number of the shale-bearing formations in these basins, including the Cretaceous Kiowa Formation and Graneros Shale (Macfarlane et al., 1993), the Mississippian Fayetteville Shale (Ratchford et al., 2006; Li et al., 2010), the upper Devonian/lower Mississippian Woodford Shale (e.g., Amsden, 1975; 1980; Cardott and Lambert, 1985; Rottmann, 2000; Blackford, 2007; Party et al., 2008; Cardott, 2012), the Devonian Chattanooga Shale (Li et al., 2010), and the Ordovician Sylvan Shale (Amsden, 1975).

The Hugoton Embayment of the Anadarko Basin in southwestern Kansas contains a sequence of Paleozoic, Mesozoic, and Cenozoic sedimentary rocks that reaches up to 2900 m in thickness (Macfarlane et al., 1993). In the upper portion of this basin, there are several Cretaceous shale units, including the Kiowa Formation (Figure 2-9) and the Graneros Shale (Figure 2-10), which serve as regional aquitards.

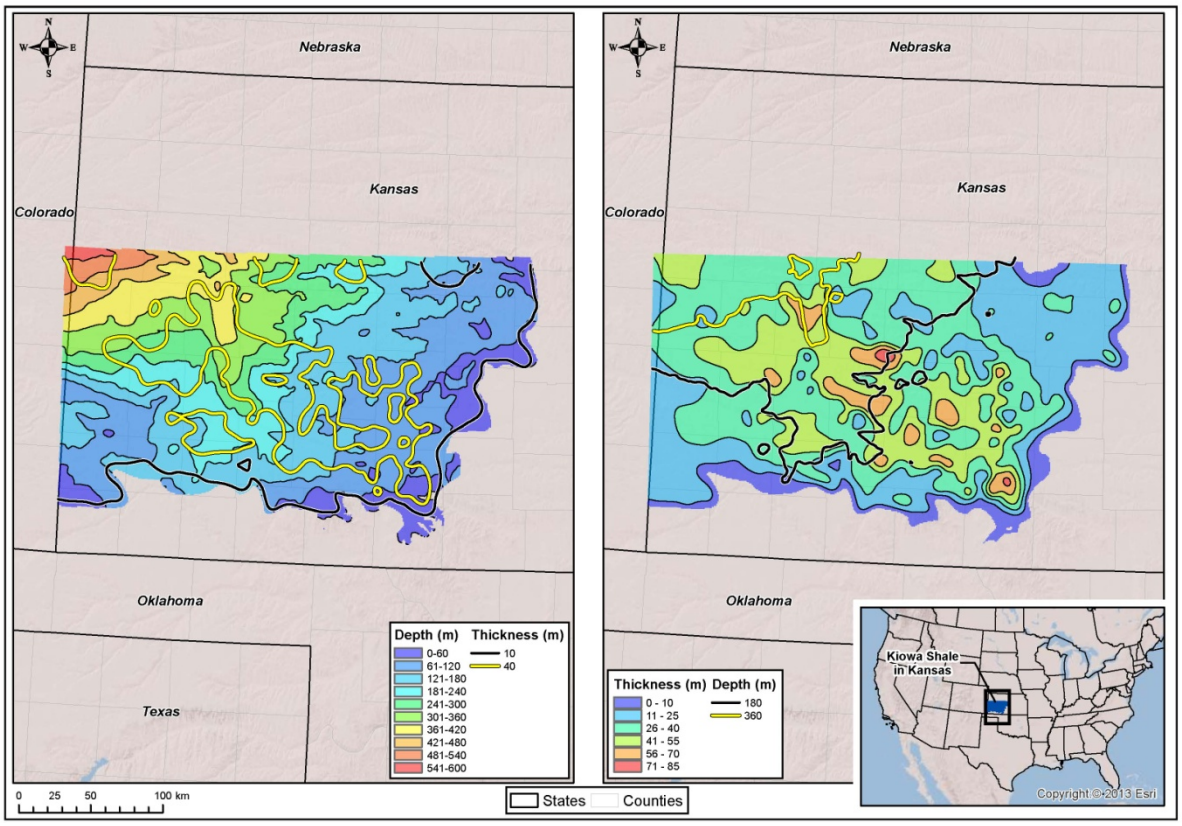

Figure 2-9. Depth and isopach maps of the Kiowa Shale, Anadarko Basin. Figure produced by LANL from shale data populated into the GIS database.

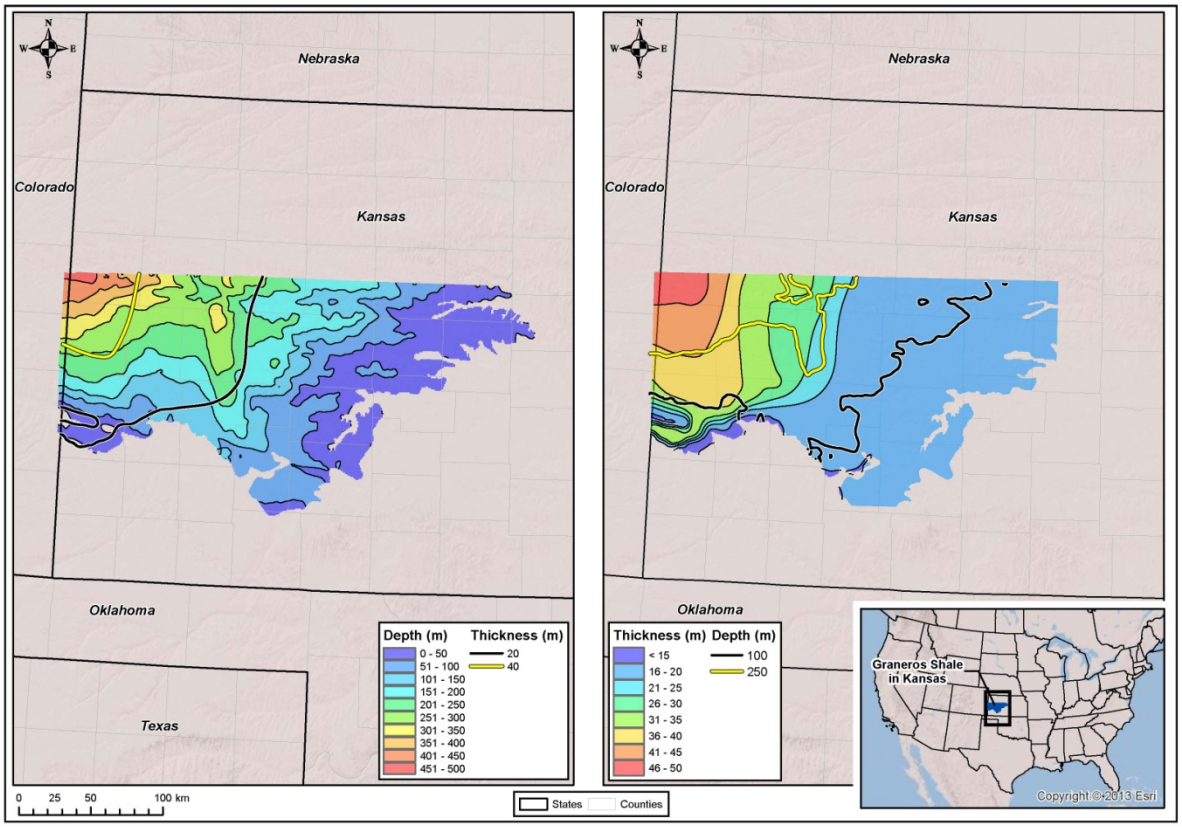

Figure 2-10. Depth and isopach maps of the Graneros Shale, Anadarko Basin. Figure produced by LANL from shale data populated into the GIS database.

Data on the Mississippian Fayetteville Shale and Devonian Chattanooga Shale reported by Ratchford et al. (2006) and Li et al. (2010) were used to construct structure and isopach maps for this unit in the Arkoma Basin in Arkansas (Figures 2-11 and 2-12). These studies also contain extensive geochemical data on the total organic carbon (TOC) and vitrinite reflectance of the shale in this basin.

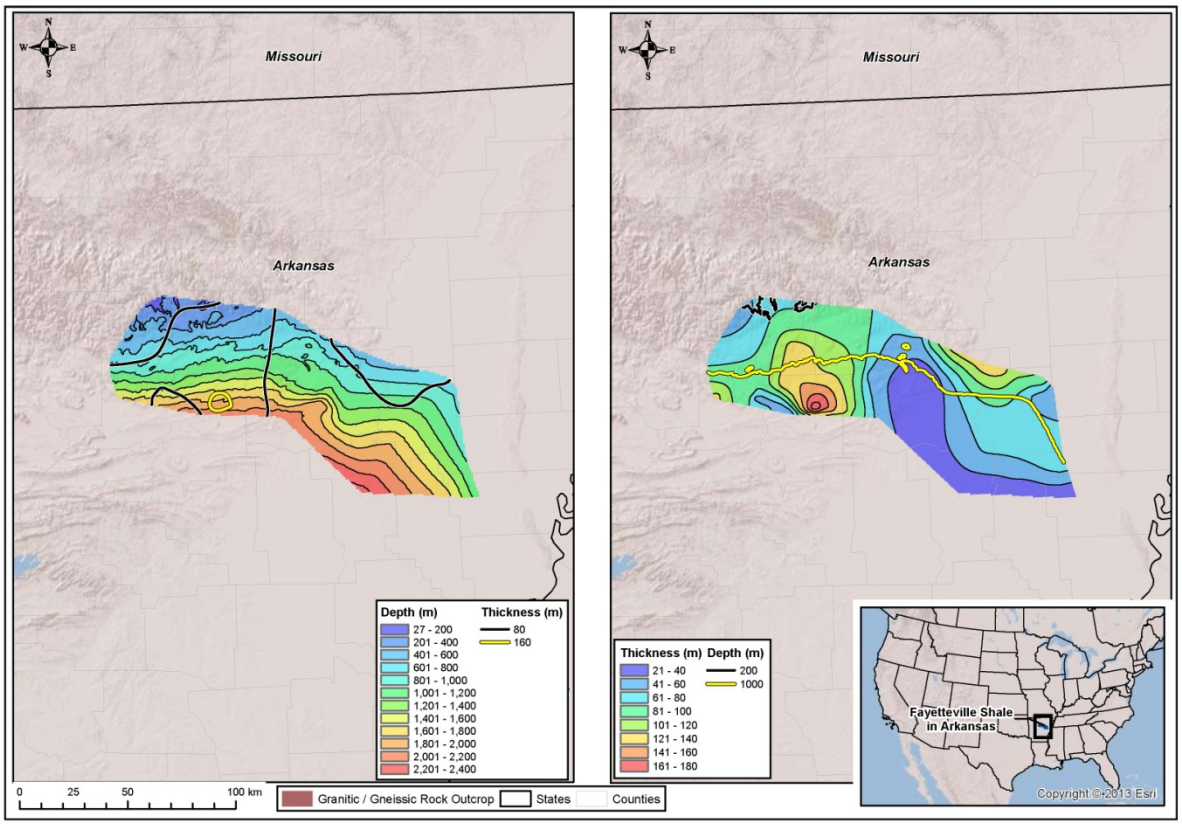

Figure 2-11. Depth and isopach maps of the Fayetteville Shale, Arkoma Basin. Figure produced by LANL from shale data populated into the GIS database.

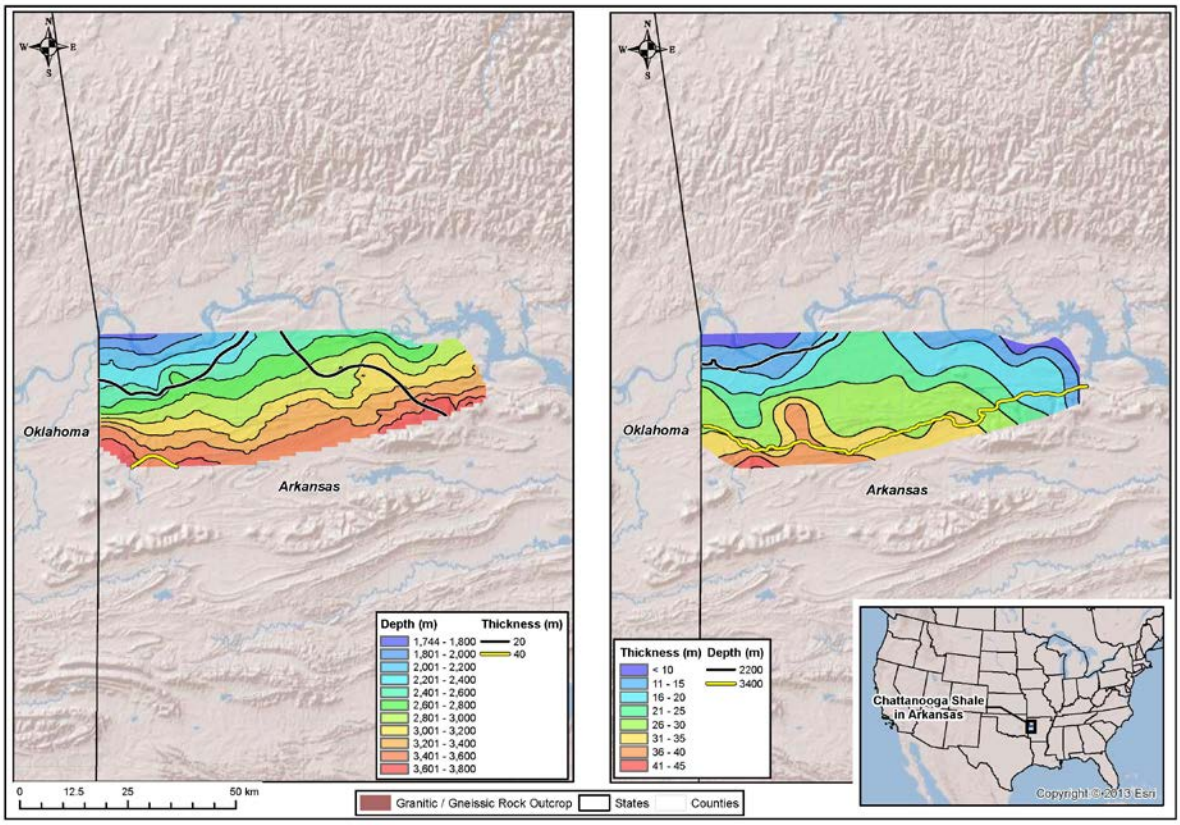

Figure 2-12. Depth and isopach maps of the Chattanooga Shale, Arkoma Basin. Figure produced by LANL from shale data populated into the GIS database.

The Upper Devonian/Lower Mississippian Woodford Shale (e.g., Amsden, 1975; 1980; Cardott and Lambert, 1985; Rottmann, 2000; Blackford, 2007; Party et al., 2008; Cardott, 2012) is a major shale gas play and hydrocarbon source rock in Oklahoma. Agrawal (2009) describes the depositional environment, mineralogy and TOC of the Woodford. GIS data for the Woodford Shale within the Anadarko and Arkoma Basins were generated from Amsden (1975; 1980) (Figure 2-13).

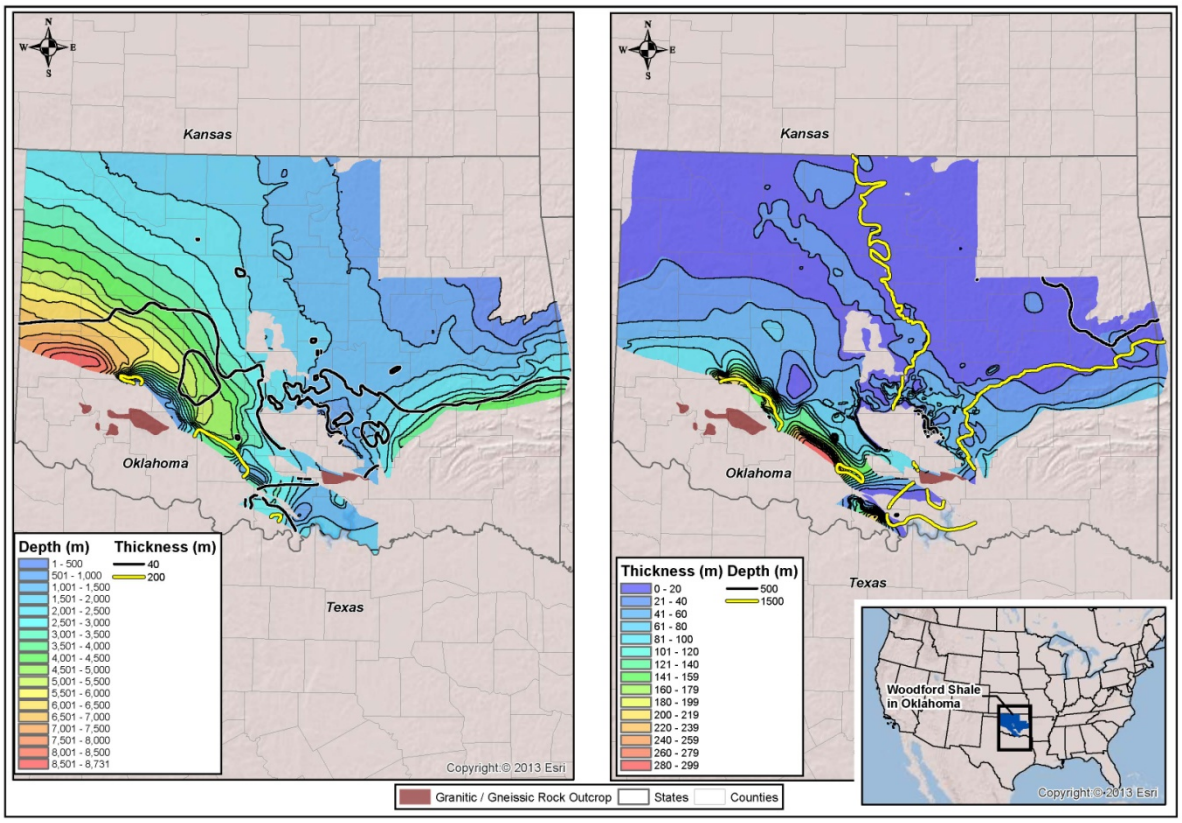

Figure 2-13. Depth and isopach maps of the Woodford Shale, Anadarko and Arkoma Basins. Figure produced by LANL from shale data populated into the GIS database.

2.3.6 Gulf of Mexico Basin

The Gulf of Mexico Basin contains extensive sedimentary accumulations both onshore and offshore, many of which host hydrocarbon deposits. Pitman (2008) generated a comprehensive GIS database of petroleum reservoirs and associated source rocks in Gulf of Mexico Basin, including delineation of the Upper Jurassic Smackover Formation, the Upper Cretaceous Eagle Ford Formation, and the Paleocene/Eocene Wilcox Formation. Hammes et al. (2011) presented a detailed description of the regional geology and stratigraphy of the Upper Jurassic Haynesville Shale, including isopach and structure maps of this important shale gas play unit; these maps were digitized to generate GIS data to create depth and isopach maps for this unit (Figure 2-14). Agrawal (2009) describes the depositional environment, mineralogy and TOC of the Haynesville. Surles (1987) constructed isopach maps for the entire Eagle Ford shale and its members, as well as compiled information on the amount of sand and organic matter. Harbor (2011) conducted a detailed study of the lithofacies and stratigraphy of the Eagle Ford Formation. GIS data obtained from the US EIA (EIA, 2010) was used to construct depth and isopach maps for the Eagle Ford Formation (Figure 2-15).

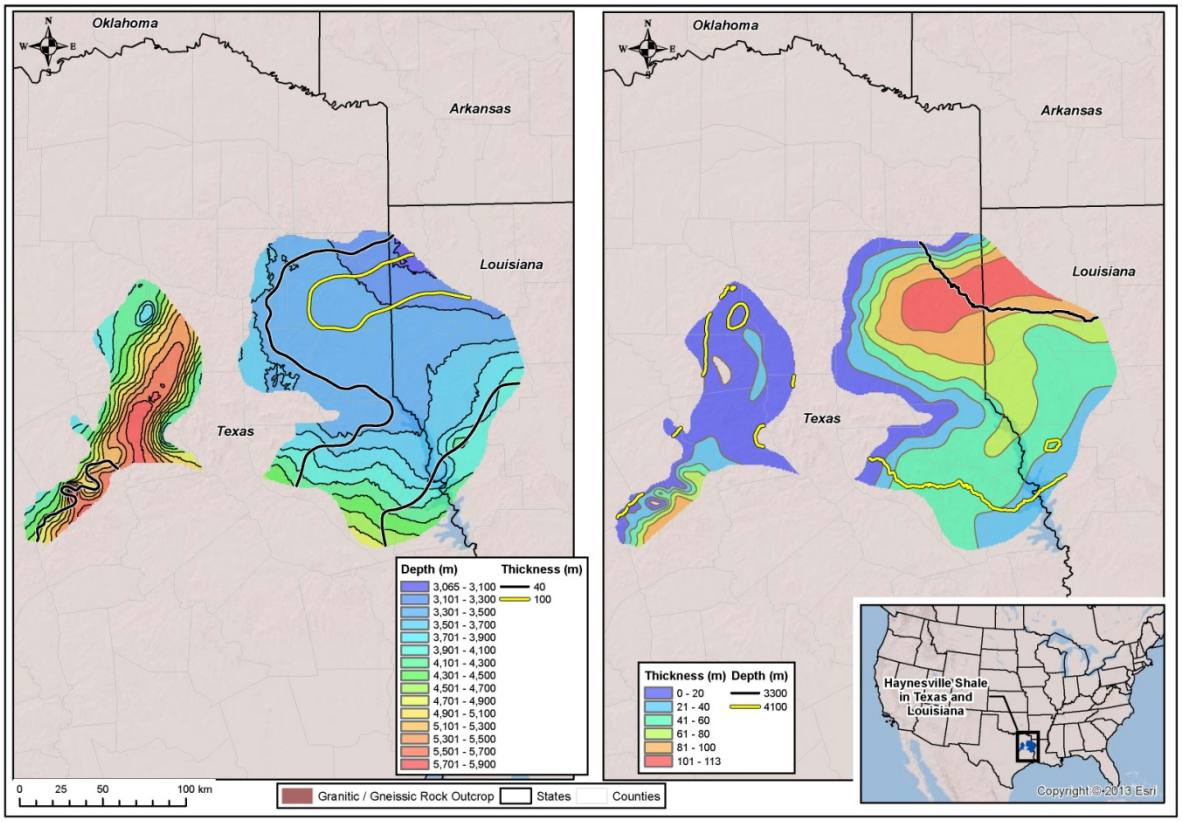

Figure 2-14. Depth and isopach maps of the Haynesville Shale, Gulf of Mexico Basin. Figure produced by LANL from shale data populated into the GIS database.

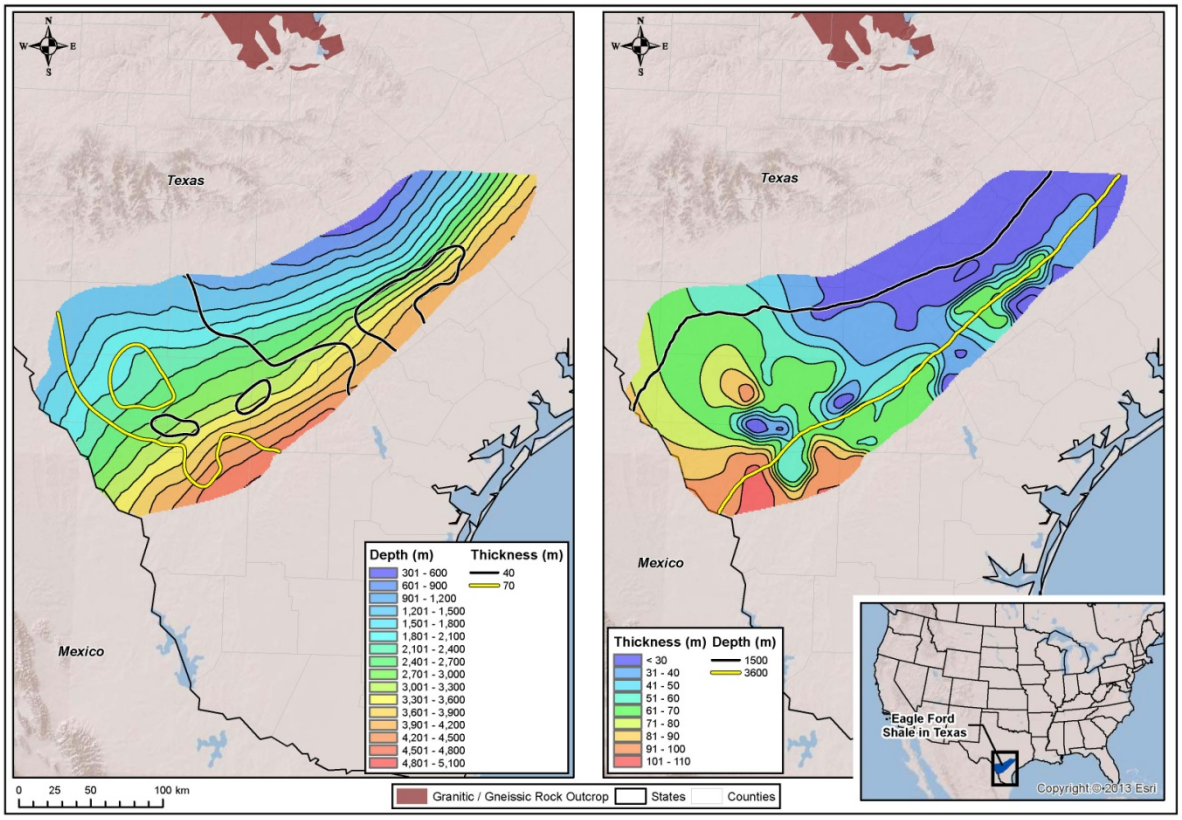

Figure 2-15. Depth and isopach maps of the Eagle Ford Formation, Gulf of Mexico Basin. Figure produced by LANL from shale data populated into the GIS database.

2.3.7 Fort Worth Basin

The Mississippian Barnett Shale is a major producer of shale gas in the Fort Worth Basin. Pollastro et al. (2007) conducted a detailed geologic study of this petroleum system, and generated isopach and structure maps for the Barnett Shale; these maps were digitized and integrated into the LANL GIS database (Figure 2-16). Agrawal (2009) describes the depositional environment, mineralogy and TOC of the Barnett.

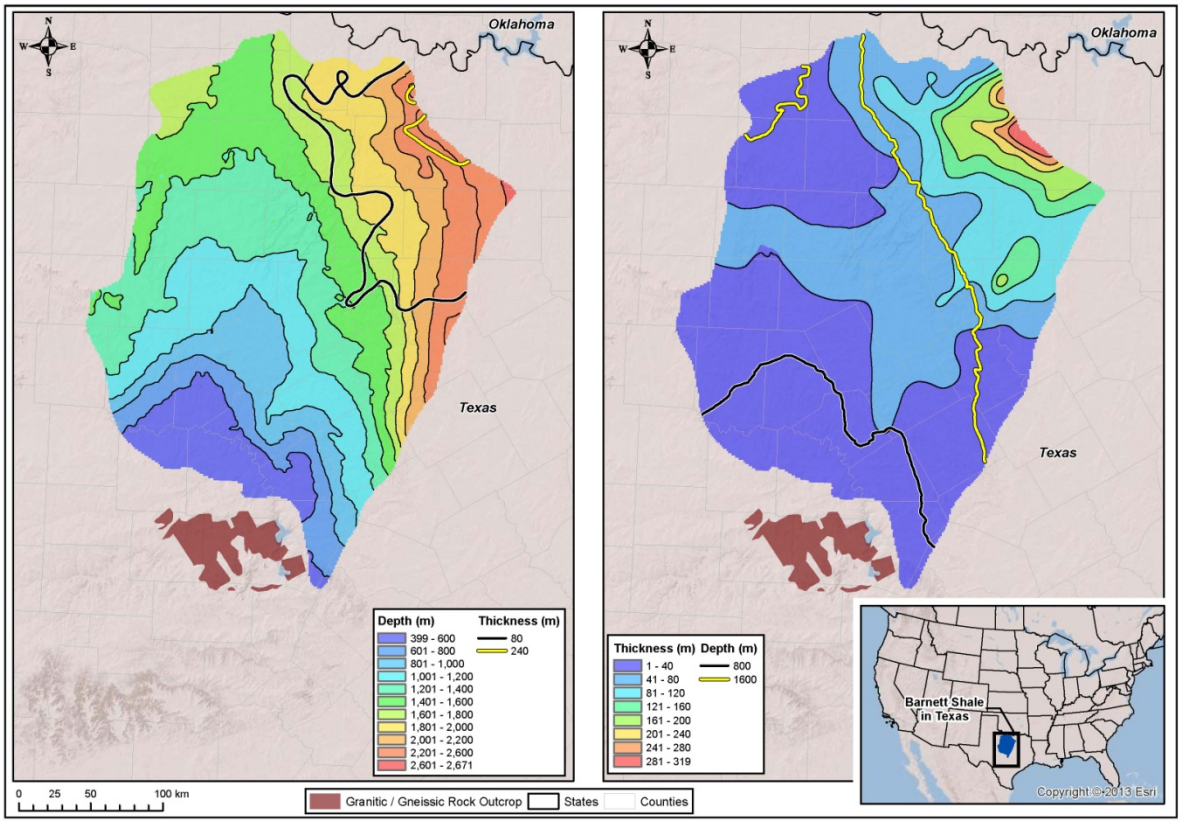

Figure 2-16. Depth and isopach maps of the Barnett Shale, Fort Worth Basin. Figure produced by LANL from shale data populated into the GIS database.

2.3.8 Permian Basin

While the Permian Basin is dominated by carbonate and evaporite sequences, it also hosts some siliciclastic units, such as the Woodford Shale. Broadhead (2010) conducted a detailed study of the distribution and source rock characteristics of the Woodford Shale located within the New Mexico portion of the Permian Basin. Structure and isopach maps for the Woodford Shale (Comer, 1991) were converted into GIS surfaces by Ruppel et al. (2005), and are depicted in Figure 2-17.

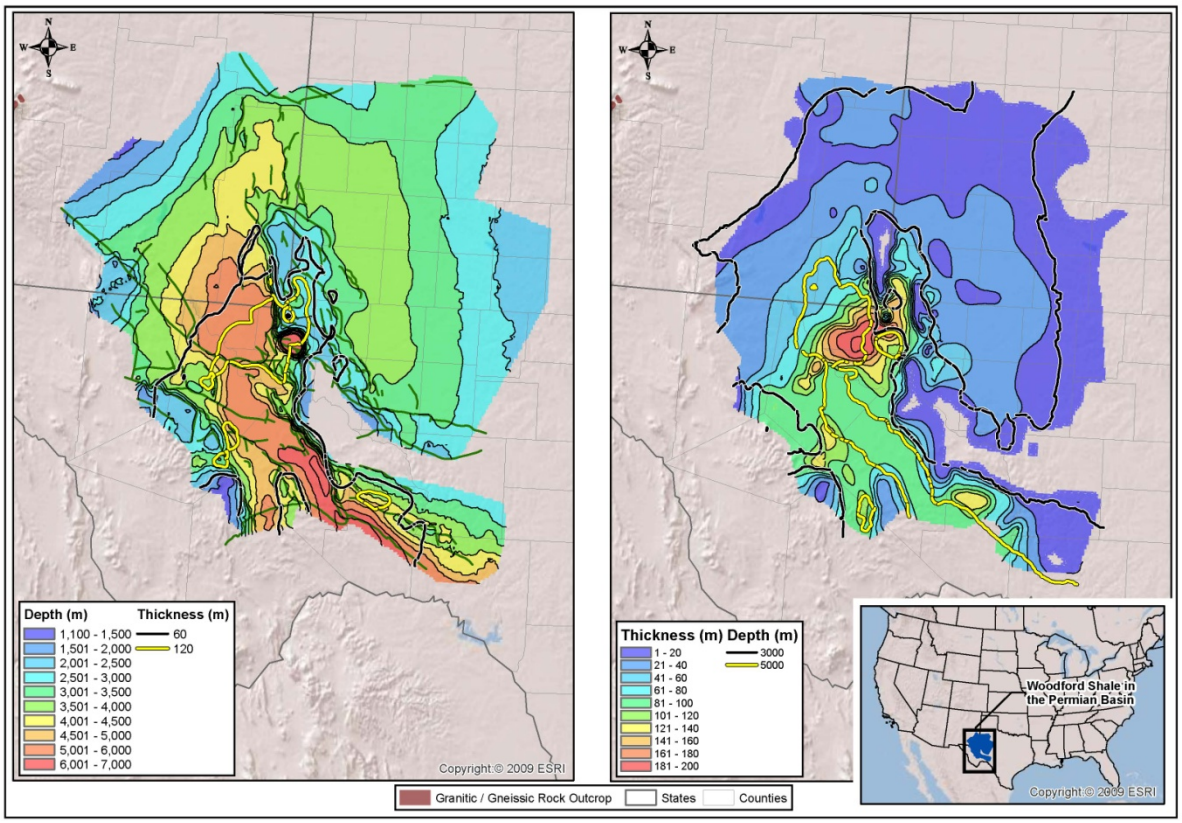

Figure 2-17. Depth and isopach maps of the Woodford Shale, Permian Basin. Figure produced by LANL from shale data populated into the GIS database.

Another major shale unit in the Permian Basin is the Mississippian Barnett Shale. Broadhead and Gillard (2007) provide detailed information on the stratigraphy, structure, and petroleum source rock characteristics, including TOC content and Rock-Eval data. Figure 2-18 depicts structural and isopach maps for the Barnett Shale in southeastern New Mexico (Broadhead and Gillard, 2007).

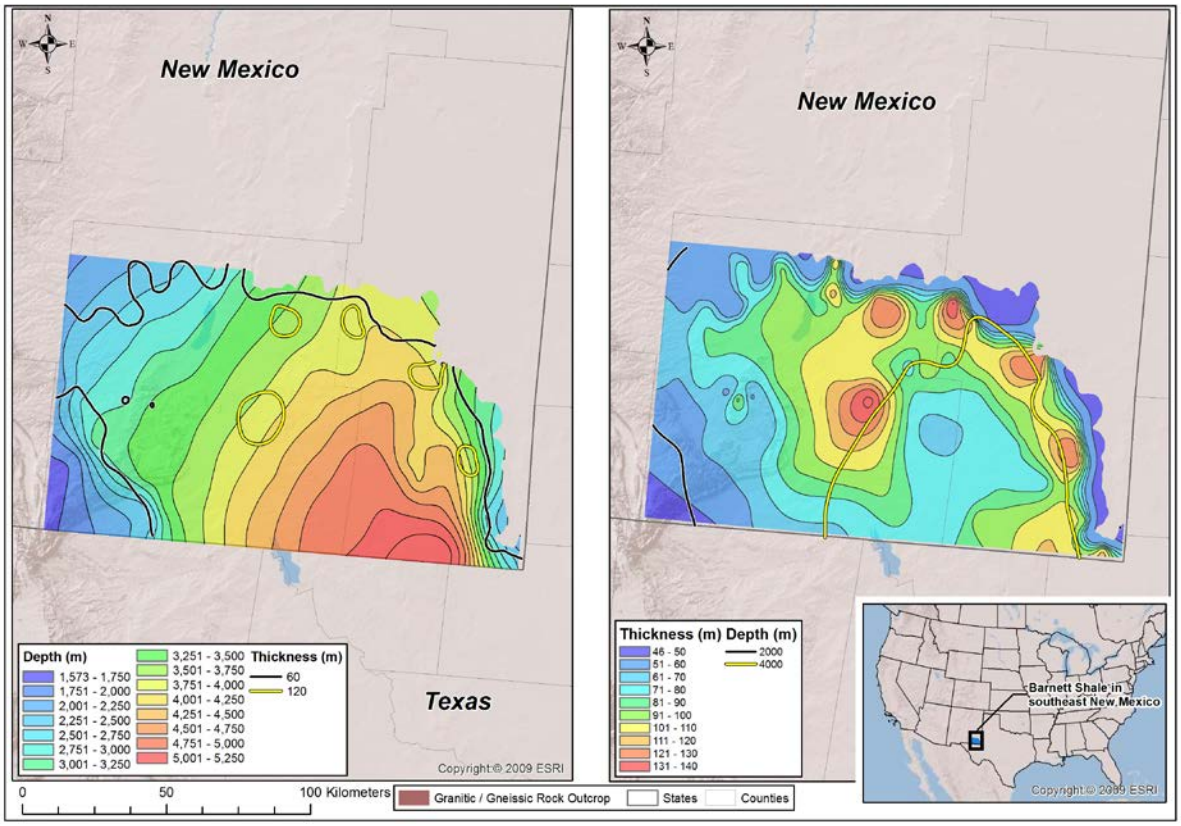

Figure 2-18. Depth and isopach maps of the Barnett Shale, Permian Basin. Figure produced by LANL from shale data populated into the GIS database.

2.3.9 Williston Basin

The Williston Basin is an intercratonic basin centered in North Dakota with sedimentary rocks consisting of carbonates, evaporites, sandstones, and shales. These rocks range in age from Precambrian to Tertiary (Gerhard et al., 1982). Shale-bearing units within the Paleozoic section include the Ordovician Ice Box Formation and the Mississippian Bakken and Otter Formations. The Bakken Formation has upper and lower shale members and a middle sandstone member (Pollastro et al., 2008) and contains significant (3.59 billion barrels) reserves of oil shale (EIA, 2011b). GIS data for the Bakken (Figure 2-19) are based on constraints provided by LeFever (2008) and LeFever et al. (2012).

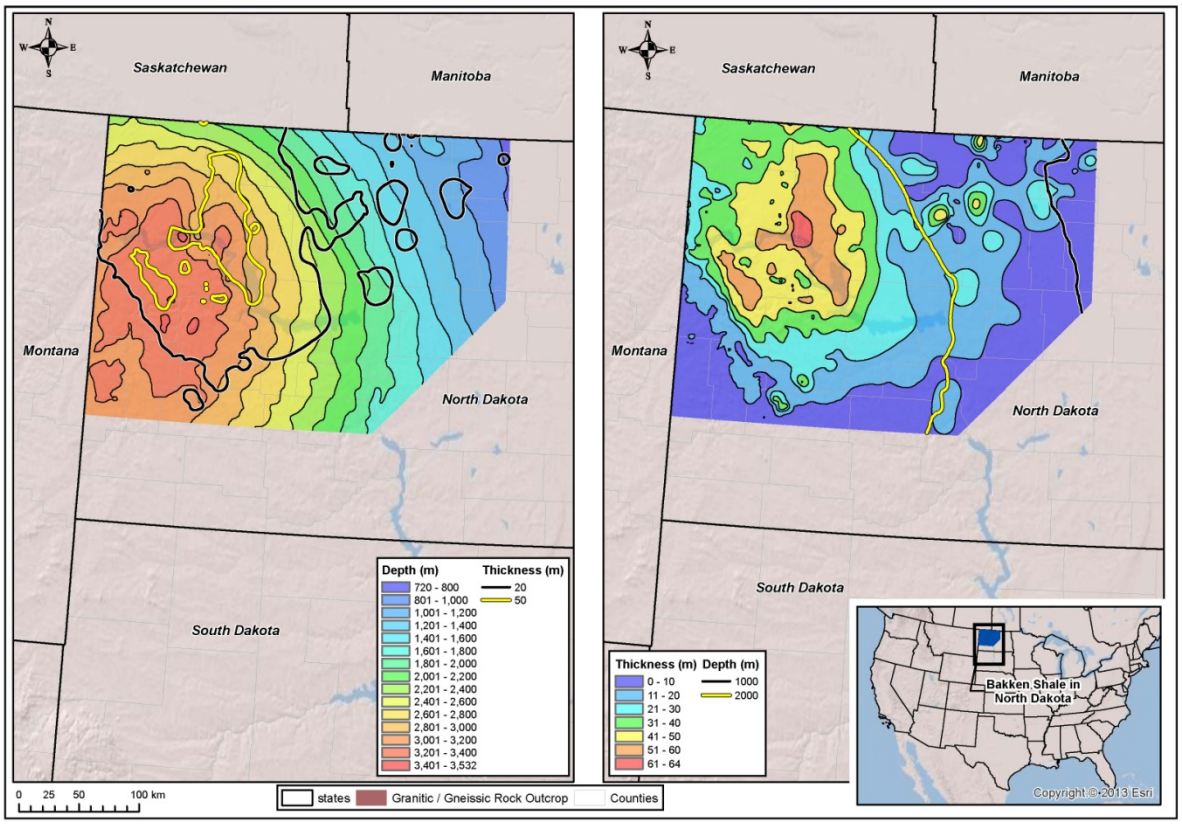

Figure 2-19. Depth and isopach maps of the Bakken Formation, Williston Basin. Figure produced by LANL from shale data populated into the GIS database.

The Williston Basin also contains a sequence of Cretaceous shales, including the Skull Creek, Mowry, Belle Fourche, Carlile, and Pierre (Bearpaw) Shales. There are a number of published isopach and structural maps of the Pierre Shale and its correlative unit, the Bearpaw, for this region (Shurr, 1977; Carlson, 1982; Smith, 1999; Condon, 2000); data from Condon (2000) for eastern Montana were used to generate GIS data for the Bearpaw (Figure 2-20).

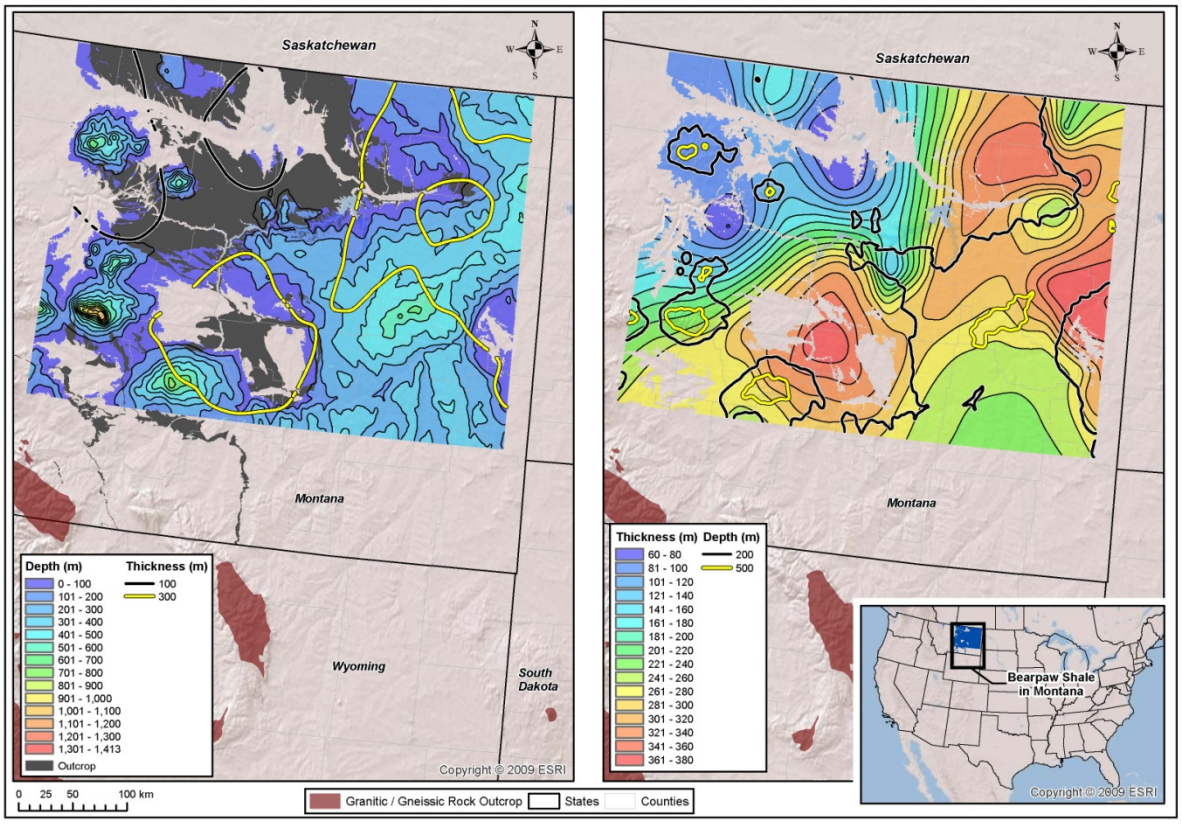

Figure 2-20. Depth and isopach maps of the Bearpaw Shale, Williston Basin. Figure produced by LANL from shale data populated into the GIS database.

2.3.10 Powder River Basin

The Powder River Basin contains a thick sequence of Paleozoic, Cretaceous, and Tertiary sediments (Anna, 2009), and is best known for its vast coal resources, consisting of thick deposits of subbituminous or lignite coal occurring at shallow depths. The Pierre Shale (Figure 2-21) forms part of the thick Cretaceous section of sediments (Denson et al., 1993a, b, c, d). As part of a hydrogeologic study of this basin, Lewis and Hotchkiss (1981) generated isopach and structure maps for the Lebo Shale member of the Paleocene Ft. Union Formation (Figure 2-22) and the Upper Hell Creek (or Lance) Formation, which is Upper Cretaceous in age.

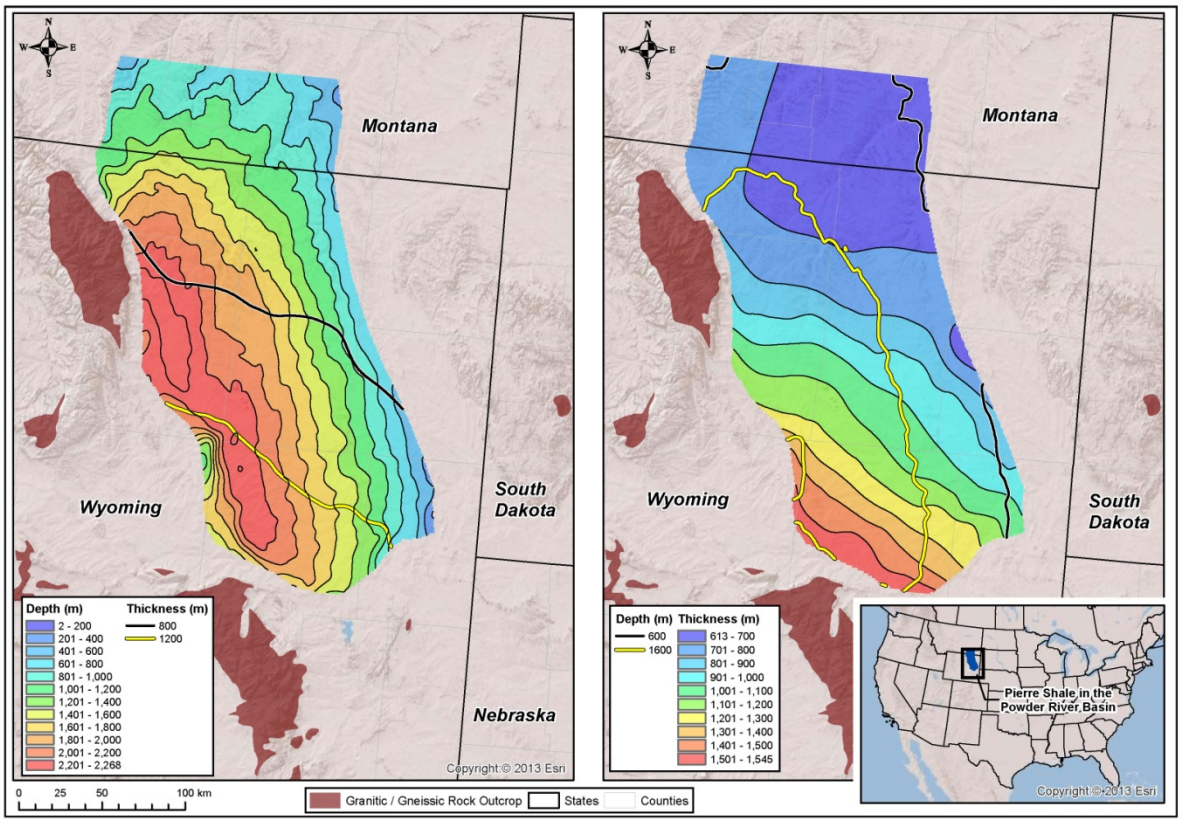

Figure 2-21. Depth and isopach maps of the Pierre Shale, Powder River Basin. Figure produced by LANL from shale data populated into the GIS database.

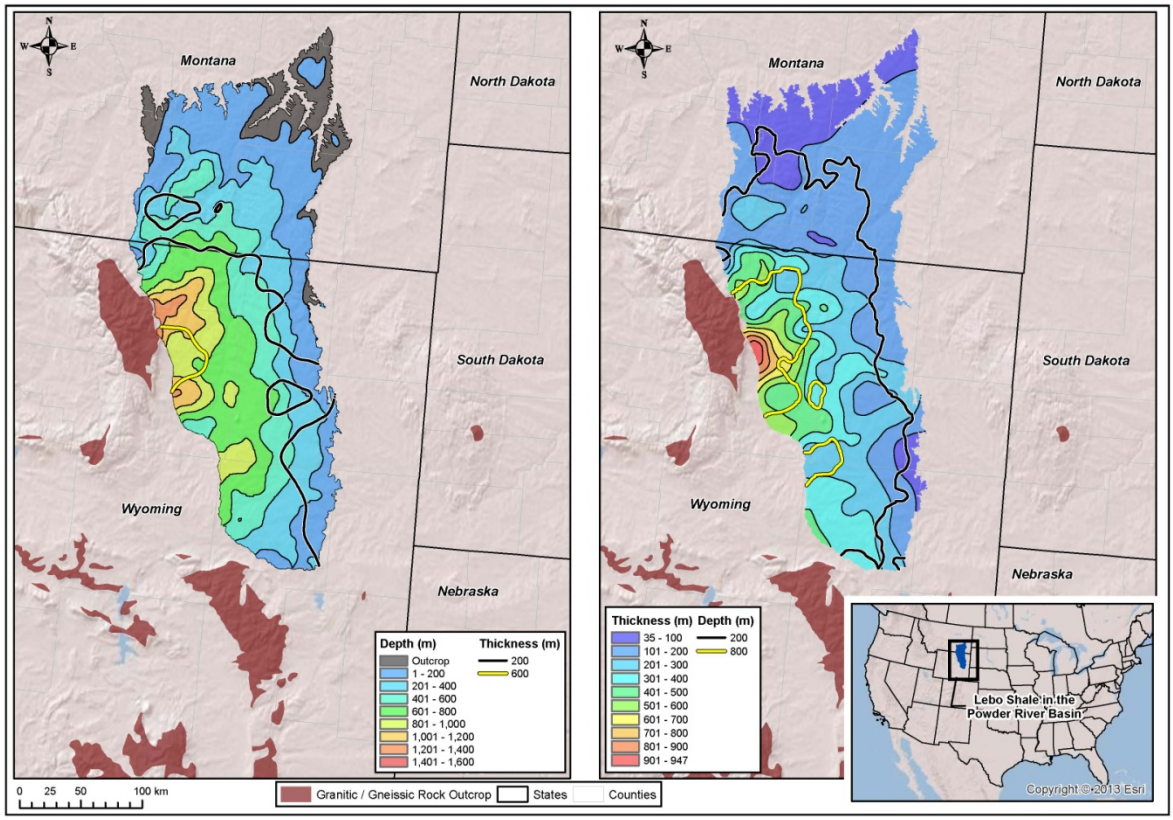

Figure 2-22. Depth and isopach maps of the Lebo Shale, Powder River Basin. Figure produced by LANL from shale data populated into the GIS database.

2.3.11 Denver Basin

The Denver Basin is a foreland structural basin bounded to the west by the Rocky Mountains. Most of the sediments in the basin are Cretaceous sandstones, shales, and carbonates (Higley and Cox, 2007); the shale units include the Skull Creek, Mowry, Graneros, Carlile, Niobrara (Smoky Hills Shale Member), and Pierre. The Pierre Shale is the most prominent of these units, and its distribution and thickness (Figure 2-23) has been characterized by Shurr (1977), who conducted an extensive study of this unit as a possible host for radioactive waste, and Dechesne et al. (2011).

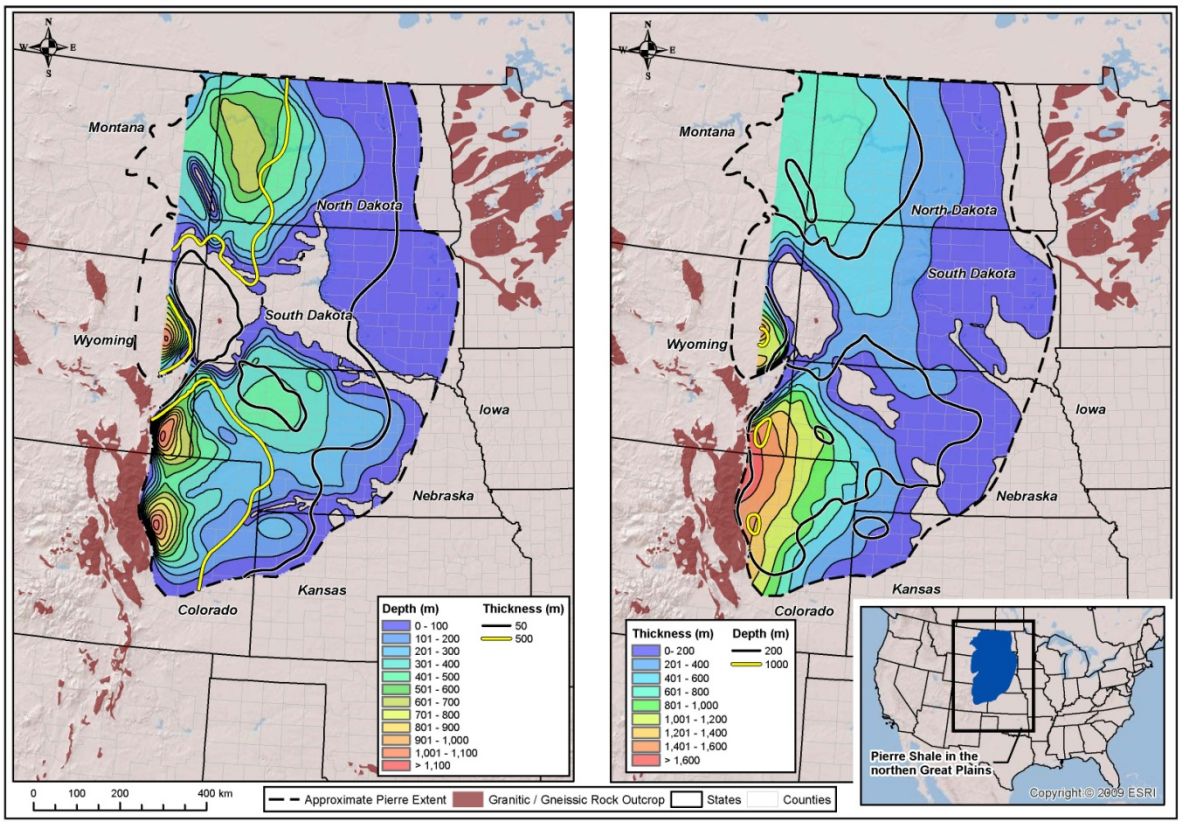

Figure 2-23. Depth and isopach maps of the Pierre Shale in the Williston and Denver Basins. Figure produced by LANL from shale data populated into the GIS database.

2.3.12 San Juan Basin

The San Juan Basin is located in southwestern Colorado and northwestern New Mexico. It contains a thick section of Jurassic and Cretaceous sands and shales, including the Upper Cretaceous Mancos Shale (Ridgley et al., 2013). This unit ranges in thickness from less than 30 m up to more than 600 m within the San Juan Basin, and is a source rock for hydrocarbon production in the basin. Isopach and structure maps from Ridgley et al. (2013) were used to develop GIS data for the Mancos in this basin (Figure 2-24).

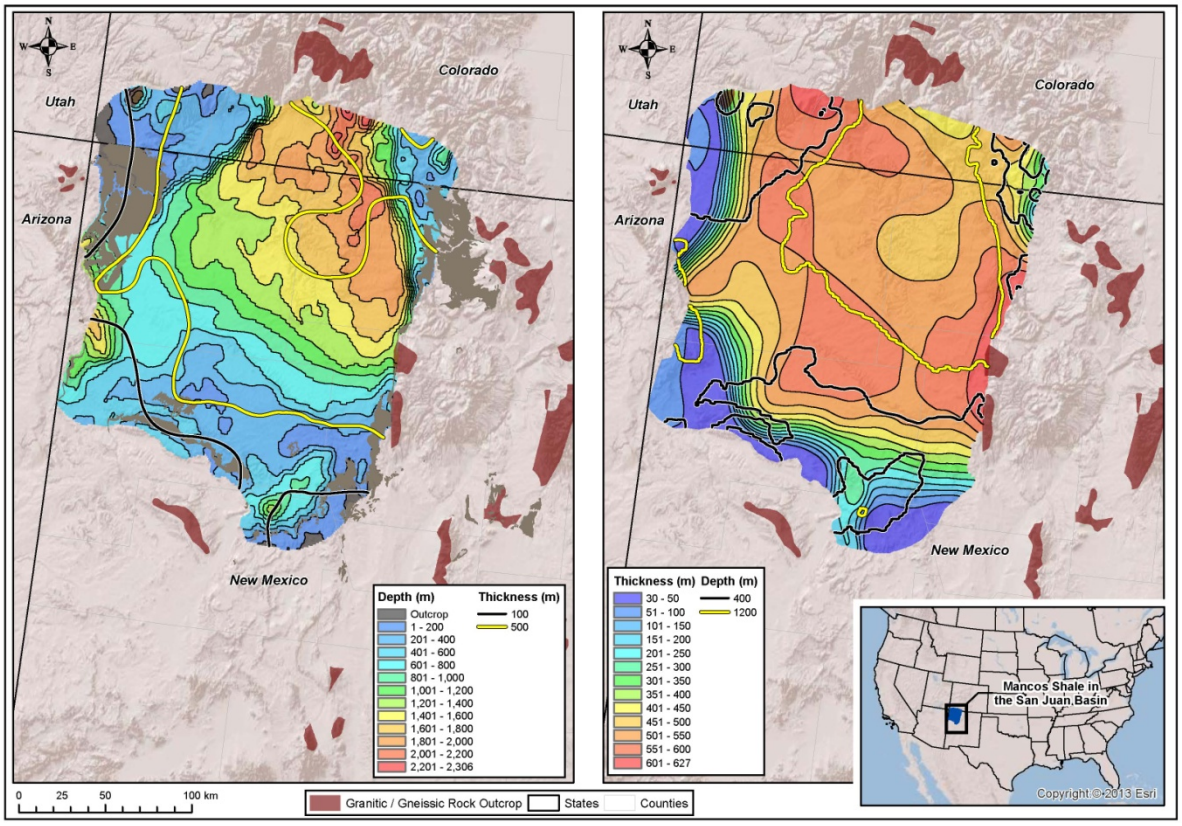

Figure 2-24. Depth and isopach maps of the Mancos Shale in the San Juan Basin. Figure produced by LANL from shale data populated into the GIS database.

2.3.13 Green River, Piceance, and Uinta Basins

The Greater Green River, Piceance, and Uinta Basins are located in Wyoming, Utah and Colorado. These basins contain major shale-bearing intervals (USGS Southwestern Wyoming Province Assessment Team, 2005; Dubiel, 2003; Johnson, 2003; Kirshbaum, 2003; USGS Uinta-Piceance Assessment Team, 2003; Johnson et al., 2010). The oldest of these units is the Permian Phosphoria Formation, which contains organic-rich mudstones. These basins also contain a number of shales that are Cretaceous in age, including the Baxter, Hillard, Steele, Lewis, Mancos and Mowry Shales. Present in all three of these basins is the Eocene Green River Formation, which contains the world's largest oil-shale deposit, with about 1.2 trillion barrels of oil in place (Dubiel, 2003). The Green River Formation consists of interbedded oil shales (such as the Parachute Creek Member), organic shales, evaporites, siltstones, sandstones, and mudstones. The Greater Green River Basin contains a number of sub-basins, including the Hoback Basin, the Green River Basin, the Great Divide Basin, the Washakie Basin, and the Sand Wash Basin (Self et al., 2011). The USGS has generated GIS data (Figure 2-25) that maps the thickness and structure of different members of the Green River Formation in these three basins as part of an oil shale resource assessment (Mercier et al., 2010a, b, c; Mercier and Johnson, 2012).

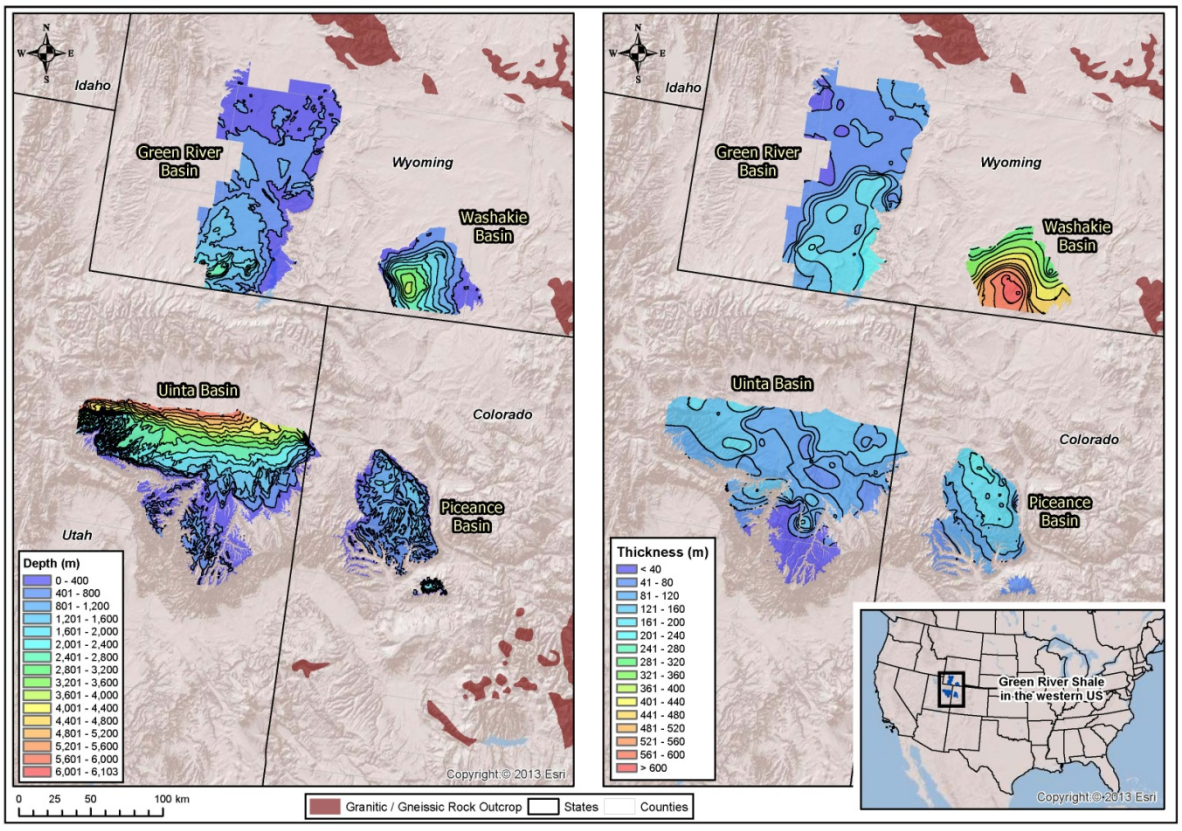

Figure 2-25. Depth and isopach maps of the Green River Shale in the Greater Green River, Uinta, and Piceance Basins. Figure produced by LANL from shale data populated into the GIS database.

2.3.14 San Joaquin, Santa Maria, and Cuyama Basins

There are a number of sedimentary basins in central and coastal California which contain thick sequences of siliciclastic rocks; these include the Los Angeles Basin, the San Joaquin Basin, the Ventura Basin, the Santa Maria Basin, and the Cuyama Basin. Most of these sediments are Tertiary in age. The two main shale-rich sedimentary units (which serve as major hydrocarbon source rocks) in these basins are the Miocene Monterey Formation and the Eocene Kreyenhagen Formation (Magoon et al., 2009). The Monterey Formation has a wide variety of lithologies present (Williams, 1982), including diatomite, porcelanite, siliceous, organic-rich and clay shales, chert, dolomite, calcareous siliceous sediments, and siltstones. Sweetkind et al. (2010; 2013) created digital tabulations of stratigraphic well data for the Santa Maria and Cuyama Basins. Hosford Scheirer (2013) developed a 3-D basin model that includes isopach and structural surface maps of the Monterey Formation for the San Joaquin Basin (Figure 2-26).

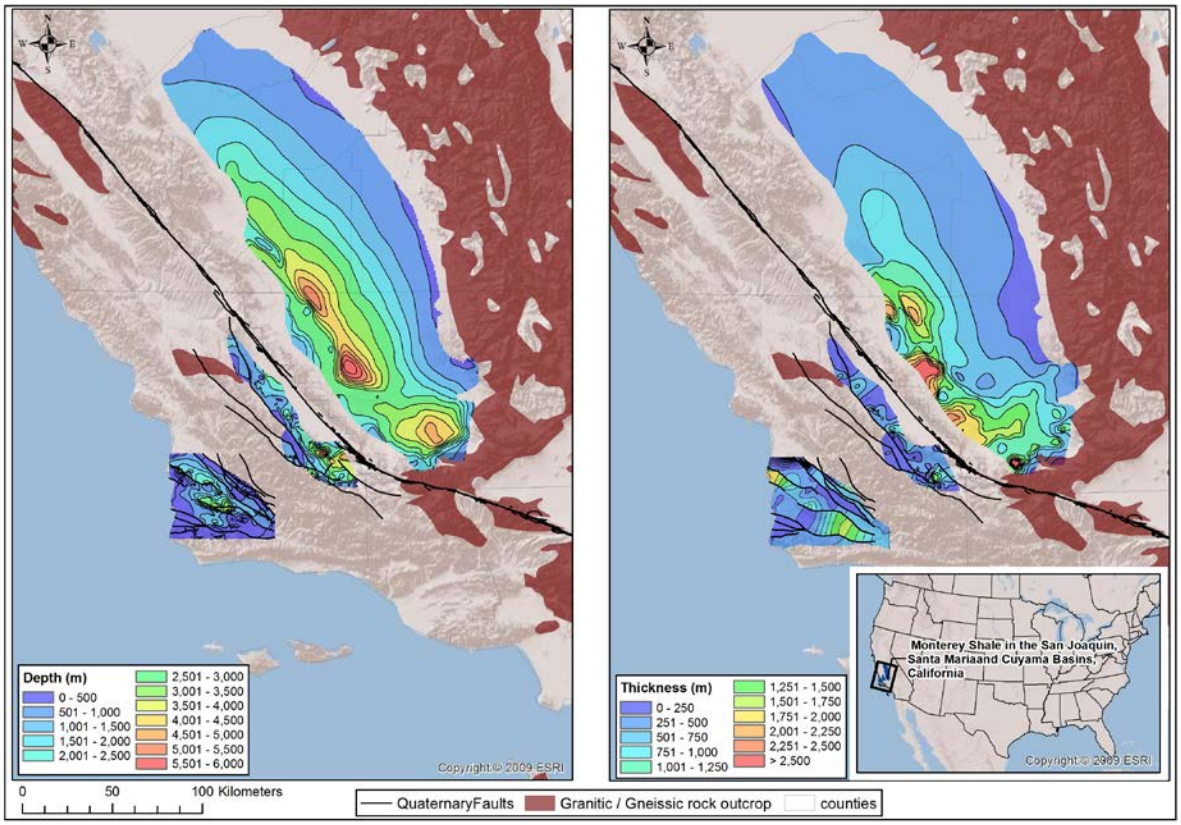

Figure 2-26. Depth and isopach maps of the Monterey Formation in the San Joaquin, Cuyama, and Santa Maria Basins. Figure produced by LANL from shale data populated into the GIS database.

2.4 TOTAL ORGANIC CARBON AND THERMAL MATURITY MAPS

The rock properties of shales can impact their viability as a rock barrier for the migration of radionuclides. In many shale sequences, the amount and thermal maturity of organic matter have been studied to determine their viability as potential source and reservoir rocks for the production of oil and gas. The thermal history of shales can also impact their rock properties, as burial diagenesis will result in sediment compaction and mineralogic changes. The integrated thermal history of sedimentary rocks can be evaluated using established techniques such as vitrinite reflectance and changes in conodont color.

Maps depicting lateral variations in total organic carbon (TOC) content and the thermal maturity of shale units were created for the following units as organized by sedimentary basin. Table 2-2 summarizes formations for which TOC and/or thermal maturity data (typically as vitrinite reflectance) have been obtained.

Table 2-2. Identified data sources for TOC and thermal maturity for shale formations within major sedimentary basins.

Appalachian Basin	
Utica Shale	**TOC data**: Engelder, 2011 (Figure 4.12); Patchen et al., 2006 (Figures 7-3, 7-4 & 7-5); Ohio Department of Natural Resources, 2013a **Thermal maturity data**: Repetski et al., 2008 (Figure 6); Patchen et al., 2006 (Figures 7-5 & 7-7); Ohio Department of Natural Resources, 2013b
Illinois Basin	
New Albany Shale	**Thermal maturity data**: Strapoc et al., 2010 (Figure 5); Mastalerz et al., 2013 (Figure 1)
Arkoma Basin	
Chattanooga Shale	**TOC and thermal maturity data:** Li et al., 2010 (Plate 2)
Fayetteville Shale	**TOC and thermal maturity data:** Ratchford et al., 2006 (Plate 23); Li et al., 2010 (Plate 1)
Fort Worth Basin	
Barnett Shale	**Thermal maturity data**: Pollastro et al., 2007 (Figure 12); Montgomery et al., 2005 (Figure 6); Zhao et al., 2007 (Figure 6)
Permian Basin	
Barnett Shale	**TOC and thermal maturity data:** Broadhead and Gillard, 2007 (Plates IX & X) (GIS data obtained from New Mexico Bureau of Geology and Mineral Resources)
San Joaquin Basin	
Monterey Formation	**Thermal maturity data:** Magoon et al., 2009 (Figures 8.9 & 8.14)

The compositions and rock properties of the Utica and Marcellus shales were studied in an analog assessment of their viability as a rock barrier for the migration of radionuclides as part of an evaluation of the proposed Ontario Power Generation Deep Geologic Repository at the Bruce site in Ontario for storage of low and intermediate radioactive waste (Engelder, 2011). High natural gas contents related to the burial and maturation of organic-rich shales can lead to the development of natural hydraulic fractures, which could compromise the integrity of the shales as fluid flow barriers. The Utica Shale has a total organic carbon (TOC) content that varies from 0.28 to 4.26 wt. % (Figure 2-27), with a median value just less than 2% (Ryder et al., 1998). In contrast, the Marcellus has TOC values that generally range from 2 to 12 wt. %, with values typically between 2 and 10% (Bruner and Smosna, 2011). Organic-rich black shales are often characterized by elevated gamma signatures. Agrawal (2009) describes the depositional environment, mineralogy and TOC of the Marcellus.

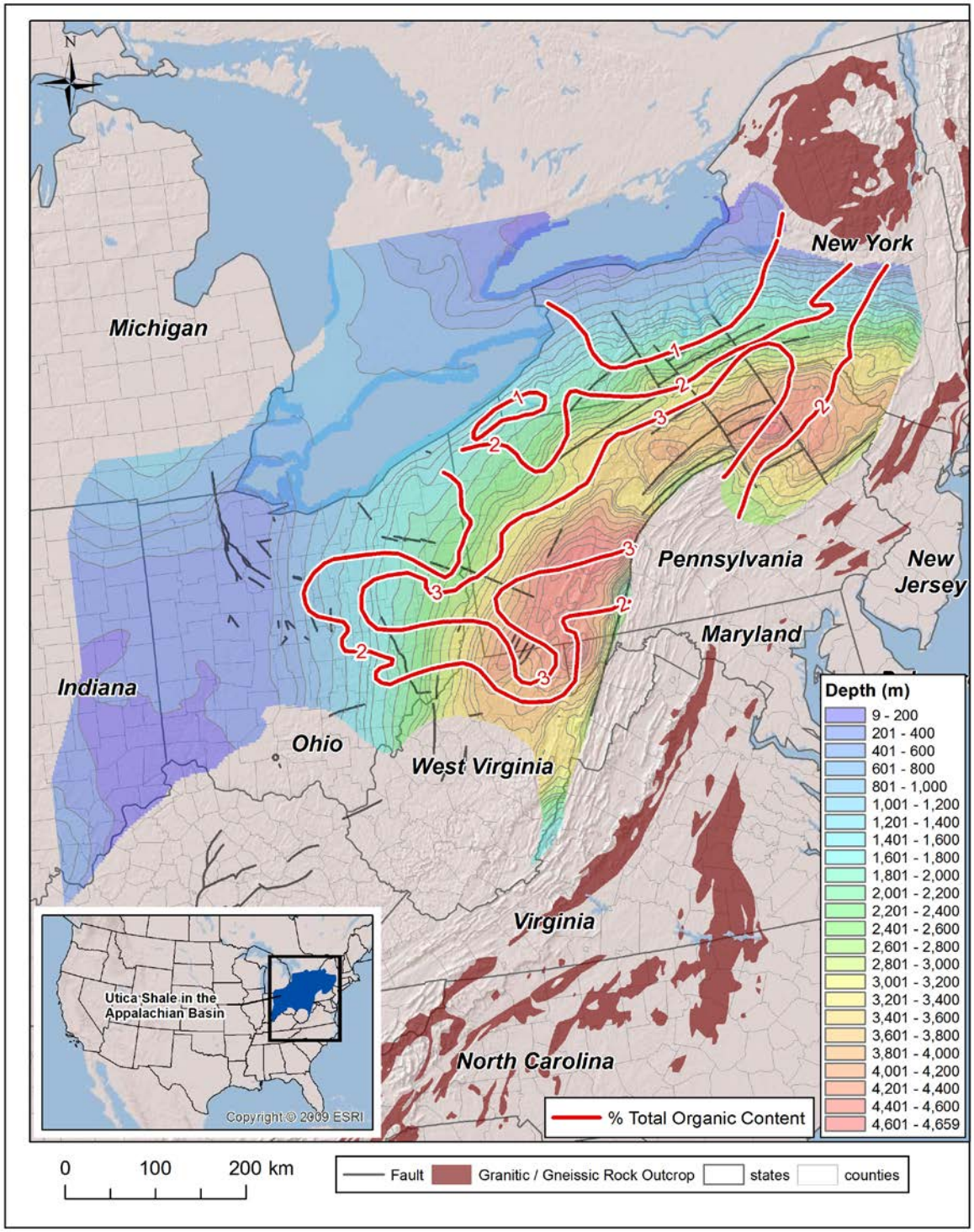

Figure 2-27. Variation in total organic carbon in the Utica Shale, Appalachian Basin. Figure produced by LANL from shale data populated into the GIS database.

Vitrinite reflectance data were used to create thermal maturity maps for the New Albany Shale in the Illinois Basin (Fig. 2-28), the Fayetteville Shale in the Arkoma Basin (Fig. 2-29) (this also has TOC data), the Barnett Shale in the Fort Worth Basin (Fig. 2-30), and the Monterey Formation in the San Joaquin Basin (Fig. 2-31). As expected, deeper portions of the basins typically have higher % vitrinite reflectance.

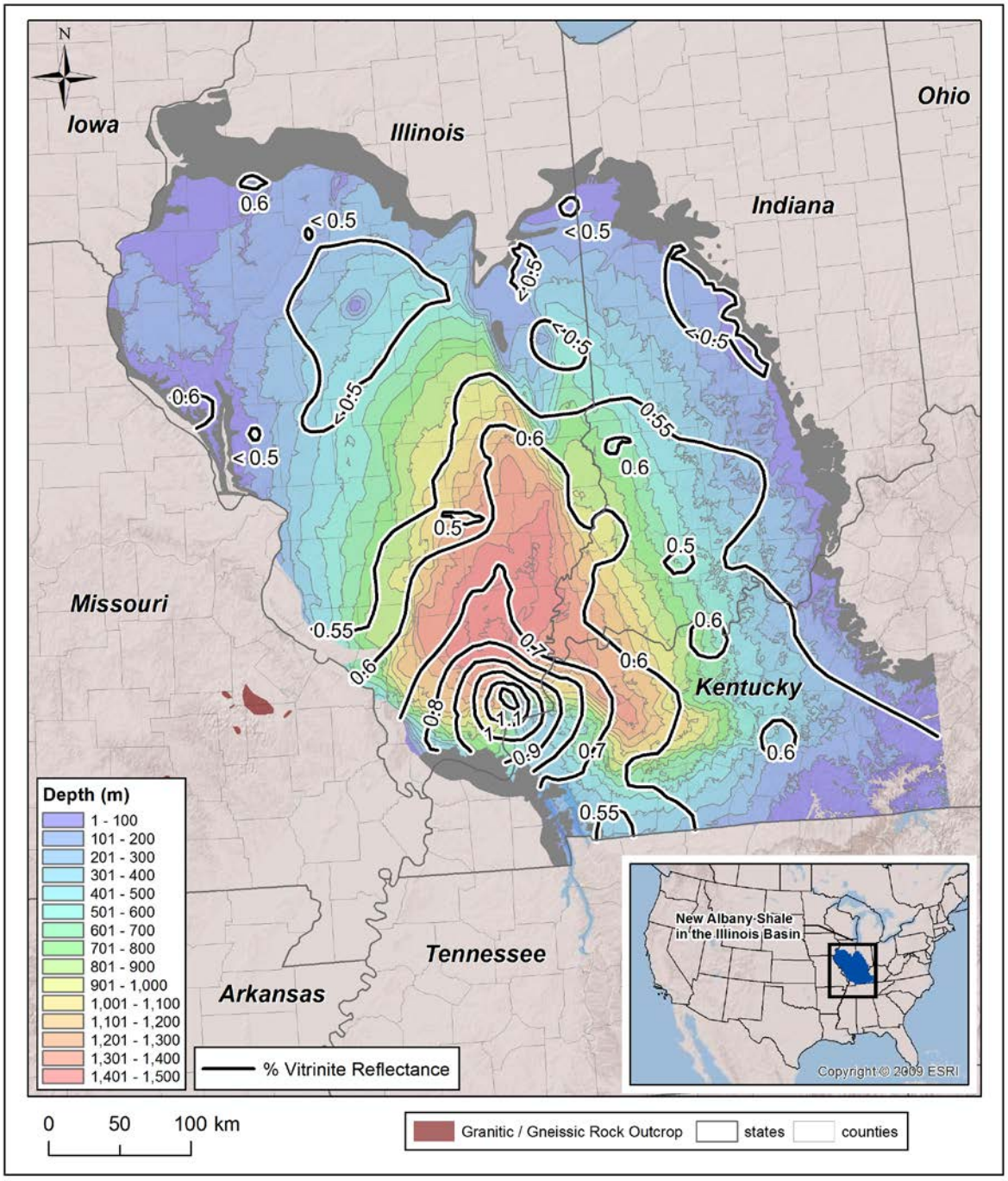

Figure 2-28. Variation in percent vitrinite reflectance in the New Albany Shale, Illinois Basin. Figure produced by LANL from shale data populated into the GIS database.

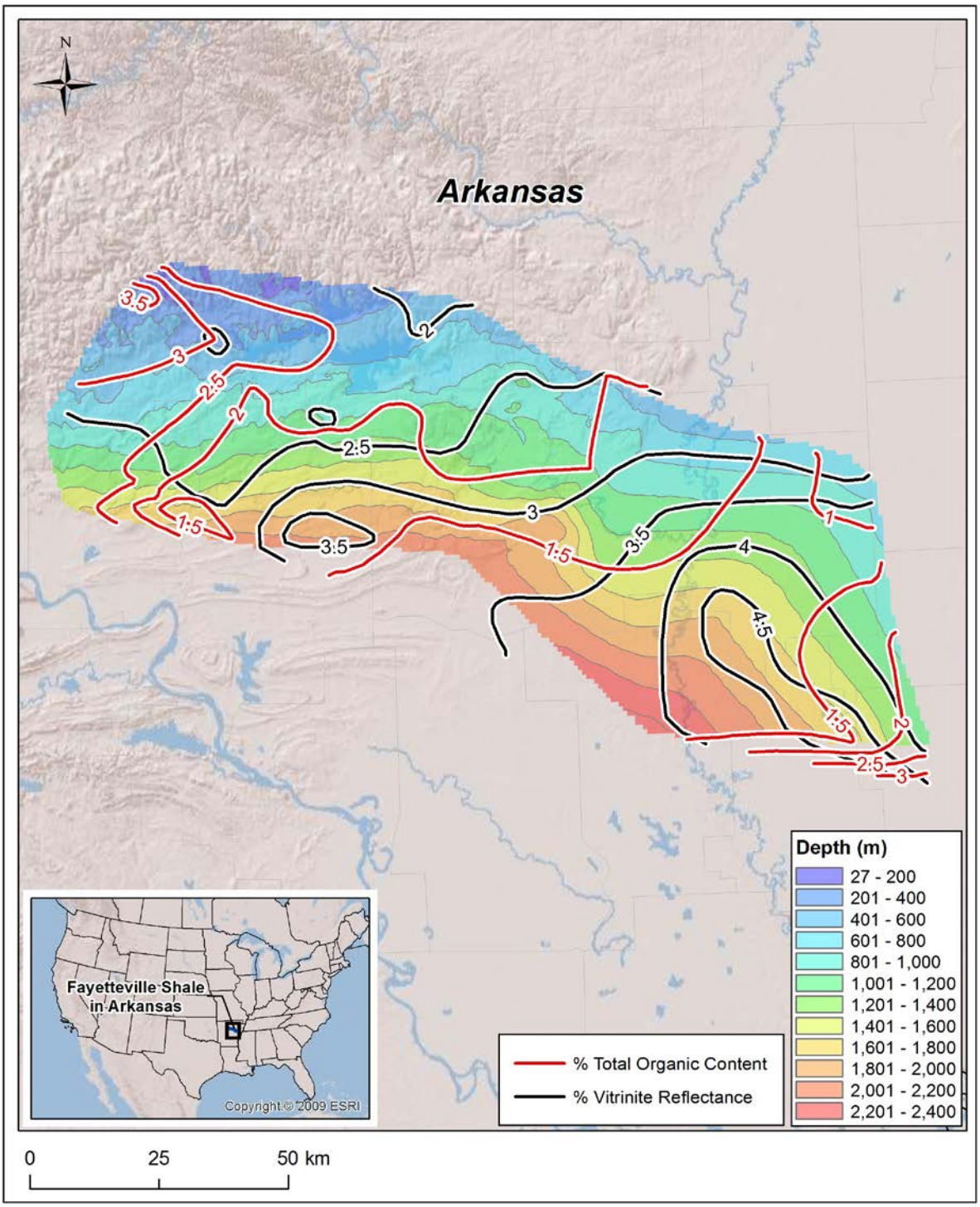

Figure 2-29. Variation in total organic carbon and percent vitrinite reflectance in the Fayetteville Shale, Arkoma Basin. Figure produced by LANL from shale data populated into the GIS database.

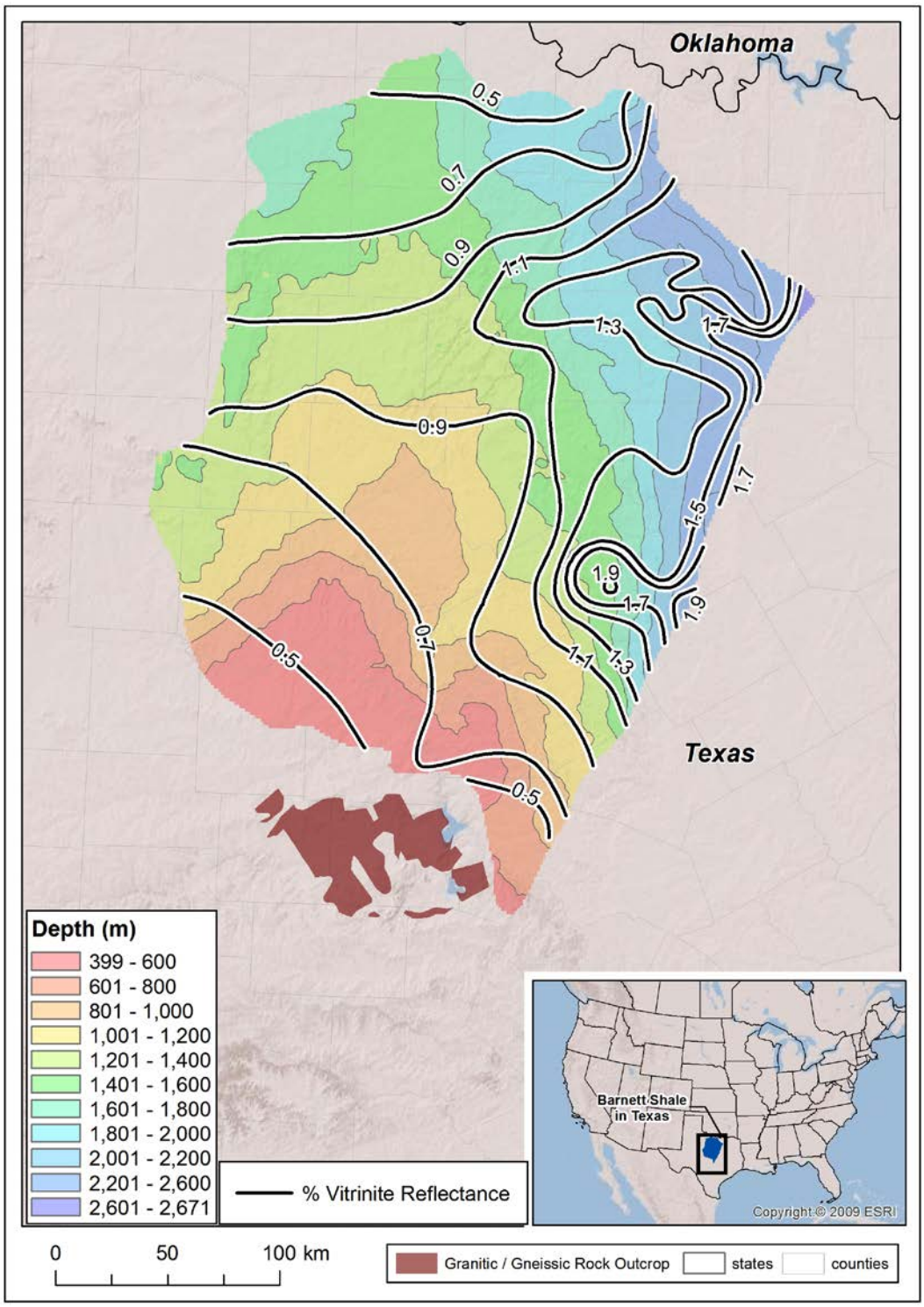

Figure 2-30. Variation in percent vitrinite reflectance in the Barnett Shale, Fort Worth Basin. Figure produced by LANL from shale data populated into the GIS database.

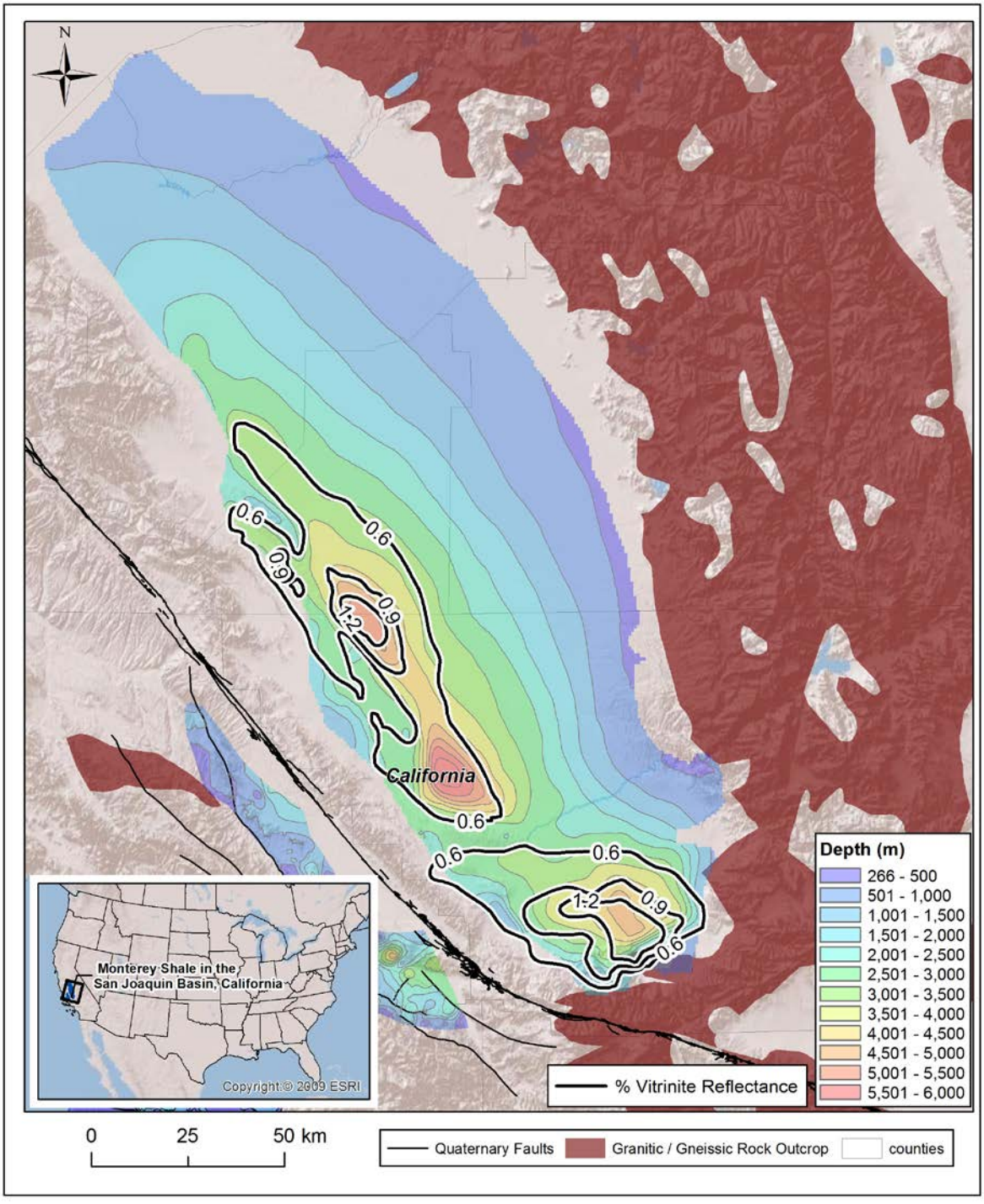

Figure 2-31. Variation in percent vitrinite reflectance in the Monterey Formation, San Joaquin Basin. Figure produced by LANL from shale data populated into the GIS database.

Total organic carbon data were also utilized to create a map for the Barnett Shale in the Permian Basin of SE New Mexico (Fig. 2-32).

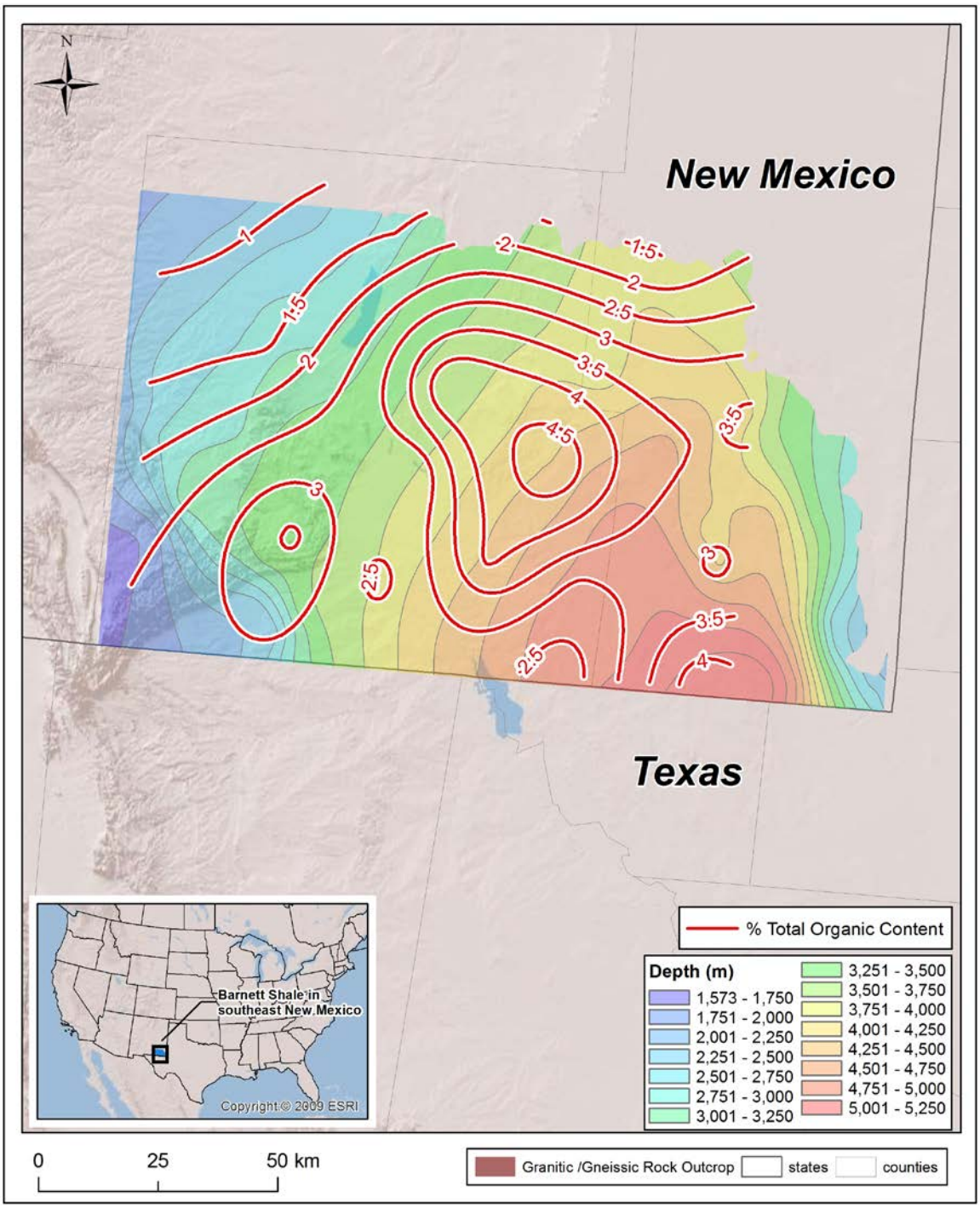

Figure 2-32. Variation in total organic carbon in the Barnett Shale, Permian Basin. Figure produced by LANL from shale data populated into the GIS database.

2.5 CONCLUSIONS

This report serves as an update relating to the progress of obtaining shale formation extent, thickness and depth data for the LANL geologic database. GIS data have been obtained for many shale formations associated with unconventional shale oil and gas deposits, such as the Marcellus, Utica, Barnett, New Albany, Antrim, Haynesville and Woodford Shales and the Bakken, Eagle Ford, Monterey, and Green River Formations; Figure 2-33 summarizes the shale formations that have been incorporated into the LANL database. Additional GIS data are in the process of being generated through the digitization of published isopach and structure maps. Continued efforts are being made to obtain additional GIS and map data for other shale formations that can be used to augment the GIS database. Associated rock property data such as total organic carbon and thermal maturity data are also being collected and integrated into the GIS database.

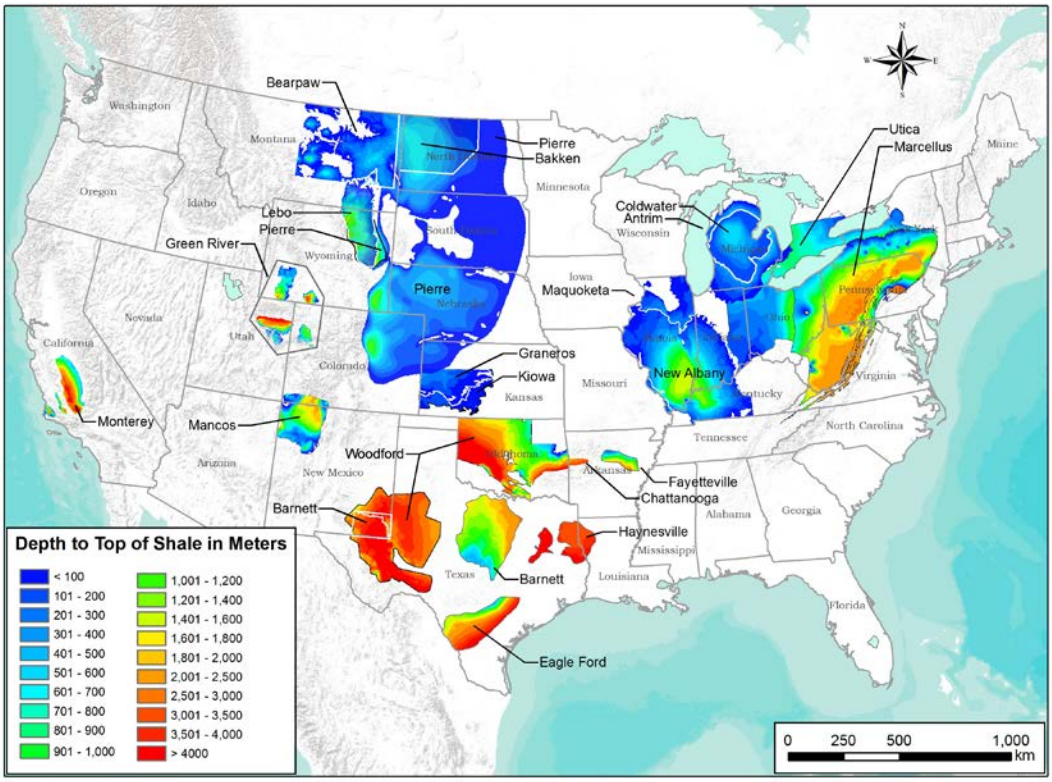

Figure 2-33. Summary of GIS data for depth to top of shale formations within major sedimentary basins in the US currently incorporated in the LANL GIS database. Figure produced by LANL from shale data populated into the GIS database.

3. ROCK PROPERTIES AND IN-SITU CONDITIONS FOR SHALE ESTIMATED FROM SONIC VELOCITY MEASUREMENTS

3.1 Introduction and Recap of Previous Work

Shale is a sedimentary rock type that is being considered for geologic disposal of high-level radioactive waste. The regional geology task within the UFDC has been tasked to identify shale formations within the United States that should be evaluated as potential "host" formations for this waste disposal activity. Identification and evaluation of shale formations includes description of the formation geometric characteristics (area, depth, and thickness) as well as relevant physical characteristics. Physical characteristics can be measured directly using in-situ measurement methods or on rock samples (core or in some cases drill cuttings) taken during drilling of boreholes into the formation. Although such direct measurements are the most accurate was to determine physical characteristics, they are likely to be prohibitively expensive for initial assessments of possibly numerous shale formations that might need to be evaluated. The alternative pursued here is to estimate various physical characteristics of the formation based on correlations with the compressional (or sonic) velocity of the rock. The advantage of this approach is that sonic velocity is a standard geophysical log that is routinely performed on boreholes and as such is more readily available than direct in-situ or core measurements of properties. If an existing log is not available, it is possible to conduct a log measurement if an existing borehole is available. This can typically be done for less cost than direct in-situ measurements (if such measurements are even possible) or sampling and laboratory measurements on core. Furthermore, a sonic log provides a continuous measure of sonic velocities along the borehole which can be used to evaluate heterogeneities in the formation.

The sonic velocity is used because of the range of properties that have already been identified by other researchers as having a robust correlation with sonic velocity (e.g., porosity, Young's modulus, shear modulus, uniaxial compressive strength) for shale lithologies (Ingram and Urai, 1999; Horsrud, 2001). In a previous report (Dobson and Houseworth, 2013), these correlations were expanded based on additional data available from European investigations of nuclear waste disposal in shale lithologies. Additional correlations with sonic velocity were also developed for bulk density, clay content, Poisson's ratio, cohesive strength, friction angle, and tensile strength. A published correlation relating porosity, clay content, and permeability for mudrock (Yang and Aplin, 2010) was used in combination with the porosity and clay content correlations with sonic velocity to allow estimation of permeability from sonic velocity. The correlation is valid over a wide range of clay content (mass fraction of sub 2 micron particulates), from 12% to 97%, and porosity from 0.04 to 0.78. Similarly, an additional published correlation relating porosity, clay content, and maximum effective stress (Yang and Aplin, 2004) was used in combination with published correlations relating sonic velocity, uniaxial compressive strength and brittleness index (BRI), and the brittleness index with the overconsolidation ratio, to allow an estimate of in-situ pore pressure based on the sonic velocity.

Anisotropic behavior is common for shale and mudrock and is usually found to be a particular type of anisotropy known as *transversely isotropic*. This type of anisotropy is caused by the bedding structure of shales and mudrock. It means that potentially directionally sensitive property values are isotropic for any orientation restricted to be parallel to the bedding plane, but display anisotropy normal to the bedding plane. Anisotropic effects for some of the properties known to be directional such as permeability and Young's modulus were also estimated based on measurements (or estimates) of sonic velocity anisotropy. This was done by using a scaling factor equal to the ratio of sonic velocities parallel and normal to bedding raised to a power (determined empirically). The property value normal to bedding was multiplied by this scaling factor, A, to obtain a property value parallel to bedding. The anisotropy scaling factor is

given by $A = \left(V_{pp}/V_{pn}\right)^{\omega}$, where V_{pn} is the sonic velocity normal to bedding, V_{pp} is the sonic velocity parallel to bedding, and ω is an empirical anisotropy coefficient. To be consistent for properties that do not show directional behavior, the correlations with sonic velocity were conducted using the geometric mean sonic velocity, $V_{pm} = \sqrt{V_{pn}V_{pp}}$, where V_{pn} is the sonic velocity normal to bedding and V_{pp} is the sonic velocity parallel to bedding. Anisotropic property correlations were established by correlating the property normal to bedding with V_{pm}. Then, the property parallel to bedding was established by scaling the same correlation by the anisotropy factor, A.

The correlation between clay content and sonic velocity presented in Dobson and Houseworth (2013) showed a bit more scatter than most of the correlations, which lead to the question as to whether or not it is reasonable to expect a correlation between sonic velocity and clay content. Some additional literature on this subject has been reviewed in Section 2 and supports the use of such a correlation. Data that allows the investigation of a correlation between the sonic velocity and thermal properties, i.e., thermal conductivity and specific heat, have been analyzed and correlations have been developed that provide a means to estimate these properties sonic velocities. Additional published correlations that link permeability and air entry pressure along with a correlation between air entry pressure and the van Genuchten capillary strength parameter (α) allow a linkage between sonic velocity and α. An additional relationship from the literature between the air entry pressure and the van Genuchten pore-size-distribution index (m) permits the evaluation of this parameter from the sonic velocity. From these, capillary pressure and relative permeability parameter functions of saturation can be computed.

3.2 ESTIMATING CLAY CONTENT

The clay content of shales was empirically correlated with the geometric mean sonic velocity in Dobson and Houseworth (2013). The clay content is defined as the clay mineral mass fraction. Several authors have reported on the correlation of sonic velocity, porosity, and clay content for more general sandstone rock types with widely varying clay content (Tosaya and Nur, 1982; Kowallis et al., 1984; Castanaga et al., 1985, Han et al., 1986).

Tosaya and Nur present data for sonic velocity, porosity, and clay content. In their data, porosity ranges from 4 to 20 percent and the volume fraction of clay content ranges from 0 to 72 percent. These data are correlated to give the following:

$$V_p = -2.4C - 8.6\phi + 5.8C_v \qquad (3\text{-}1)$$

where V_p is the sonic velocity in km/s, C_v is the volume fraction clay content, and ϕ is the fractional porosity. The relationship indicates the general expected trend of reduced sonic velocities with increased porosity or clay content, with greater sensitivity to changes in porosity, as found by Dobson and Houseworth (2013). Tosaya and Nur (1982) data, shown in Figure 3.1, span different rock types (sandstones, siltstones, and shales) that contain different types of clay (illite, kaolinite, mixed-layer illite-montmorillonite, and illite-chlorite). However, the correlation did not appear to be sensitive to differences in clay mineralogy. Furthermore, the spatial distribution of clay within the samples, observed to vary between pores (authigenic clay) and grain contacts (allogenic clay) did not impact the correlation.

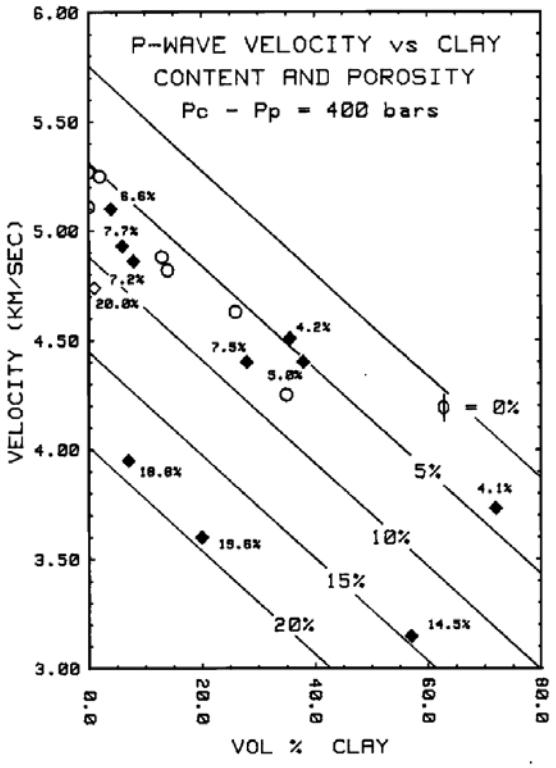

Figure 3.1 Compressional velocity as a function of clay content and porosity at a confining stress of 800 bars and a pore pressure of 400 bars, Tosaya and Nur (1982).

The work of Tosaya and Nur (1982) was extended by Kowallis et al. (1984) to include additional samples that ranged up to 29 percent porosity. A similar linear correlation between sonic velocity, clay content, and porosity was found.

Castanaga et al. (1985) developed correlations for sonic velocity, clay content, and porosity and for shear velocity, clay content, and porosity. Their data also spans sandstones, siltstones, and shales as does Toyasa and Nur (1982), but contain a much larger number of samples. An analysis of the mudrock (shale) samples revealed a unique linear relationship between the sonic (V_p) and shear (V_s) velocities,

$$V_p = 1.16V_s + 1{,}360 \qquad (3\text{-}2)$$

where both velocities are in m/s. The data and correlation line from Castanaga et al., (1985) are shown in Figure 3.2.

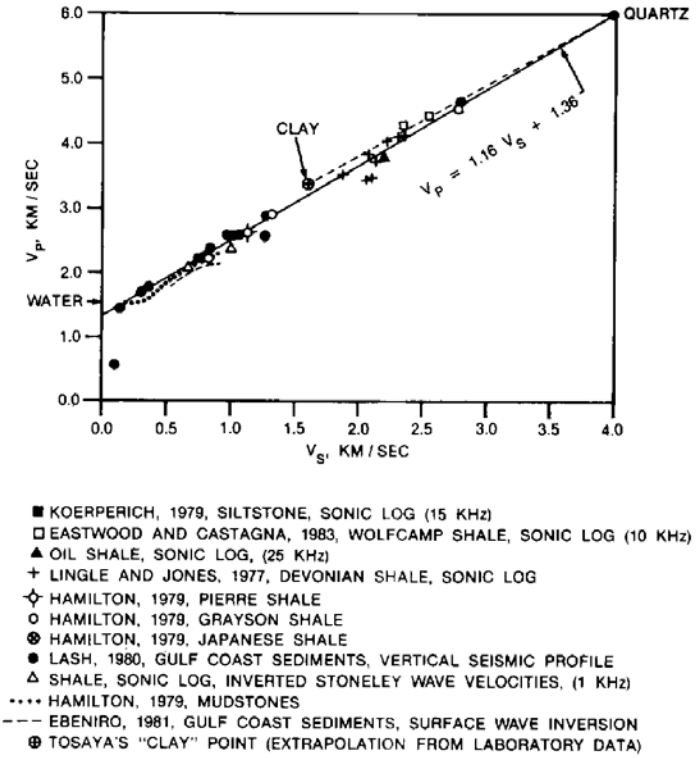

Figure 3.2 In-situ and seismic measurements of sonic and shear wave velocities in mudrocks (Castanaga et al. (1985).

Castanaga et al. (1985) found that the mudrock line could also be used to approximate the relationship between the sonic and shear velocities for sandstones.

Han et al. (1986) developed independent correlations for sonic and shear velocities as functions of porosity and clay volume fraction for shaly sandstones as shown in Equations (3.3) and (3.4).

$$V_p = 5{,}590 - 6{,}930\phi - 2{,}180C_v \quad (3\text{-}3)$$

$$V_s = 3{,}520 - 4{,}910\phi - 1{,}890C_v \quad (3\text{-}4)$$

where the velocities are in m/s, ϕ is the porosity (as a fraction), and C_v is the clay volume fraction. In theory, Equations (3-2), (3-3), and (3-4) could be combined to give a relationship between V_p and C_v. However, such a combination does not produce a valid result — C_v is found to be greater than 1 for all reasonable values of V_p.

Shale porosity can be reasonably represented as a function of the sonic velocity alone as shown in Dobson and Houseworth (2013). Therefore, including both velocity and porosity in a correlation for clay content may not improve the correlation. This conclusion was also reached by Cosenza et al. (2014) who analyzed similar correlations for the Callovo-Oxfordian Clay. Instead of clay volume fraction, Cosenza et al. (2014) used the weight fraction of clay, X. Cosenza et al. (2014) investigated several correlation forms including correlations between V_p, X, and ϕ, but found that a simple $V_p - X$ correlation performed as well

as or better than correlations including porosity as an independent variable. Figure 3.3 shows correlations found between X and V_p and X and V_s.

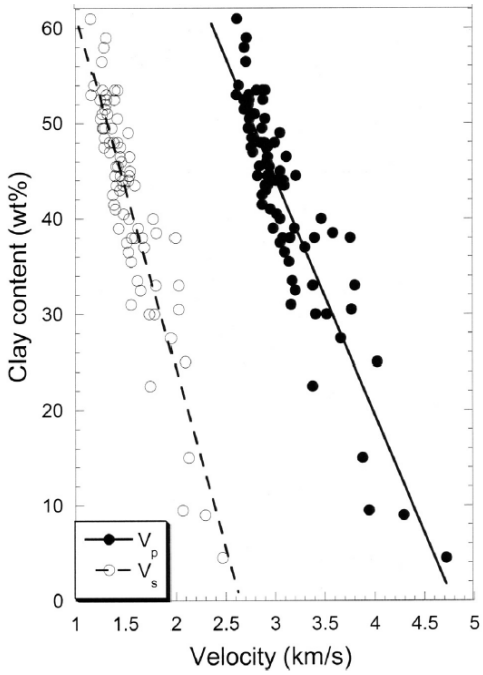

Figure 3-3. Correlation between clay content and sonic and shear velocities for the Callovo-Oxfordian clay. Solid line is for Equations (3-5) (for V_p) and dotted line for (3-6) (for V_s). (Cosenza et al., 2014).

The Cosenza et al. (2014) correlations for X and V_p and X and V_s are:

$$X = 1.186 - 0.000248\, V_p \tag{3-5}$$

$$X = 0.996 - 0.000376\, V_s \tag{3-6}$$

where the velocities are in m/s. Cosenza et al. (2014) does not distinguish between sonic velocity normal or perpendicular to bedding, therefore, these velocities are assumed to represent a mean velocity. Equations (3-5) and (3-6) may be combined to eliminate X to give,

$$V_p = 1.52 V_s + 766 \tag{3-7}$$

Equation (3-7) may be compared with the correlation in Equation (3-2). Equation (3-7) gives a relatively low value of $V_p = 766$ m/s at $V_s = 0$ as compared with Equation (3-2), which gives 1,360 m/s. The sonic velocity at a shear velocity of zero may also be compared with the sonic velocity in water (see Figures 3-2 and 3-4). The predicted values of V_p for Equations (3-2) and (3-7) cross over at a shear velocity of 1,650 m/s, and for $V_s \geq 1{,}650$, the predicted values of V_p from Equation (3-7) is greater than the value predicted from Equation (3-2). Although the two correlations are different, within the main middle region (sonic velocities from 2000 to 5000 m/s) the lines are reasonably close as shown in Figure 3-4

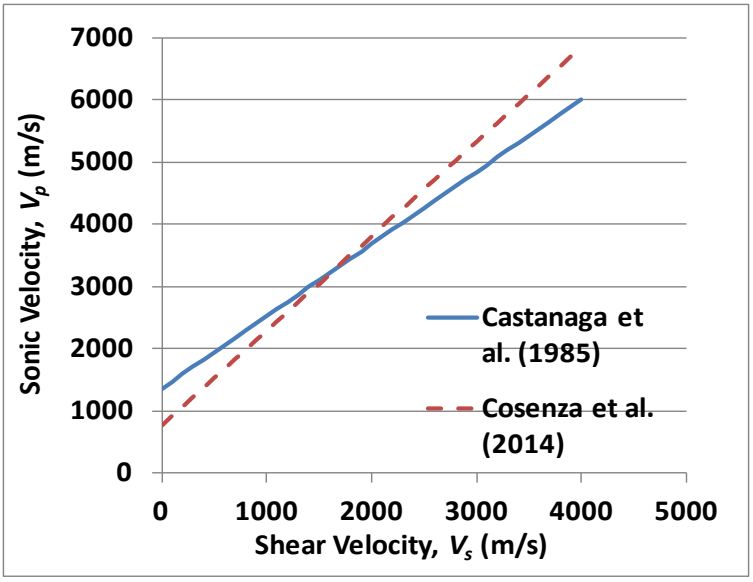

Figure 3-4. Use of Equation (3-5) needs to be truncated at high velocities because $X \leq 0$ for for $V_p \geq 4782$. Therefore, X will be set to zero for $V_p \geq 4782$.

The correlation proposed by Cosenza et al. (2014) is similar to the correlation developed by Dobson and Houseworth (2013) in that clay content is correlated with compressional seismic velocity and found to decrease monotonically with increasing velocity. However, the two correlations are substantially different in terms of quantitative predictions. The correlations are compared in Figure 3-5. The reason for the significant differences, particularly at high velocities, is not understood at this time.

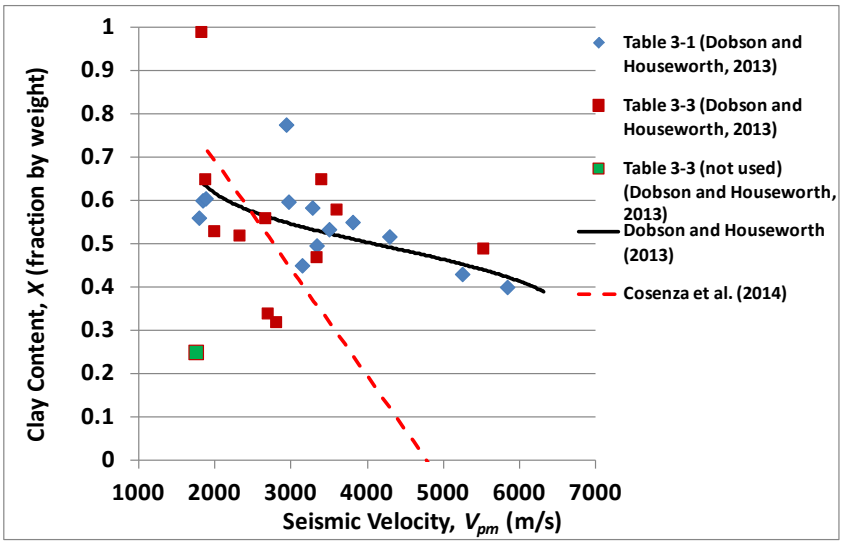

Figure 3-5. Correlation developed by Dobson and Houseworth (2013) compared with the V_p- clay content correlation developed by Cosenza et al. (2014) (also shown in Figure (3-3)).

3.3 ESTIMATING THERMAL CONDUCTIVITY AND SPECIFIC HEAT CAPACITY

Data that includes measurements of sonic velocity and thermal conductivity or heat capacity for shales have not been identified. However, sonic velocity has been used as a correlation variable thermal conductivity of other types of geologic materials (Boulanouar, et al., 2013; Fuchs and Förster, 2013). Goto and Matsubayashi (2009) derived correlations for thermal conductivity and specific heat using porosity as the correlation variable.

3.3.1 Thermal Conductivity

Thermal conductivity measurements in shales, mudrocks, and claystones have been reported by several investigators (Blackwell and Steele, 1989; Midttømme et al., 1997; 1998; Midttømme and Roaldset, 1999; Waples and Tirsgaarde, 2002; Garitte et al., 2012). While none of these have attempted to link thermal conductivity with seismic velocity, Midttømme et al. (1997), Midttømme et al. (1998), and Midttømme and Roaldset (1999) tested arithmetic, geometric, and harmonic mixing-law models as a way to predict thermal conductivity based on porosity and mineral composition. Midttømme et al. (1997) found that there was some dependency seen in the data between thermal conductivity and porosity, however, the relationship between thermal conductivity and mineral composition was found to be weak. In some of these data sets only water content is reported instead of porosity (Midttømme et al., 1997 and Midttømme and Roaldset, 1999). For these cases, the water content was used as a proxy for porosity. The two values can differ when minerals contain waters of hydration as part of the mineral structure, which is counted towards water content but not porosity. Midttømme et al. (1998) measured both for four high-clay-content samples (clay content 44% to 65%); the root-mean-square average difference was about 0.07.

The data for thermal conductivity normal to bedding (K_{thn}) is plotted against porosity (ϕ) for all but the Waples and Tirsgaarde (2002) data (Figure 3-6). Although there is considerable scatter, a trend can be seen between these variables. These data were obtained either from field measurements in boreholes or laboratory measurements using the divided bar method.

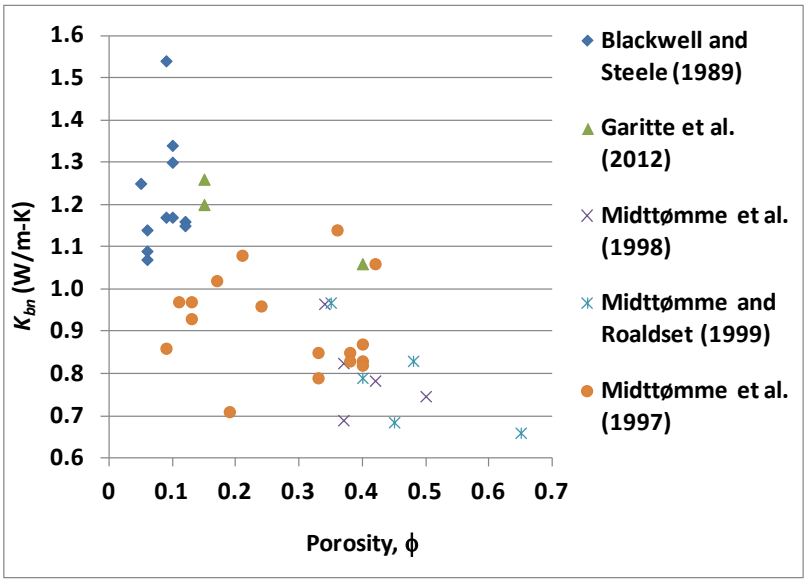

Figure 3-6. Field measurements and lab measurements (divided bar method) for thermal conductivity normal to bedding.

A large data set reported by Waples and Tirsgaarde (2002) is added to the data shown in Figure 3-7. This data was measured in the laboratory using the needle probe method.

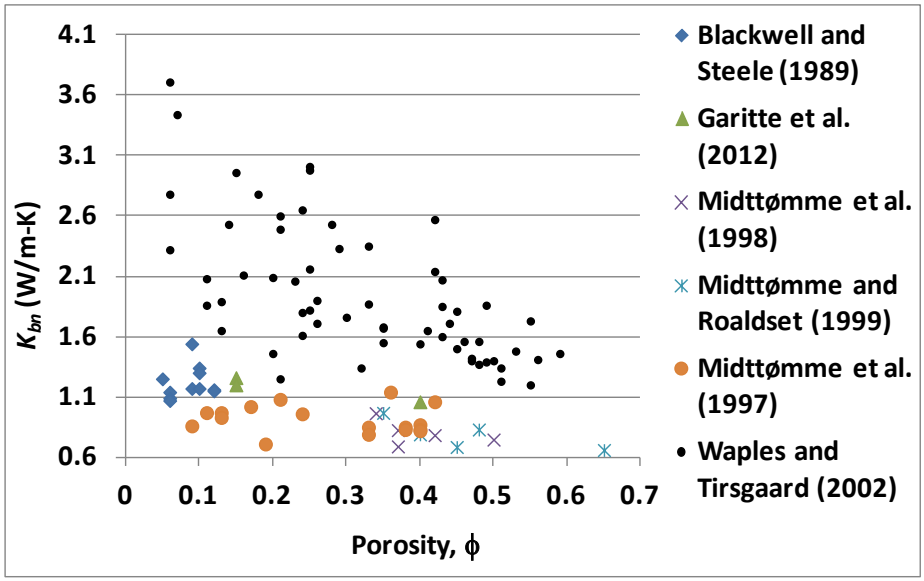

Figure 3-7. Field measurements and lab measurements (both divided bar and needle probe methods) for thermal conductivity normal to bedding.

The clear distinction between the measurements reported by Waples and Tirsgaarde (2002) and the other data sets is apparent. The needle probe measurements give values that are distinctly higher than the field measurements and the divided bar measurements at the same porosity, and lie considerably outside the scatter of these data (Midttømme et al., 1998). This difference caused by measurement methodology was investigated by Midttømme et al. (1999) and similar trends were found comparing needle probe measurements with divided bar measurements. Blackwell and Steele (1989) also comment on discrepancies between laboratory and field measurements of thermal conductivity. Given the differences between the needle probe measurements and other measurement techniques, the data from Waples and Tirsgaarde (2002) are not included in the development of a correlation.

Thermal conductivity studies conducted by Midttømme et al. (1997) found that thermal conductivity showed the strongest relationship with water content (or porosity) and a weaker relationship with mineral content (Midttømme et al., 1997). Three mixing models (arithmetic, geometric, and harmonic) for estimating thermal conductivity were investigated by Midttømme and Roaldset (1999); the best model was found to be the geometric mixing model:

$$K_{bn} = K_w^{\phi} K_g^{1-\phi} \tag{3-8}$$

where, K_{bn} is the bulk saturated rock thermal conductivity normal to bedding, K_w is the thermal conductivity of the pore fluid (water), K_g is the thermal conductivity of the solid, and ϕ is the porosity.

The approach for developing a thermal conductivity correlation is to take the logarithm of Equation (3-8) and average the quantity $\overline{\log(K_s)}$ for the data in Figure 3-6,

$$\overline{\log(K_g)} = \frac{\log(K_{bn}) - \phi \log(K_w)}{1-\phi} \tag{3-9}$$

The value of K_w is taken to be 0.6 W/m-K (Midttømme and Roaldset, 1999). A representative value for the thermal conductivity of the solid is $\overline{K_g} = 10^{\overline{\log(K_g)}}$, and is found to be $\overline{K_g} = 1.1$ W/m-K. Thermal conductivities are then computed from

$$K_{bn} = K_w^{\phi} \overline{K_g}^{1-\phi} \tag{3-10}$$

This correlation is shown in Figure 3-8. By using the correlation between porosity and sonic velocity in Dobson and Houseworth (2013), the thermal conductivity can also be computed from a measurement of the compressional seismic velocity. The root-mean square error (RMSE) for the correlation is 0.154 W/m-K.

The correlation for thermal conductivity parallel to bedding (K_{bp}) is computed using the same methodology for anisotropic materials as describe in Dobson and Houseworth (2013). The thermal conductivity normal to bedding is scaled by the velocity ratio (V_{pr}^{ω}) raised to the power ω. The velocity ratio is given by the sonic velocity parallel to bedding divided by the sonic velocity normal to bedding. If sonic velocity parallel to bedding is not available, a method to estimate this from the normal sonic velocity is described in Dobson and Houseworth (2013). The correlation equation is then,

$$K_{bp} = K_w^{\phi} \overline{K_g}^{1-\phi} V_{pr}^{\omega} \tag{3-11}$$

The power ω is determined by fitting the correlation to the thermal conductivity data parallel to bedding. Doing this gives a value of ω of 2.3.

This fit is shown in Figure 3-9 and has an RMSE of 0.215.

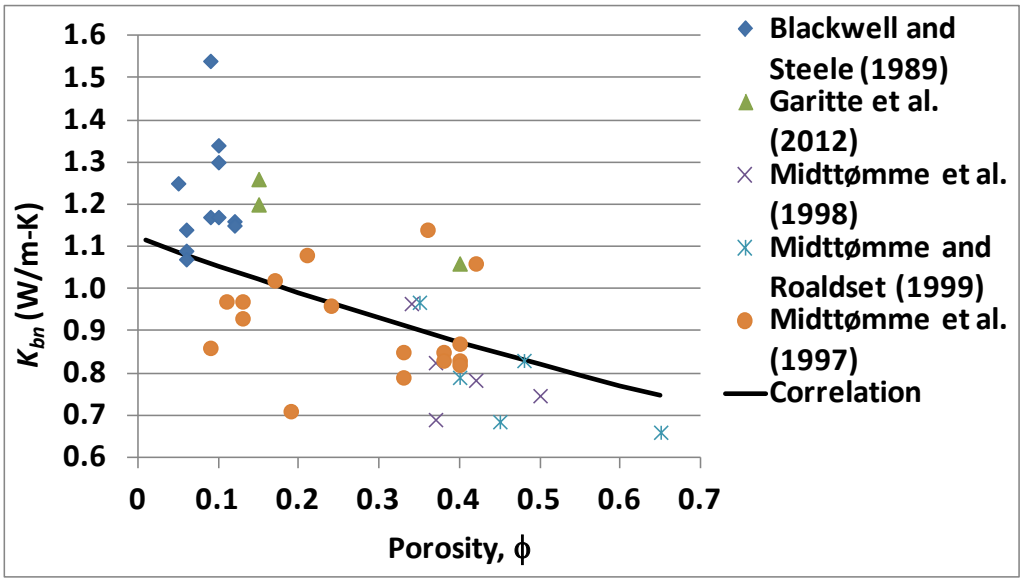

Figure 3-8. Thermal conductivity normal to bedding; data and correlation.

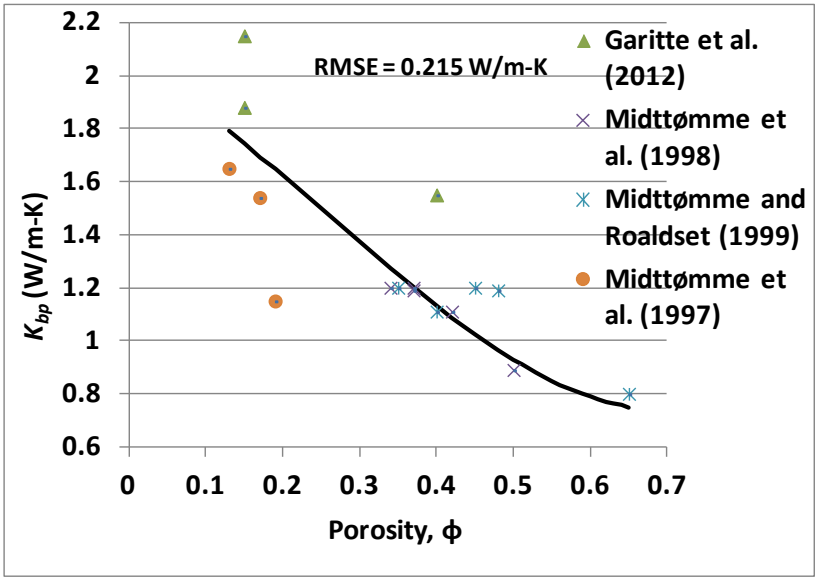

Figure 3-9. Thermal conductivity parallel to bedding; data and correlation.

For unsaturated systems, the thermal conductivity may be estimated from the following logical extensions of Equations (3-10) and (3-11):

$$K_{bn} = K_w^{S_w\phi} K_a^{(1-S_w)\phi} \overline{K_g}^{1-\phi} \tag{3-12}$$

$$K_{bp} = K_w^{S_w\phi} K_a^{(1-S_w)\phi} \overline{K_g}^{1-\phi} V_{pr}^{\omega} \tag{3-13}$$

where the fluid thermal conductivity raised to the power of the porosity, K_w^{ϕ}, has been replaced by the product of the thermal conductivity of water raised to the power of the water content, $K_w^{S_w\phi}$, times the thermal conductivity of air raised to the power of the air content, $K_a^{(1-S_w)\phi}$ in Equation (3-12). This reduces to K_w^{ϕ} when $S_w = 1$ where the fluid thermal conductivity is for water and reduces to K_a^{ϕ} when $S_w = 0$. Equation (3-13) is the expression in Equation (3-12) with the anisotropy factor, exactly as Equation (3-11) is formulated relative to Equation (3-10).

3.3.2 Specific Heat

The approach to estimate specific heat follows that of Goto and Matsubayashi (2009) in which the specific heat is computed from an arithmetic average of the rock and fluid components,

$$\rho_b c_b = \phi\rho_w c_w + (1-\phi)\rho_g c_g \tag{3-14}$$

where ρ_b is the bulk density of the saturated rock, ρ_w is the pore fluid density, and ρ_g is the grain density, c_b is the bulk specific heat of the saturated rock, c_w is the specific heat of the pore fluid (water), and c_g is the specific heat of the rock grains. The pore fluid is approximated as water with a density of 1000 kg/m^3 and the pore fluid specific heat is 4126 J/kg-C. As discussed in Section 3.3.1, the previous work of Dobson and Houseworth (2013) has defined a correlation between sonic velocity and porosity (ϕ). A

correlation was also defined for the saturated rock bulk density and sonic velocity. The grain density can then be computed given the porosity, bulk density, and pore fluid density. Therefore, all parameters in Equation (3-14) can be computed given the sonic velocity except for c_b and c_s. However, Waples and Waples (2004) have derived a correlation for the rock grain specific heat as a function of the grain density for low- and moderate-density mineral grains for the range of approximately 2000 to 4000 kg/m^3. This range is covers the range of grain densities encountered in shale and mudrocks. This correlation is given by,

$$\rho_g c_g = 1.0263 \times 10^{-6} \exp\left(0.0002697 \rho_g\right) \tag{3-15}$$

where ρ_g is in kg/m^3 and $\rho_g c_g$ is in J/m^3-K. The data and correlation function plot from Waples and Waples (2004) is given in Figure 3-10.

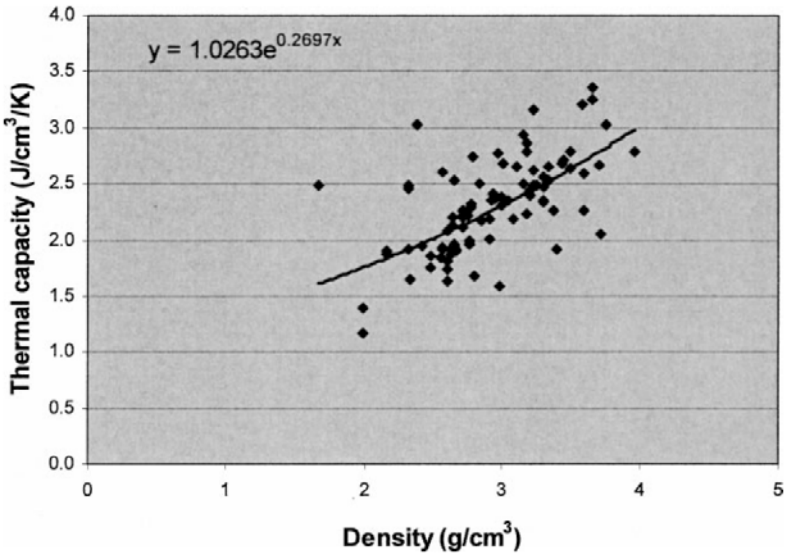

Figure 3-10. Data and correlation between rock grain volumetric specific heat and grain density (Waples and Waples 2004)

Using Equations (3-14) and (3-15) the value of the bulk specific heat of the saturated rock may be computed as a function of porosity. Lab and field measurements of specific heat on clay/shale rocks from the Opalinus Clay (Wileveau and Rothfuchs, 2007), Boom Clay (Li et al., 2007), Callovo-Oxfordian Clay (Delay et al., 2011), and Ypresian Clay (Piña-Diaz, 2011) are shown along with the correlation for specific heat as a function of porosity in Figure 3-11. The correlation is found to have an RMSE relative to the data of 186 J/kg-K. By using the correlation between porosity and sonic velocity in Dobson and Houseworth (2013), the specific heat can also be computed from a measurement of the compressional seismic velocity.

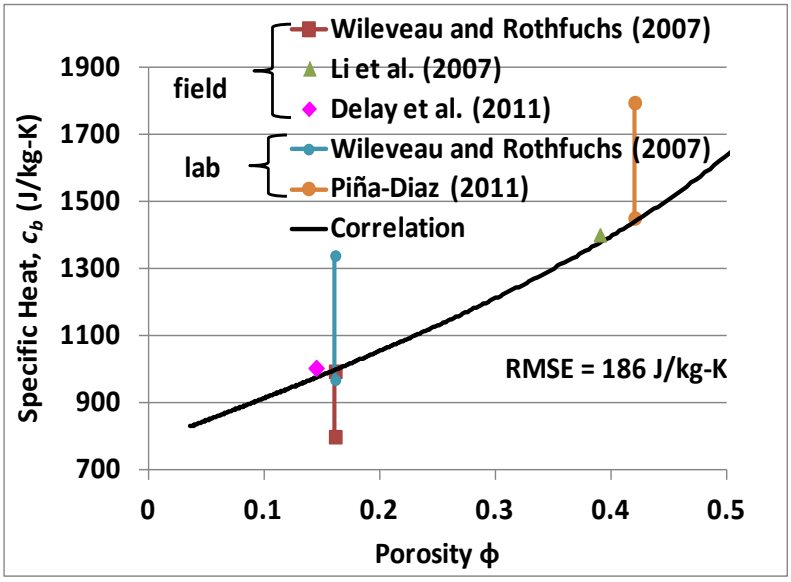

Figure 3-11. Bulk rock specific heat correlation with lab and field data.

The extension of Equation (3-14) for unsaturated conditions is,

$$\rho_b c_b = \phi S_w \rho_w c_w + \phi(1 - S_w)\rho_a c_a + (1 - \phi)\rho_g c_g \tag{3-16}$$

where ρ_w and ρ_a are the water and air mass densities and c_w and c_a are the water and air specific heat capacities.

3.4 ESTIMATING TWO-PHASE FLOW PARAMETERS

Two-phase flow processes are of interest for radioactive waste disposal in shale primarily because of the introduction of a gas phase into a water-saturated shale environment during ventilation for repository construction and waste emplacement. Repository heating may also result in the generation of a gaseous phase of H_2O (steam). The introduction of a second immiscible phase results in a phase pressure difference, or capillary pressure, between the gas and liquid phases. Capillary pressure is an additional driving force for flow processes. The presence of two phases also reduces the effective permeability of each phase relative to the intrinsic (phase-saturated) permeability. This reduction is typically represented as a relative permeability, which is the ratio of the effective permeability divided by the intrinsic permeability. Both capillary pressure and relative permeability are functions of phase saturation.

There are a number of models for representing capillary pressure and relative permeability for two-phase systems as functions of saturation. A model that has been widely used for soil systems was developed by van Genuchten (1980). This model uses two independent parameters to describe the capillary pressure parameter function of saturation. The relative permeability parameter function does not introduce any further parameters, as it is derived from the capillary pressure parameter function. The expressions for capillary pressure and relative permeability are:

$$P_c(S_{wn}) = \frac{1}{\alpha}\left\{S_{wn}^{-\frac{1}{m}} - 1\right\}^{1-m} \tag{3-17}$$

$$k_{rw}(S_{wn}) = S_{wn}^{\frac{1}{2}}\left\{1-\left(1-S_{wn}^{\frac{1}{m}}\right)^{m}\right\}^{2} \quad (3\text{-}18)$$

Where P_c is the capillary pressure, S_{wn} is the normalized water saturation, k_{rw} is the dimensionless relative permeability to water, α is a parameter (with units of inverse pressure) referred to as capillary strength, and m is a dimensionless parameter referred to as the pore-size distribution index. The normalized water saturation is given by

$$S_{wn} = \frac{S_w - S_{wr}}{S_{wm} - S_{wr}} \quad (3\text{-}19)$$

where S_{wr} is the residual water saturation at which water ceases to flow, S_{wm} is the maximum water saturation at which gas ceases to flow, and S_w is the physical water saturation (fraction of pore space occupied by water).

The relative permeability parameter function for the gas phase (k_{rg}) also needs to be specified for a two-phase flow model. Charlier et al. (2013) was able to approximate experimental data for gas relative permeability in the Callovo-Oxfordian Clay using the following cubic function (Figure 3-12),

$$k_{rg}(S_{wn}) = (1 - S_{wn})^3 \quad (3\text{-}20)$$

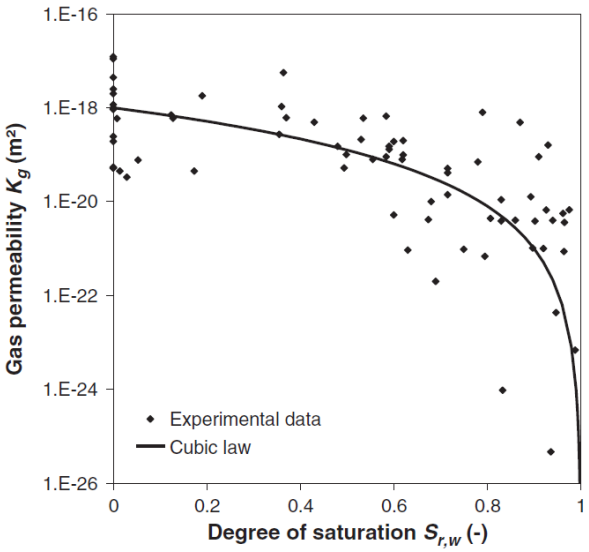

Figure 3-12. Gas relative permeability data and model for the Callovo-Oxfordian Clay (Charlier et al., 2013)

3.4.1 Estimating van Genuchten α

Thomas et al. (1968) investigated the relationship between the threshold (or air entry) pressure and permeability. The air entry pressure is the pressure required for air to enter and start flowing in a water-saturated system. Although the study was not specifically for shale or mudstone, it did involve low-permeability rocks down to microdarcy levels. The correlation is given in Equation (3-21) and shown in Figure 3-13.

$$P_T = 7.37k^{-0.43} \quad (3\text{-}21)$$

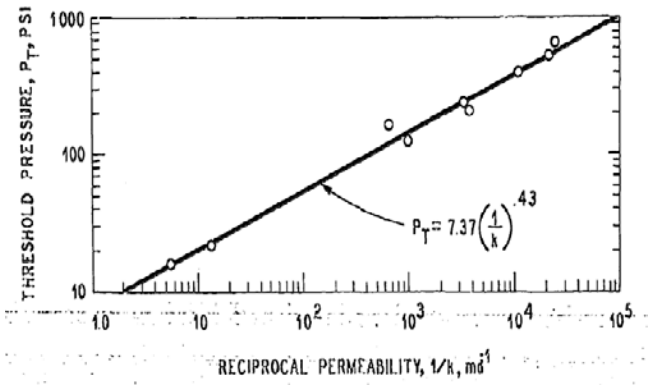

Figure 3-13. Threshold pressure permeability correlation (Thomas et al., 1968)

where P_T is the air entry pressure in pounds per square inch (psi) and k is the intrinsic permeability in millidarcies (md). This relationship is supported by more recent evidence for clay and shale rock types as shown in Figure 3-14. A comparison between Equation (3-21) and the Davies (1991) shale model shown in Figure 3-14 is given in Figure 3-15. The difference in the models is not considered significant in comparison with the data shown in Figure 3-14.

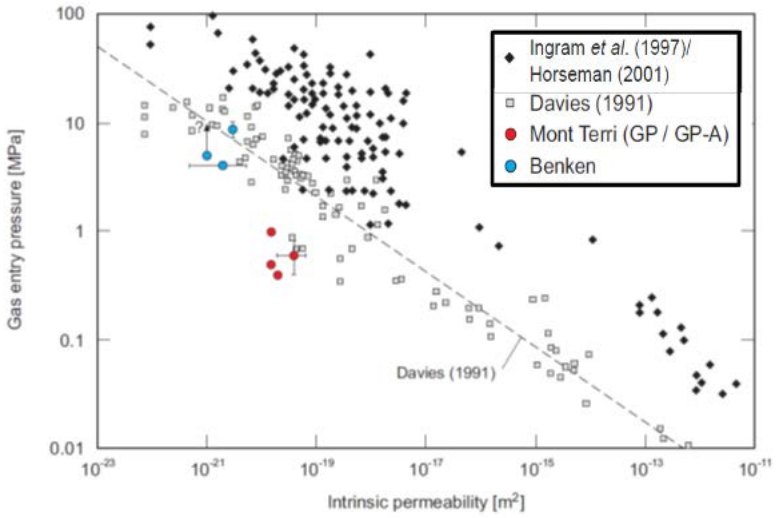

Figure 3-14. Data and correlation between permeability and gas entry pressure (Johnson et al., 2004; Marschall et al., 2005).

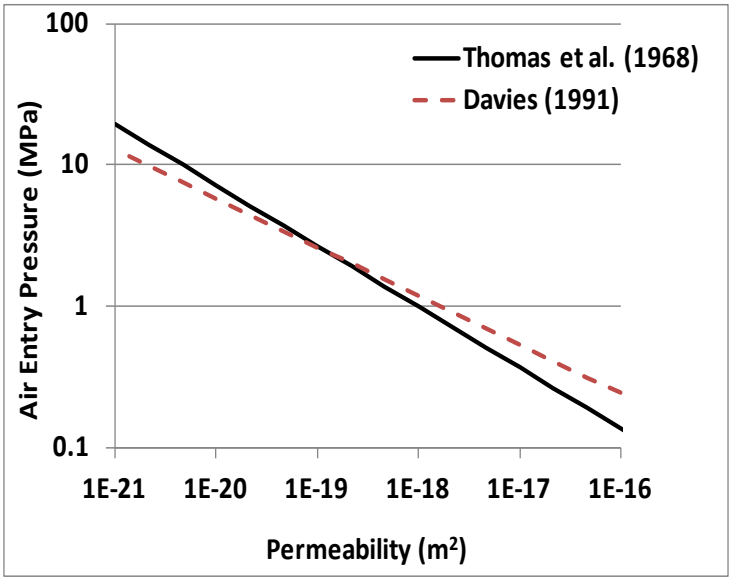

Figure 3-15. Comparison of correlations for air entry pressure as a function of permeability.

A relationship between the air entry pressure and capillary strength was found by Tinjum et al. (1997) to be,

$$\alpha = 0.78 P_T^{-1.26} \tag{3-22}$$

where P_T is expressed in kPa (instead of psi as used for P_T in Equation (3-21)) and α is given in kPa^{-1}. The correlation found by Tinjum et al. (1997) is shown in Figure 3-16.

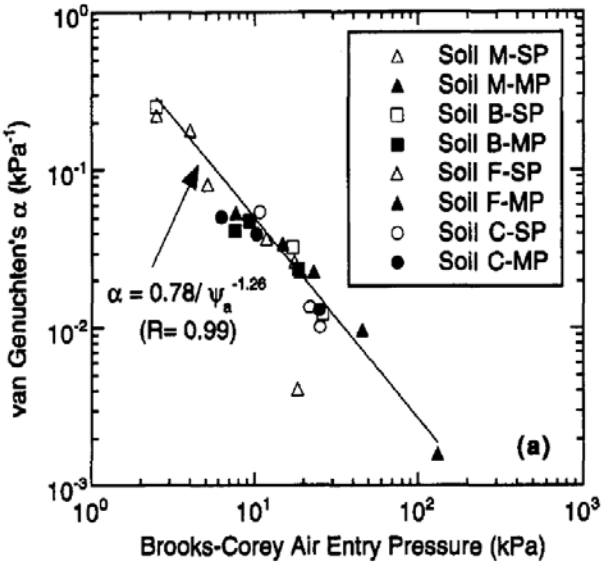

Figure 3-16. Correlation for soils between van Genuchten α and air entry pressure (Tinjum et al., 1997).

The Tinjum et al. (1997) correlation is for soils and does not cover the parameter space for typical claystones and shales investigated here, where air-entry pressures are generally on the order of 1 MPa or more. Therefore, this type of relationship was calibrated to the few clay-shale data points available shown in Figure 3-17. In this figure, the air-entry pressure was computed from Equation (3-21) using the known permeability and plotted against the van Genuchten α. For anisotropic materials, the geometric mean permeability between bedding normal and bedding parallel permeability values was used.

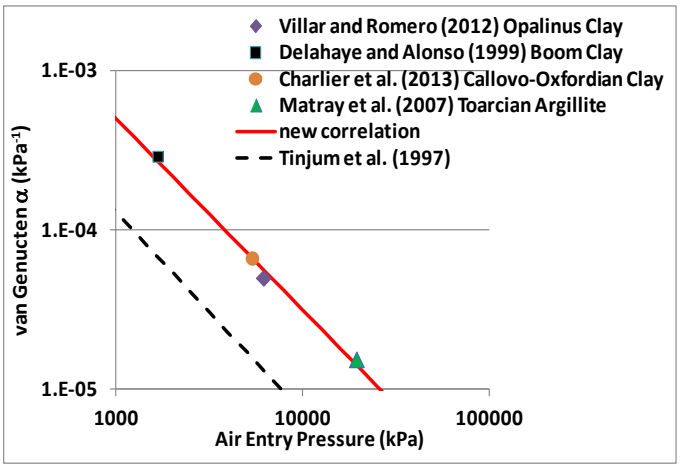

Figure 3-17. Correlation and data for van Genucten α as a function of air-entry pressure for shales and claystones compared with Tinjum et al. (1997) correlation for soils.

The new correlation lies above the Tinjum et al. (1997) correlation with nearly the same slope. The correlation equation is,

$$\alpha = 2.01 P_T^{-1.20} \qquad (3\text{-}23)$$

where, as for Equation (3-22), P_T is expressed in kPa (instead of psi as used for P_T in Equation (3-21)) and α is given in kPa^{-1}.The correlation has a root-mean square error (RMSE) of 0.034 for $\log(\alpha)$ (in kPa), or a factor of 1.08 on α. Using Equations (3-21) and (3-23), an estimate of capillary strength α can be made given the intrinsic permeability. The intrinsic permeability can be estimated from seismic velocity as described in Dobson and Houseworth (2013). Therefore, α may be estimated from the seismic velocity.

3.4.2 Estimating van Genuchten m

As for van Genuchten α, there is very little data available for the van Genuchten pore-size distribution index m for shales and claystones. The limited data available has been plotted in Figure 3-17 against permeability. These data are for m as used in a drainage (or desaturation) capillary pressure curve. In some cases, measurements found distinctions for the value of m were found for relative permeability and for imbibition processes (see references listed in Figure 3-18). Figure 3-18 shows a trend of decreasing values of m with increasing permeability. The correlation is given in Equation (3-24), which has an RMSE of 0.053. An error function model was used to ensure that m does not go beyond the limits of 0 and 1 at low and high permeabilities, respectively. By using the relationship between the seismic velocity and permeability in Dobson and Houseworth (2013), an estimate of m may be made from the seismic velocity.

$$m = 0.5 - 0.5\text{erf}\left\{\frac{\log(k) + 20.34}{3.94}\right\} \quad (3\text{-}24)$$

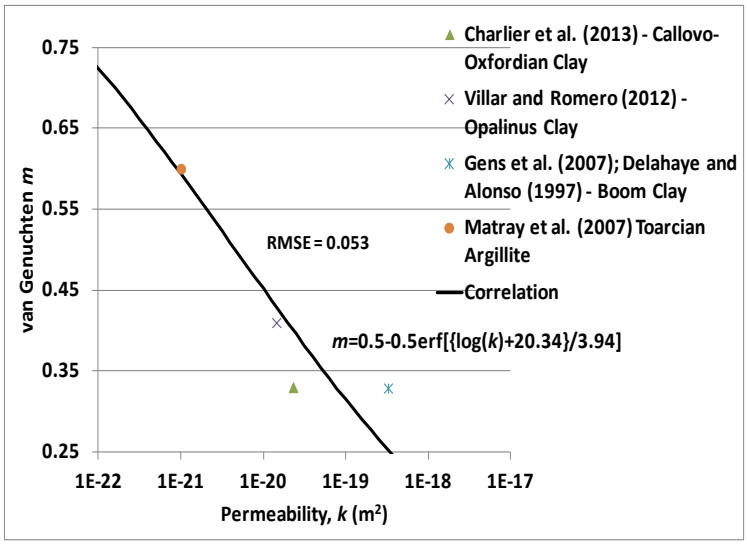

Figure 3-18. Correlation of the van Genucten pore-size distribution index with permeability.

3.4.3 Estimating Residual Saturations

Estimates of the residual saturations (S_{wr} and S_{wm}) are needed for the van Genuchten parameter functions describing capillary pressure and water relative permeability. They are also needed for the Corey parameter function for gas relative permeability. However, very little direct information from shales and mudrocks are available for determining these parameters. A number of relationships relating porosity, permeability and residual water saturation are presented by Alavi et al. (2014). However, these were developed for sandstones and do not give reasonable results for clay/shale rock types. The existence of a residual wetting-phase saturation for a drainage process has been questioned for water-wet materials (such as organic-poor clays and shales) because water maintains hydraulic continuity within the porous material as films on the grain surfaces down to very low water saturations (Dullien et al., 1986). This is particularly true for water-gas fluid systems because gases are typically strongly non-wetting relative to water on mineral surfaces. Therefore, a value of $S_{wr} = 0$ is suggested if no additional site-specific information is available. The maximum wetting phase saturation, S_{wm}, has traditionally been taken to be 1 for the van Genuchten formulation. The maximum wetting-phase saturation corresponds to the residual non-wetting phase saturation for two-phase systems, i.e., $S_{wm} = 1 - S_{gr}$, where S_{gr} is the residual gas saturation. Although a value of $S_{wm} = 1$ (or $S_{gr} = 0$) is true for primary drainage in which gas displaces water from a water-saturated system, this is not the case for imbibition in which water displaces gas. The existence of a residual non-wetting phase saturation for imbibition processes has been well established (e.g., Chatzis et al., 1988). However, because of a lack of data on residual gas saturations for clays and shales, a value of $S_{wm} = 1$ is recommended if site-specific information is not available. For the Opalinus Clay, Marschall et al. (2005) cite the following ranges: $0 \leq S_{wr} \leq 0.5$ and $0 \leq S_{gr} \leq 0.05$.

3.5 APPLICATION TO US SHALE FORMATIONS

Given the changes and additions of property estimates introduced here, the application of the correlations to US Shale Formations has been revised from that given in Section 3.3 of Dobson and Houseworth (2013). Figure 3-19 shows the location of formations evaluated.

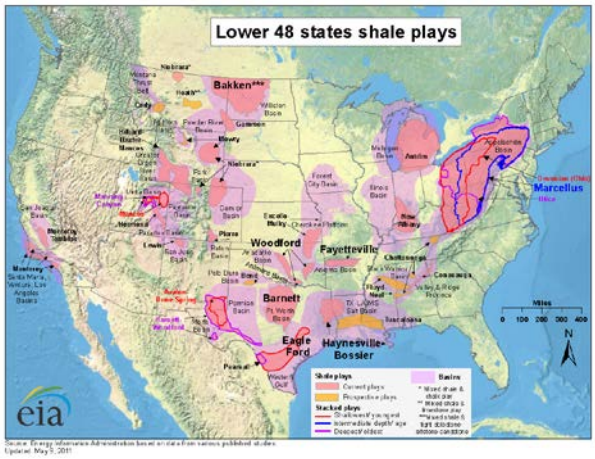

Figure 3-19. Map of U.S. shale gas and shale oil plays (EIA, 2011b).

The correlation inputs are the normal and parallel sonic velocities and an average formation depth. As for the development of correlations described in Section 3.2, if the velocity parallel to bedding is not available, it is estimated using the velocity ratio correlation given by Equation (3-1). Table 3-1 (Dobson and Houseworth, 2013) gives the requisite inputs for the formations, which are the sonic velocity normal to bedding (V_{pn}), the sonic velocity perpendicular to bedding (V_{pp})(where available) and the formation depth (D). The formation water density is also an input, however, for the current analysis, a fresh water density of 1000 kg/m^3 was assumed.

Table 3-1. Inputs for Properties Estimation.

Formation	V_{pn} (m/s)	V_{pp} (m/s)	D (m)
Barnett Shale	4031[(1)]	NA	1000[(2)]
Haynesville Shale	3628[(1)]	NA	3000[(3)]
Pierre Shale (1)	2164[(4)]	2243[(4)]	152[(4)]
Pierre Shale (2)	3140[(5)]	3768[(5)]	1520[(5)]
New Albany Shale	3600[(6)]	4500[(6)]	520[(7)]
Antrim Shale	3174[(8)]	4057[(8)]	328[(8)]
Eagle Ford Shale	4016[(9)]	4083[(9)]	3234[(9)]
Marcellus Shale	3500[(10)]	NA	1920[(10)]
Woodford Shale	4008[(11)]	NA	1220[(11)]
Monterey Shale	4844[(12)]	5310[(12)]	2.7[(12)]

Sources: [(1)] Montaut (2012); [(2)] Bruner and Smosna (2011); [(3)] Nunn (2012); [(4)] McDonal et al. (1958); [(5)] Tosaya (1982); [(6)] Johnston and Christensen (1995); [(7)] CNX/GTI (2008); [(8)] Liu (1997); [(9)] Sondhi (2011); [(10)] Hardage et al. (2013); [(11)] Verma et al. (2013); [(12)] Liu (1994)

3.5.1 Correlations Results

With the sonic velocities from Section 3.3.1, the correlations from Section 3.2 may be used to compute thermal, hydrological, and geomechanical parameters. These results are shown in Table 3-2. Outputs shaded in blue are rock parameters, while outputs shaded in rose are formation conditions (e.g., effective stress, brittleness index, and overconsolidation ratio) that lead to the estimation of pore pressure. The new correlation for this table that supersedes Dobson and Houseworth (2013) is for clay content. New correlations here, beyond those documented in Dobson and Houseworth (2013), are for thermal conductivity (both normal and parallel to bedding), specific heat, and two-phase flow parameters, van Genuchten capillary strength (α) and van Genuchten pore-size distribution index (m).

Table 3-2. Estimated Parameters Using Seismic Velocity Correlations.

Parameters	Barnett Shale	Haynesville Shale	Pierre Shale (1)	Pierre Shale (2)	New Albany Shale
Inputs (from Table 3-1)					
V_{pn} (m/s)	4031	3628	2164	3140	3600
V_{pp} (m/s)	NA	NA	2243	NA	4500
D(m)	1000	3000	152	1524	518
Outputs					
V_{pp} (m/s)	5226	4665	2530	3975	4626
ϕ	0.056	0.087	0.36	0.14	0.094
e	0.060	0.095	0.56	0.16	0.103
ρ_b (kg/m^3)	2640	2590	2220	2520	2580
ρ_{bd} (kg/m^3)	2580	2500	1860	2380	2490
ρ_g (kg/m^3)	2740	2740	2890	2760	2740
X (fraction)	0.48	0.50	0.60	0.52	0.50
k_n(m^2)	6.1E-22	1.3E-21	7.4E-20	3.2E-21	1.4E-21
k_p(m^2)	1.8E-21	3.5E-21	8.6E-20	8.5E-21	3.6E-21
UCS (MPa)	43	31	5.9	21	29
E_n (GPa)	8.1	6.1	0.70	4.1	5.8
E_p (GPa)	23	17	0.81	10.6	14
G (GPa)	3.2	2.5	0.29	1.7	2.4
υ	0.13	0.17	0.39	0.22	0.18
c_n (MPa)	7.9	5.3	0.66	3.2	4.9
c_p (MPa)	20	12.8	0.7	7.4	11
φ (degrees)	24	23	21	23	23
τ_n (MPa)	2.7	1.9	0.24	1.1	1.7
τ_p (MPa)	6.4	4.3	0.27	2.5	3.6
K_{bn} (W/m-K)	0.98	0.96	0.86	0.94	0.96
K_{bp} (W/m-K)	1.78	1.72	0.94	1.62	1.61
c_b (J/kg-K)	856	896	1316	966	905
α (MPa^{-1})	1.47E-02	2.12E-02	1.38E-01	3.40E-02	2.21E-02
m	0.59	0.55	0.33	0.49	0.54
σ'_v (MPa)	47	41	9.3	32	40
σ_{NC} (MPa)	16	47	1.8	23	8.0
UCS$_{NC}$ (MPa)	8.0	23	0.9	11	4.0
BRI	5.3	1.3	6.5	1.8	7.3
OCR	3.2	1.2	3.7	1.5	4.0
σ_{pd} (MPa)	15	33	2.5	21	10
p (MPa)	11	43	0.79	17	3
p_{hs} (MPa)	9.8	29	1.5	15	5.1
p_{op} (MPa)	1.41	13	-0.70	1.9	-1.8

Table 3-2 (continued). Estimated Parameters Using Seismic Velocity Correlations.

Parameters	Antrim Shale	Eagle Ford Shale	Marcellus Shale	Woodford Shale	Monterey Shale
Inputs (from Table 3-1)					
V_{pn} (m/s)	3174	4016	3500	4008	4844
V_{pp} (m/s)	4057	4843	NA	NA	5310
D(m)	328	3234	1920	1219	2.7
Outputs					
V_{pp} (m/s)	4024	5206	4485	5195	6339
ϕ	0.13	0.067	0.10	0.058	0.033
e	0.15	0.071	0.11	0.061	0.035
ρ_b (kg/m^3)	2530	2620	2570	2640	2680
ρ_{bd} (kg/m^3)	2390	2550	2470	2580	2650
ρ_g (kg/m^3)	2760	2740	2740	2740	2740
X (fraction)	0.52	0.49	0.50	0.48	0.46
k_n(m^2)	2.9E-21	8.0E-22	1.6E-21	6.3E-22	3.0E-22
k_p(m^2)	8.1E-21	1.7E-21	4.4E-21	1.8E-21	4.4E-22
UCS (MPa)	22	38	28	42	60
E_n (GPa)	4.3	7.3	5.6	7.9	10.4
E_p (GPa)	11	15	15	22	15
G (GPa)	1.8	2.9	2.3	3.1	3.9
υ	0.22	0.14	0.18	0.13	0.094
c_n (MPa)	3.4	6.8	4.7	7.7	12
c_p (MPa)	8.0	13	11.1	19	17
φ (degrees)	23	23	23	24	24
τ_n (MPa)	1.2	2.4	1.6	2.7	4.1
τ_p (MPa)	2.7	4.4	3.7	6.3	5.6
K_{bn} (W/m-K)	0.95	0.97	0.96	0.98	0.99
K_{bp} (W/m-K)	1.66	1.50	1.70	1.77	1.22
c_b (J/kg-K)	958	870	912	858	826
α (MPa^{-1})	3.27E-02	1.57E-02	2.39E-02	1.50E-02	8.54E-03
m	0.50	0.58	0.53	0.59	0.65
σ'_v (MPa)	33	45	39	47	53
σ_{NC} (MPa)	4.9	51	30	20	0.045
UCS_{NC} (MPa)	2.5	26	15	9.8	0.023
BRI	8.9	1.5	1.9	4.3	2700
OCR	4.6	1.3	1.6	2.8	250.0
σ_{pd} (MPa)	7	34	25	17	0.21
p (MPa)	1.01	49	24	15	-0.14
p_{hs} (MPa)	3.2	32	19	12	0.027
p_{op} (MPa)	-2.2	17	5.0	2.6	-0.17

V_{pn}: compressional sonic velocity normal to bedding; V_{pp}: compressional sonic velocity parallel to bedding; D: present-day formation depth; ϕ: porosity; e: void ratio; ρ_b: brine-saturated bulk density; ρ_{bd}: dry bulk density; ρ_g: grain density; X: mass fraction of clay minerals; k_n: brine permeability normal to bedding; k_p: brine permeability parallel to bedding; UCS: uniaxial compressive strength normal to bedding; E_n: Young's modulus normal to bedding; E_p: Young's modulus parallel to bedding; G: shear modulus normal to bedding; υ: Poisson's ratio (isotropic); c_n: cohesive strength normal to bedding; c_p: cohesive strength parallel to bedding; φ: friction angle (isotropic); τ_n: tensile strength normal to bedding; τ_p: tensile strength parallel to bedding; K_{bn}: thermal conductivity of water-saturated rock normal to bedding; K_{bp}: thermal conductivity of water-saturated rock parallel to bedding; c_b: specific heat capacity of water-saturated rock; α: van Genuchten capillary strength parameter for capillary pressure parameter function; m: van Genuchten pore-size distribution index for capillary pressure and relative permeability parameter functions; σ_v': maximum effective stress experienced by the formation; σ_{NC}: effective stress at the present-day depth for normal consolidation at hydrostatic pore pressure; $\mathrm{UCS_{NC}}$: uniaxial compressive strength for normal consolidation at present-day depth; BRI: brittleness index; OCR: overconsolidation ratio; σ_{pd}: present-day effective stress; p: present-day pore-fluid pressure; p_{hs}: hydrostatic pressure at present-day depth; p_{op}: pore-fluid overpressure (or underpressure if negative) $(p - p_{hs})$.

3.6 CONCLUSIONS

Correlations for estimating hydrological and geomechanical formation properties and in-situ conditions from sonic velocities have been developed from data on shale formations that lie outside the United States. These correlations have been applied to estimate properties for several large shale formations in the United States. The advantage of using correlations based on sonic velocity is that properties can be estimated from geophysical logs. This information is often more readily available and in greater quantity than direct property measurements on core that would otherwise be required. Furthermore, geophysical logs provide a continuous readout along wells that can be more readily used to characterize spatial variability in properties.

Previous work (Dobson and Houseworth, 2013) found that several properties (porosity, bulk density, clay content, permeability, uniaxial compressive strength, Young's modulus, shear modulus, Poisson's ratio, cohesive strength, friction angle, and tensile strength) could be correlated with the compressive seismic velocity. In addition, the in-situ conditions for effective stress, overconsolidation ratio, and pore pressure could also be linked to the compressive seismic velocity. The work presented here extends and enhances the correlations developed in Dobson and Houseworth (2013). A study reported by Cosenza et al. (2014) for the Callovo-Oxfordian Clay lends support to the use of seismic velocity correlations for estimating clay content. However the correlations developed by Dobson and Houseworth (2013) differ significantly from the correlation proposed by Cosenza et al. (2014) in terms of quantitative estimates of clay content. These differences remain unresolved.

Correlations for thermal conductivity (including anisotropic effects) and specific heat have been developed based on traditional models representing mixtures of rock grains and pore fluids. The mixing models are based on geometric averaging for thermal conductivity and arithmetic averaging for specific heat. The literature on thermal conductivity measurements indicates that some measurement bias may be present in certain types of thermal conductivity measurements. The data that best represent the physical system have been evaluated and selected for use in the development of the correlation.

Correlations for two-phase flow properties have been developed in terms of the van Genuchten two-phase flow parameters for capillary strength (α) and pore-size distribution index (m). The correlation for van Genuchten capillary strength is based on data that relate permeability to air entry pressure along with data linking air-entry pressure to the capillary strength parameter. Similar correlations have been commonly used for applications to soils and have been extended here for claystones and shales. A similar approach has been used for the pore-size distribution index in that the parameter is correlated with permeability.

The correlations require additional development and verification. In particular, the correlations for the van Genuchten two-phase flow parameters require additional data. Further verification is also needed for many of the parameter estimates in Table 3-2; therefore, they should be viewed as initial estimates.

4. ACKNOWLEDGMENTS

Funding for this work was provided by the Used Fuel Disposition Campaign, Office of Nuclear Energy, of the U.S. Department of Energy under Contract Number DE-AC02-05CH11231 with Berkeley Lab.

From Lawrence Berkeley National Laboratory, Curt Oldenburg reviewed this report and his feedback was greatly appreciated. Editorial assistance was also provided by Helen Prieto and Peter Persoff.

Section 2 of this report represents a major collaborative effort with Frank Perry and Rick Kelley of Los Alamos National Laboratory (LANL). They have scanned and generated GIS data from pdf versions of isopach and structure maps, and have uploaded existing GIS data into their database. They used the resulting GIS data to create contoured structure and isopach maps.

In addition, many individuals generously shared their knowledge and data to help populate the GIS database described in Section 2. Steve Ruppel and Cari Breton of the University of Texas, Bureau of Economic Geology, provided us with their GIS dataset for the Woodford Shale in the Permian Basin. John Bocan, with the West Virginia Geological and Economic Survey, provided us with GIS data for the Utica Shale that had been developed by the Trenton-Black River Research Consortium. Jim McDonald of the Ohio Department of Natural Resources shared with us a regional GIS dataset for the Marcellus Shale. Christopher Korose of the Illinois State Geological Survey provided us with GIS data for the New Albany Shale that was developed by the Illinois Basin Consortium. Jeff Zimmerman of the Susquehanna River Basin Commission provided us with some USGS GIS data for the Utica and Marcellus Shales. David Effert of the Louisiana Department of Natural Resources gave us access to GIS data for the Haynesville Shale. Brian Cardott of the Oklahoma Geological Survey provided us with additional references on the Woodford Shale and Sue Palmer (also of the Oklahoma Geological Survey) provided us with pdf copies of plates depicting the thickness and depth of the Woodford Shale in the Anadarko Basin. Sue Hovorka of the University of Texas, Bureau of Economic Geology, pointed us towards a study conducted by the Gulf Coast Carbon Center, which contains abundant information regarding seals (i.e., shales) in many sedimentary basins in the US. Prof. James Wood (Michigan Tech) provided us with a copy of his digital dataset for the Antrim Shale in the Michigan Basin. Julie LeFever (North Dakota Geological Survey) shared her GIS data for the Bakken Formation. Sam Limerick helped us track down the source files for the EIA shale play maps, and Jack Perrin and Meg Coleman (US EIA) generously provided us with the associated GIS data. Don Sweetkind (USGS) shared the GIS data associated with his reports on the Monterey Formation in the Cuyama and Santa Maria Basins. Many thanks for all of their contributions.

5. REFERENCES

Agrawal, A., 2009. A technical and economic study of completion techniques in five emerging U.S. gas shale plays. M.S. thesis, Texas A&M University, 135 p.

Alavi, M.F., Alavi, M.F., Alavi, M.F. (2014). Determination of Relative Permeability Based on Irreducible Water Saturation and Porosity from Log Data and Flow Zone Indicator (FZI) from Core Data, International Petroleum Technology Conference, Doha, Qatar, January 20-22, 2014, 18 p.

Amsden, T.W., 1975. Hunton Group (Late Ordovician, Silurian, and Early Devonian) in the Anadarko Basin of Oklahoma. Oklahoma Geological Survey Bulletin 121, 214 p.

Amsden, T.W., 1980. Hunton Group (Late Ordovician, Silurian, and Early Devonian) in the Arkoma Basin of Oklahoma. Oklahoma Geological Survey Bulletin 129, 136 p.

Anna, L.O., 2009. Geologic assessment of undiscovered oil and gas in the Powder River Basin Province: U.S. Geological Survey Digital Data Series DDS-69-U, 93 p.

Blackford, M.A., 2007. Electrostratigraphy, thickness, and petrophysical evaluation of the Woodford Shale, Arkoma Basin, Oklahoma. Master's thesis, Oklahoma State University, 84 p.

Blackwell, D.D., Steele, J.L., (1989). Heat Flow and Geothermal Potential of Kansas, in Geophysics in Kansas: Kansas Geological Survey, Bulletin 226, Steeples, D.W. (ed), pp. 267-295.

Boulanouar, A., Rahmouni, A., Boukalouch, M., Samaouali, A., Géraud, Y., Harnafi, M., Sebbani, J. (2013). Determination of Thermal Conductivity and Porosity of Building Stone from Ultrasonic Velocity Measurements, Geomaterials, 2013, 3, pp. 138-144.

Bristol, H.M., and Buschbach, T.C., 1973. Ordovician Galena Group (Trenton) of Illinois - Structure and oil fields. Illinois State Geological Survey, Illinois Petroleum 99, 38 p.

Broadhead, R.F., 2010. The Woodford Shale in southeastern New Mexico: distribution and source rock characteristics. New Mexico Geology, v. 32, pp. 79-90.

Broadhead, R.F., and Gillard, L., 2007. The Barnett shale in southeastern New Mexico: Distribution, thickness, and source rock characterization. New Mexico Bureau of Geology and Mineral Resources, Open-File Report 502, 56 p.

Bruner, K.R., and Smosna, R., 2011. A comparative study of the Mississippian Barnett Shale, Fort Worth Basin, and Devonian Marcellus Shale, Appalachian Basin. National Energy Technology Laboratory Report, DOE/NETL-2011/1478.

Cardott, B.J., 2012. Thermal maturity of Woodford Shale gas and oil plays, Oklahoma, USA, International Journal of Coal Geology, doi:10.1016/j.coal.2012.06.004

Cardott, B.J., and Lambert, M.W., 1985. Thermal maturation by vitrinite reflectance of Woodford Shale, Anadarko Basin, Oklahoma. American Association of Petroleum Geologists Bulletin, v. 69, pp. 1982-1998.

Carlson, C.G., 1982. Structure map on top of the Cretaceous Pierre Formation in North Dakota. North Dakota Geological Survey, Miscellaneous Map No. 23.

Castagna, J.P., Batzle, M.L., Eastwood, R.L. (1985). Relationships Between Compressional-Wave and Shear-Wave Velocities in Elastic Silicate Rocks, Geophysics Vol. 50, No. 4, pp. 571-581.

Catacosinos, P.A., and Daniels, P.A., Jr., 1991, Stratigraphy of middle Proterozoic to Middle Ordovician formations of the Michigan basin. Geological Society of America Special Paper 256, pp. 53-72.

Catacosinos, P.A., Harrison, W.B., III, and Daniels, P.A., Jr., 1991. Structure, stratigraphy, and petroleum geology of the Michigan Basin, Chapter 30, in Leighton, M.W., Kolata D.R., Oltz, D.F., and Eidel,

J.J., eds., Interior cratonic basins: American Association of Petroleum Geologists Memoir 51, pp. 561-601.

Charlier, R., Collin, F., Pardoen, B., Talandier, J., Radu J.-P., Gerard, P. (2013). An Unsaturated Hydro-Mechanical Modelling of Two In-Situ Experiments in Callovo-Oxfordian Argillite, Engineering Geology, 165, pp. 46–63.

Chatzis, I., Kuntamukkula, M.S., Morrow, N.R. (1988). Effect of Capillary Number on the Microstructure of Residual Oil in Strongly Water-Wet Sandstones, SPE Reservoir Engineering, pp. 902-912.

CNX/GTI (2008). New Albany Shale RVSP, New Albany Shale Gas Project, RVSP Seismic Project Report.

Coleman, J.L, Jr., and Cahan, S.M., 2012. Preliminary catalog of the sedimentary basins of the United States. U.S. Geological Survey Open-File Report 2012-1111, 27 p.

Collinson, C., Sargent, M. L., and Jennings, J. R., 1988, Chapter 14: Illinois Basin region, in Sloss, L. L., ed., The Geology of North America, v. D-2, Sedimentary Cover-North American Craton: U.S.: Decade of North American Geology: Geological Society of America, pp. 383-426.

Comer, J.B., 1991. Stratigraphic analysis of the Upper Devonian Woodford Formation Permian Basin West Texas and Southeastern New Mexico. The University of Texas at Austin, Bureau of Economic Geology Report of Investigations No. 201, 63 p.

Condon, S.M., 2000. Stratigraphic framework of Lower and Upper Cretaceous rocks in central and eastern Montana. U.S Geological Survey Digital Data Series DDS-57, 12 p, 23 plates.

Cosenza, P., Robinet, J.C., Prêt, D., Huret, E., Fleury, M., Géraud, Y., Lebon, P., Villiéras, F., Zamora, M. (2014). Indirect Estimation of the Clay Content of Clay-Rocks Using Acoustic Measurements: New Insights from the Montiers-Sur-Saulx Deep Borehole (Meuse, France), Marine and Petroleum Geology, 53, pp. 117-132.

Cuadros, J., 2008. Clay as sealing material in nuclear waste repositories. Geology Today, v. 24, p. 99-103.

Davies, P.B. (1991). Evaluation of the Role of Threshold Pressure in Controlling Flow of Waste-Generated Gas into Bedded Salt at the Waste Isolation Pilot Plant, Sandia Report, SAND90–3246, UC–721, 44 p.

Dechesne, M., Raynolds, R.G., Barkmann, P.E., and Johnson, K.R., 2011. Notes on the Denver Basin geologic maps: Bedrock geology, structure, and isopach maps of the Upper Cretaceous to Paleogene strata between Greeley and Colorado Springs, Colorado. Colorado Geological Survey, 35 p.

Delahaye, C.H., Alonso, E.E. (1999). Modeling of Gas Migration in Clay, MECOM 99, Mendoza, Mecánica Computacional Volume XIX. Number 3. Solid Mechanics, 12 p.

Delay, J., Conil, N., de La Vaissière, R. Meuse/Haute-Marne Underground Research Center – Technologies and Techniques for Studying Gas Flow and Thermal Properties of an Indurated Clay-Rock, i-DUST 2010, 03001 (2011) DOI: 10.1051/idust/201103001.

Denson, N.M., Gibson, M.L., and Sims, G.L., 1993a. Geologic and structure map, with contours on top of the Pierre Shale, for the north half of the Powder River Basin, southeastern Montana and northeastern Wyoming. U.S. Geological Survey Miscellaneous Investigations Series Map I-2343-A.

Denson, N.M., Gibson, M.L., and Sims, G.L., 1993b. Geologic and structure map, with contours on top of the Pierre Shale, for the south half of the Powder River Basin, northeastern Wyoming. U.S. Geological Survey Miscellaneous Investigations Series Map I-2343-B.

Denson, N.M., Gibson, M.L., and Sims, G.L., 1993c. Geologic map showing thickness of the Upper Cretaceous Pierre Shale in the north half of the Powder River Basin, southeastern Montana and northeastern Wyoming. U.S. Geological Survey Miscellaneous Investigations Series Map I-2380-A.

Denson, N.M., Gibson, M.L., and Sims, G.L., 1993d. Geologic map showing thickness of the Upper Cretaceous Pierre Shale in the south half of the Powder River Basin, northeastern Wyoming and adjacent areas. U.S. Geological Survey Miscellaneous Investigations Series Map I-2380-B.

Dobson, P., 2011. Survey of clay/shale formations in the US. In: FY11 Report on Unsaturated Flow and Transport, FCRD-USED-2011-000296.

Dobson, P., 2012. Status of Shale Geology: Information on Extent, Thickness and Depth of Shale Deposits, FCRD-UFD-2012-000296.

Dobson, P., and Houseworth, J., 2013. Inventory of shale formations in the US including geologic, hydrological, and mechanical characteristics, FCRD-UFD-2014-000513.

Dobson, P., Houseworth, J.E. (2013). Inventory of Shale Formations in the US Including Geologic, Hydrological, and Mechanical Characteristics, U.S. DOE Fuel Cycle Research & Development, Used Fuel Disposition Campaign, Lawrence Berkeley National Laboratory, FCRD-UFD-2014-000513.

Dubiel, R.F., 2003. Geology, depositional models, and oil and gas assessment of the Green River Total Petroleum System, Uinta-Piceance Province, Eastern Utah and Western Colorado, Chapter 5 of Petroleum systems and geologic assessment of oil and gas in the Uinta-Piceance Province, Utah and Colorado, USGS Uinta-Piceance Assessment Team, U.S. Geological Survey Digital Data Series DDS-69-B. http://pubs.usgs.gov/dds/dds-069/dds-069-b/REPORTS/Chapter_5.pdf

Dullien, F.A.L., Lai, F.S.Y., Macdonald, I.F. (1986). Hydraulic Continuity of Residual Wetting Phase in Porous Media, Journal of Colloid and Interface Science, Vol. 109, No, 1, pp. 201-218.

Eastwood, R.L., Castagna, J.P. (1983). Basis for Interpretation of Ratios in Complex Lithologies, Sot. Prof. Well Log Analysts 24th Annual Logging Symp.EIA (Energy Information Administration), 2010, Eagle Ford Shale Play, Western Gulf Basin, South Texas. Map date May 29, 2010. http://www.eia.gov/oil_gas/rpd/shaleusa9.pdf

EIA (Energy Information Administration) (2011a). http://www.eia.gov/pub/oil_gas/natural_gas/analysis_publications/maps/maps.htm

EIA (Energy Information Administration), 2011b. Review of Emerging Resources: U.S. Shale Gas and Shale Oil Plays. www.eia.gov/analysis/studies/usshalegas/pdf/usshaleplays.pdf

Engelder, T., 2011. Analogue study of shale cap rock barrier integrity. Report for the Nuclear Waste Management Organization, NWMO DGR-TR-2011-23, 108 p.

Erenpreiss, M.S., Wickstrom, L.H., Perry C.J., Riley, R.A., Martin, D.R., and others, 2011. Regional organic-thickness map of the Marcellus Shale with additional organic-rich shale beds in the Hamilton Group included for New York, Pennsylvania, and West Virginia. Ohio Department of Natural Resources, Division of Geological Survey, scale 1 inch equals 52 miles.

Ettensohn, F.R., 2008. The Appalachian foreland basin in Eastern United States. In: Miall, A.D. (ed.) The Sedimentary Basins of the United States and Canada, Vol. 5, Sedimentary Basins of the World. Elsevier, Amsterdam, pp. 105-179.

Fuchs, S., Förster, A. (2013). Well-Log Based Prediction of Thermal Conductivity of Sedimentary Successions: A Case Study from the North German Basin, Geophys. J. Int., doi: 10.1093/gji/ggt382.

Gale, J.F.W., and Holder, J., 2010. Natural fractures in some US shales and their importance for gas production. In: Vining, B.A., and Pickering, S.C., eds., Petroleum Geology: From Mature Basins to New Frontiers. Proceedings of the 7th Petroleum Geology Conference, pp. 1131-1140.

Garitte, B., Gens, A., Vaunat J., Armand, G. (2012). Thermal Conductivity of Argillaceous Rocks: Determination Methodology Using In Situ Heating Tests, Rock Mech Rock Eng, 47, pp. 111–129.

Gens, A., Vaunat, J., Garitte, B., Wileveau, Y. (2007). In Situ Behaviour of a Stiff Layered Clay Subject to Thermal Loading: Observations and Interpretation, Géotechnique, 57, No. 2, pp. 207–228.

Gerhard, L.C., Anderson, S.B., Lefever, J.A. and Carlson, C.G., 1982. Geological development, origin, and energy mineral resources of Williston Basin, North Dakota. American Association of Petroleum Geologists Bulletin v. 66, pp. 989-1020.

Gonzales, S., and Johnson, K.S., 1985. Shales and other argillaceous strata in the United States. Oak Ridge National Laboratory report 84-64794, 594 p.

Goto, S., Matsubayashi, O. (2009). Relations between the thermal properties and porosity of sediments in the eastern flank of the Juan de Fuca Ridge, Earth Planets Space, 61, pp. 863–870.

Gray, J.D., Struble, R.A., Carlton, R.W., Hodges, D.A., Honeycutt, F.M., Kingsbury, R.H., Knapp, N.F., Majchszak, F.L., and Stith, D.A., 1982. An integrated study of the Devonian-age black shales in eastern Ohio. Technical Information Center, US Department of Energy, DOE/ET/12131-1399.

Hamilton, E.L. (1979). VP/VS and Poisson's Ratios in Marine Sediments and Rocks, J. Acoust. Soc. Am., 66, pp. 1093-I 101.

Hammes, U., Hamlin, H.S., and Ewing, T.E., 2011. Geologic analysis of the Upper Jurassic Haynesville Shale in east Texas and west Louisiana. AAPG Bulletin, v. 95, no. 10, pp. 1643-1666.

Han, D-H, Nur, A., Morgan, D. (1986). Effects of Porosity and Clay Content on Wave Velocities in Sandstones, Geophysics, Vol. 51. No. 11, pp. 2093-2107.

Harbor, R.L., 2011. Facies characterization and stratigraphic architecture of organic-rich Mudrocks, Upper Cretaceous Eagle Ford Formation, South Texas. M.S. Thesis, University of Texas, Austin, 184 p.

Hardage, B.A., Alkin, E., Backus, M.W., DeAngelo, M.V., Sava, D., Wagner, D., Graebner, R.J. (2013). Evaluation of Fracture Systems and Stress Fields Within the Marcellus Shale and Utica Shale and Characterization of Associated Water-Disposal Reservoirs: Appalachian Basin, Final Report to RPSEA, RPSEA Subcontract: 08122-55.

Hasenmueller, N.R., and Comer, J.B., eds., 1994. Gas potential of the New Albany Shale (Devonian and Mississippian) in the Illinois Basin, Gas Research Institute Technical Report GRI-92/0391.

Hasenmueller, N.R., and Comer, J.B., eds., 2000. GIS compilation of gas potential of the New Albany Shale in the Illinois Basin, Gas Research Institute Technical Report GRI-00/0068.

Higley, D.K. and Cox, D.O., 2007. Oil and gas exploration and development along the front range in the Denver Basin of Colorado, Nebraska, and Wyoming, in Higley, D.K., compiler, Petroleum systems and assessment of undiscovered oil and gas in the Denver Basin Province, Colorado, Kansas, Nebraska, South Dakota, and Wyoming-USGS Province 39: U.S. Geological Survey Digital Data Series DDS-69-P, ch. 2, 41 p. http://pubs.usgs.gov/dds/dds-069/dds-069-p/REPORTS/69_P_CH_2.pdf

Horseman, S.T. (2001) Gas Migration through Indurated Clays (Mudrocks). In: Gas Generation and Migration in Radioactive Waste Disposal. Proc. of the NEA Workshop in Reims 2000, France.

Horsrud, P. (2001). Estimating Mechanical Properties of Shale From Empirical Correlations, SPE Drilling & Completion.

Hosford Scheirer, A., 2013. The three-dimensional geologic model used for the 2003 National Oil and Gas Assessment of the San Joaquin Basin Province, California: Chapter 7 in Petroleum systems and geologic assessment of oil and gas in the San Joaquin Basin Province, California, U.S. Geological Survey Professional Paper 1713-7, 81 p.

Hovorka, S.D., Romero, M.L., Warne, A.G., Ambrose, W.A., Tremblay, T.A., Treviño, R.H., and Sasson, D., 2003. Technical summary: Optimal geological environments for carbon dioxide disposal in brine formations (saline aquifers) in the United States. Gulf Coast Carbon Center, University of Texas, Bureau of Economic Geology, http://www.beg.utexas.edu/gccc/finalreport.pdf

Ingram G.M., Urai, J.L. and Naylor, M.A. (1997) Sealing Processes and Top Seal Assessment. In: Hydrocarbon Seals: Importance for Petroleum Exploration and Production (eds. P. Molle-Pedersen and A.G. Koesler) Norwegian Petroleum Society, Special Publication 7, Elsevier, Amsterdam, 165-174.

Ingram, G.W., Urai, J.L. (1999). Top-seal leakage through faults and fractures: the role of mudrock properties, from." Aplin, A. C., Fleet, A. J., Macquaker, J. H. S. (eds) Muds and Mudstones: Physical and Fluid Flow Properties. Geological Society, London, Special Publications, 158, 125-135.

Johnson, E.A., 2003. Geologic assessment of the Phosphoria Total Petroleum System, Uinta-Piceance Province, Utah and Colorado, Chapter 9 of Petroleum systems and geologic assessment of oil and gas in the Uinta-Piceance Province, Utah and Colorado, USGS Uinta-Piceance Assessment Team, U.S. Geological Survey Digital Data Series DDS-69-B, http://pubs.usgs.gov/dds/dds-069/dds-069-b/REPORTS/Chapter_9.pdf

Johnson, L., Marschall, P., Zuidema, P., Gribi, P. (2004). Effects of Post-Disposal Gas Generation in a Repository for Spent Fuel, High-Level Waste and Long-lived Intermediate Level Waste Sited in Opalinus Clay, Nagra, Technical Report 04-06, 184 p.

Johnson, R.C., Mercier, T.J., Brownfield, M.E. and Self, J.G., 2010. Assessment of in-place oil shale resources in the Eocene Green River Formation, Uinta Basin, Utah and Colorado: U.S. Geological Survey Digital Data Series DDS-69-BB, Ch. 1, 153 p. http://pubs.usgs.gov/dds/dds-069/dds-069-bb/REPORTS/69_BB_CH_1.pdf

Johnston, J.E., Christensen, N.I. (1995). Seismic anisotropy of shales, Journal Of Geophysical Research, Vol. 100, No. B4, pp. 5991-6003.

Kirschbaum, M.A., 2003. Geologic assessment of undiscovered oil and gas resources of the Mancos/Mowry Total Petroleum System, Uinta-Piceance Province, Utah and Colorado. Chapter 6 of Petroleum Systems and Geologic Assessment of Oil and Gas in the Uinta-Piceance Province, Utah and Colorado, USGS Uinta-Piceance Assessment Team, U.S. Geological Survey Digital Data Series DDS-69-B, http://pubs.usgs.gov/dds/dds-069/dds-069-b/REPORTS/Chapter_6.pdf

Koerperich. E. A. (1979) Shear Wave Velocities Determined from Long and Short-Spaced Borehole Acoustic Devices: Sot. Petr. Eng., 8237.

Kolata, D.R., and Noger, M.C., 1990. Chapter 5: Tippecanoe I Subsequence Middle and Upper Ordovician Series. In: Interior Cratonic Basins, M.W. Leighton, D.R. Kolata, D.F. Oltz, and J.J. Eider., eds. American Association of Petroleum Geologists Memoir 51, pp. 89-99.

Kowallis, B.J., Jones, L.E.A., Wang, H.F. (1984). Velocity-Porosity-Clay Content Systematics of Poorly Consolidated Sandstones, Journal of Geophysical Research, Vol. 89, No. B12, pp. 10355-10364.

Lagoe, M.B., 1982. Stratigraphy and paleoenvironments of the Monterey Formation and associated rocks, Cuyama Basin, California. Ph.D. thesis, Stanford University, 216 p.

Lagoe, M.B., 1984. Paleogeography of Monterey Formation, Cuyama Basin, California. American Association of Petroleum Geologists Bulletin, v. 68, pp. 610-627.

Lash, C. E. 1980, Shear waves, multiple reflections, and converted waves found by a deep vertical wave test (vertical seismic profiling): Geophysics, 45, pp. 1373-1411.

Lash, G.G., and Engelder, T., 2011. Thickness trends and sequence stratigraphy of the Middle Devonian Marcellus Formation, Appalachian Basin: Implications for Acadian foreland basin evolution. American Association of Petroleum Geologists Bulletin v. 95, pp. 61-103.

LeFever, J.A., 2008. Structural contour and isopach maps of the Bakken Formation in North Dakota. North Dakota Geological Survey Geologic Investigations No. 59, 5 sheets.

LeFever, J.A., LeFever, R.D., and Nordeng, S.H., 2012. Extending the Bakken. Williston Basin Petroleum Conference.

Lewis, B.D., and Hotchkiss, W.R., 1981. Thickness, percent sand, and configuration of shallow hydrogeologic units in the Powder River Basin, Montana and Wyoming. U.S. Geological Survey Miscellaneous Investigations Series, Map I-1317.

Li, P., Ratchford, M.E., and Jarvie, D.M., 2010. Geochemistry and thermal maturation analysis of the Fayetteville Shale and Chattanooga Shale in the western Arkoma Basin of Arkansas. Arkansas Geological Survey Information Circular 40, 191 p.

Li, X., Bernier, F., Vietor, T., Lebon, P. (2007). TIMODAZ (Contract Number: FI6W-CT-036449), Deliverable (No: 2). European Commission under the Sixth Framework Programme Euratom Research and Training Programme on Nuclear Energy (2002-2006), 104 p.

Lingle, R., Jones, A. H. (1977). Comparison of Log and Laboratory Measured P-Wave and S-Wave Velocities: Trans., Soc. Prof. Well Log Analysts, 18th Annual Logging Symp.

Liu, E. (1997). Crosshole Channel Wave Analysis from Antrim Shale Gas Play, Michigan Basin, EAGE Conference and Technical Exhibition, 59th annual meeting 1997, European Association of Petroleum Geoscientists.

Liu, X. (1994). Nonlinear Elasticity, Seismic Anisotropy, and Petrophysical Properties of Reservoir Rocks, Ph.D. thesis, Stanford University.

Macfarlane, P.A., Combes, J., Turbek, S., and Kirshen, D., 1993. Shallow subsurface bedrock geology and hydrostratigraphy of southwestern Kansas. Kansas Geological Survey, Open-File Report 93-1a. (plates updated in 2010 by J.J. Woods).

Magoon, L.B., Lillis, P.G., and Peters, K.E., 2009. Petroleum systems used to determine the assessment units in the San Joaquin Basin Province, California: Chapter 8 in Petroleum systems and geologic assessment of oil and gas in the San Joaquin Basin Province, California, U.S. Geological Survey Professional Paper 1713-8, 65 p.

Marschall, P., Horseman, S., Gimmi, T. (2005). Characterisation of Gas Transport Properties of the Opalinus Clay, a Potential Host Rock Formation for Radioactive Waste Disposal, Oil & Gas Science and Technology – Rev. IFP, Vol. 60, No. 1, pp. 121-139.

Mastalerz, M., Schimmelmann, A., Drobniak, A., and Chen, Y., 2013. Porosity of Devonian and Mississippian New Albany Shale across a maturation gradient: Insights from organic petrology, gas

adsorption, and mercury intrusion. American Association of Petroleum Geologists Bulletin, v. 97 (10), 1621-1643.

Matray, J.M., Savoye, S., Cabrera, J. (2007). Desaturation and Structure Relationships around Drifts Excavated in the Well-Compacted Tournemire's Argillite (Aveyron, France), Engineering Geology, 90, pp. 1–16.

Matthews, R.D., 1993. Review and Revision of the Devonian-Mississippian Stratigraphy in the Michigan Basin: Chapter D in Petroleum Geology of the Devonian and Mississippian Black Shale of Eastern North America, J.B. Roen and R. C. Kepferle, eds., U.S. Geological Survey Bulletin 1909, D1-D85.

McDonal, F.J., Angona, F.A., Mills, R.I., Sengbush, R.L., Van Nostrand, R.G., White, J.E. (1958). Attenuation Of Shear And Compressional Waves In Pierre Shale, Geophysics, Vol. XXIII, No. 3, pp. 421-439.

Mercier, T.J., and Johnson, R.C., 2012. Isopach and isoresource maps for oil shale deposits in the Eocene Green River Formation for the combined Uinta and Piceance Basins, Utah and Colorado: U.S. Geological Survey Scientific Investigations Report 2012-5076, 85 p., 1 pl., http://pubs.usgs.gov/sir/2012/5076/SIR12-5076.pdf

Mercier, T.J., Gunther, G.L., and Skinner, C.C., 2010a. The GIS project for the geologic assessment of in-place oil shale resources of the Eocene Green River Formation, Greater Green River Basin, Wyoming, Colorado, and Utah, U.S. Geological Survey Oil Shale Assessment Team, U.S. Geological Survey Digital Data Series DDS-69-DD, http://pubs.usgs.gov/dds/dds-069/dds-069-dd/REPORTS/69_DD_CH_3.pdf

Mercier, T.J., Gunther, G.L., and Skinner, C.C., 2010b. The GIS project for the geologic assessment of in-place oil shale resources of the Piceance Basin, Colorado. In: Oil shale and nahcolite resources of the Piceance Basin, Colorado, U.S. Geological Survey Oil Shale Assessment Team, U.S. Geological Survey Digital Data Series DDS-69-Y, http://pubs.usgs.gov/dds/dds-069/dds-069-y/REPORTS/69_Y_CH_4.pdf

Mercier, T.J., Gunther, G.L., and Skinner, C.C., 2010c. The GIS project for the geologic assessment of in-place oil shale resources of the Uinta Basin, Utah and Colorado. In: Oil shale resources of the Uinta Basin, Utah and Colorado, U.S. Geological Survey Oil Shale Assessment Team, U.S. Geological Survey Digital Data Series DDS-69-BB, http://pubs.usgs.gov/dds/dds-069/dds-069-bb/REPORTS/69_BB_CH_4.pdf

Merewether, E.A., Sharps, J.A., Gill, J.R., and Cooley, M.E., 1973. Shale, mudstone, and claystone as potential host rocks for underground emplacement of waste. U.S. Geological Survey Open-File Report 73-184, 44 p.

Midttømme, K., Roaldset, E. (1999). Thermal Conductivity of Sedimentary Rocks: Uncertainties in Measurement and Modelling, in Aplin, A. C., Fleet, A.J., Macquaker, J. H. S. (eds), Muds and Mudstones: Physical and Fluid Flow Properties, Geological Society, London, Special Publications, 158, pp. 45-60.

Midttømme, K., Roaldset, E., Aagaard, P. (1997). Thermal Conductivities of Argillaceous Sediments, in McCann, D. M., Eddleston, M., Fenning, P. J. & Reeves, G. M. (eds), 1997, Modern Geophysics in Engineering Geology, Geological Society Engineering Geology Special Publication No. 12, pp. 355-363.

Midttømme, K., Roaldset, E., Aagaard, P. (1998). Thermal Conductivity of Selected Claystones and Mudstones from England, Clay Minerals, 33, pp. 131-145.

Montaut, A. 2012. Detection and Quantification of Rock Physics Properties for Improved Hydraulic Fracturing in Hydrocarbon-Bearing Shales, Master of Science in Engineering Thesis, The University of Texas at Austin.

Montgomery, S.L., Jarvie, D.M., Bowker, K.A., and Pollastro, R.M., 2005. Mississippian Barnett Shale, Fort Worth Basin, north-central Texas: Gas-shale play with multi-trillion cubic foot potential. American Association of Petroleum Geologists Bulletin, v. 89 (2), 155-175.

Nunn, J.A. 2012. Burial and Thermal History of the Haynesville Shale: Implications for Overpressure, Gas Generation, and Natural Hydrofracture, GCAGS Journal, v. 1 (2012), p. 81–96.

Ohio Department of Natural Resources, 2013a. Division of Geological Survey, Map of maximum TOC for Upper Ordovician Shales. http://geosurvey.ohiodnr.gov/portals/geosurvey/Energy/Utica/Ordov-Shale_TOC-Max_03-2013.pdf

Ohio Department of Natural Resources, 2013b, Division of Geological Survey, Map of Calculated Ro for Upper Ordovician Shales. http://geosurvey.ohiodnr.gov/portals/geosurvey/Energy/Utica/Ordov-Shale_Ro-Average_03-2013.pdf

Party, J.M., Wipf, R.A., Byl, J.M., Lawton, J., and Hill, J.M., 2008. Woodford Shale, Ardmore Basin, Oklahoma: A developing shale play. Oklahoma Geological Survey, Gas Shales Workshop, 51 slides. http://www.ogs.ou.edu/pdf/GSPartyS.pdf.

Pashin, J.C., 2008. Gas shale potential of Alabama. 2008 International Coalbed and Shale Gas Symposium, Paper 808.

Patchen, D.G., Hickman, J.B., Harris, D.C., Drahovzal, J.A., Lake, P.D., Smith, L.B., Nyahay, R., Schulze, R., Riley, R.A., Baranoski, M.T., Wickstrom, L.H., Laughrey, C.D., Kostelnik, J., Harper, J.A., Avary, K.L., Bocan, J., Hohn, M.E., and McDowell, R., 2006. A Geologic play book for Trenton-Black River Appalachian Basin exploration. DOE Award DE-FC26-03NT41856, http://www.wvgs.wvnet.edu/www/tbr/docs/41856R06.pdf

Pawlewicz, M.J. and Hatch, J.R., 2007. Petroleum assessment of the Chattanooga Shale/Floyd Shale - Paleozoic Total Petroleum System, Black Warrior Basin, Alabama and Mississippi, in Hatch, J.R., and Pawlewicz, J.J., compilers, Geologic assessment of undiscovered oil and gas resources of the Black Warrior Basin Province, Alabama and Mississippi. U.S. Geological Survey Digital Data Series DDS-69-I, chap. 3, 23 p. http://pubs.usgs.gov/dds/dds-069/dds-069-i/REPORTS/69_I_CH_3.pdf

Perry, F., Kelley, R., and Woldegabriel, G., 2011. Regional geology and tectonic hazards - FY 2011 Status Report. FCRD-USED-2012-000002.

Perry, F.V., Dobson, P.F., and Kelley, R.E., 2013. Assessment of alternative host-rock distribution in the U.S. using GIS. Proceedings, International High-Level Waste Management Conference 2013, Albuquerque, N.M., April 28-May 2, 2013, American Nuclear Society, pp. 85-93.

Perry, F.V., Kelley, R., and Dobson, P., 2012. Regional geology: Distribution of alternative host rock formations and description of siting factors that potentially influence siting and site characterization. FCRD-USED-2012-27013.

Perry, F.V., Kelley, R.E., Dobson, P.F., and Houseworth, J.E., 2014. Regional geology: A GIS database for alternative host rocks and potential siting guidelines. FCRD-UFD-2014-000068.

Peterson, J.A., 1984. Geology and hydrology of the Madison Limestone and associated rocks in parts of Montana, Nebraska, North Dakota, South Dakota, and Wyoming. U.S. Geological Survey Professional Paper 1273A, 34 p.

Piña-Diaz, Y.E. (2011). Thermo-Hydro-Mechanical Behaviour of Ypresian Clay, Dept. de Enginyeria del Terreny, Cartogràfica i Geofisica E.T.S. Enginyers de Camins, Canals i Ports, Universitat Politècnica de Catalunya.

Pitman, J.K., 2008. Reservoirs and Petroleum Systems of the Gulf Coast. AAPG Datapages GIS Open-File website. http://www.datapages.com/AssociatedWebsites/GISOpenFiles/ReservoirsandPetroleumSystemsoftheGulfCoast.aspx

Pollastro, R.M., Jarvie, D.M., Hill, R.J., and Adams, C.W., 2007. Geologic framework of the Mississippian Barnett Shale, Barnett-Paleozoic total petroleum system, Bend Arch-Fort Worth Basin, Texas. American Association of Petroleum Geologists Bulletin v. 91, pp. 405-436.

Pollastro, R.M., Roberts, L.N.R., Cook, T.A. and Lewan, M.D., 2008. Assessment of undiscovered technically recoverable oil and gas resources of the Bakken Formation, Williston Basin, Montana and North Dakota, 2008: U.S. Geological Survey Open-File Report 2008-1353, 3 sheets.

Ratchford, M.E., Bridges, L.C., Jordan, D., Dow, W.G., Colbert, A., and Jarvie, D.M., 2006. Organic geochemistry and thermal maturation analysis within the Fayetteville Shale study area - Eastern Arkoma Basin and Mississippi embayment regions, Arkansas. Arkansas Geological Survey Information Circular 37, DFF-OG-FS-EAB/ME 008, 12 p.

Rechard, R.P., Perry, F.V., and Cotton, T.A., 2011. Site selection, characterization, and research and development for spent nuclear fuel and high-level waste disposal. International High-Level Radioactive Waste Management Conference 2001, Albuquerque, NM, April 10-14, 2011, American Nuclear Society, pp. 174-181.

Repetski, J.E., Ryder, R.T., Weary, D.J., Harris, A.G., and Trippi, M.H., 2008. Thermal maturity patterns (CAI and %Ro) in Upper Ordovician and Devonian rocks of the Appalachian Basin: A major revision of USGS Map I-917-E using new subsurface collections. USGS Scientific Investigations Map 3006.

Ridgley, J.L., Condon, S.M., and Hatch, J.R., 2013. Geology and oil and gas assessment of the Mancos-Menefee Composite Total Petroleum System, San Juan Basin, New Mexico and Colorado, chap. 4 of U.S. Geological Survey San Juan Basin Assessment Team, Total petroleum systems and geologic assessment of undiscovered oil and gas resources in the San Juan Basin Province, exclusive of Paleozoic rocks, New Mexico and Colorado. U.S. Geological Survey Digital Data Series 69-F, p. 1-97.

Rottmann, K., 2000. Isopach map of Woodford Shale in Oklahoma and Texas Panhandle. In: Hunton play in Oklahoma (including northeast Texas panhandle): Oklahoma Geological Survey Special Publication 2000-2, plate 2.

Ruppel, S.C., Jones, R.H., Breton, C.L, and Kane, J.A., 2005. Preparation of maps depicting geothermal gradient and Precambrian structure in the Permian Basin: unpublished contract report prepared for the U. S. Geological Survey, 21 p. plus data CD.

Ryder, R.T., Burruss, R.C. and Hatch, J.R., 1998. Black shale source rocks and oil generation in the Cambrian and Ordovician of the central Appalachian Basin, USA. AAPG Bulletin 82, pp. 412-441.

Self, J.G., Ryder, R.T., Johnson, R.C., Brownfield, M.E., and Mercier, T.J., 2011. Stratigraphic cross sections of the Eocene Green River Formation in the Green River Basin, southwestern Wyoming, northwestern Colorado, and northeastern Utah, in U.S. Geological Survey Oil Shale Assessment Team, ed., Oil shale resources in the Eocene Green River Formation, Greater Green River Basin,

Wyoming, Colorado, and Utah. U.S. Geological Survey Digital Data Series DDS-69-DD, chap. 5, 7 p., 24 plates.

Shurr, G.W., 1977. The Pierre Shale, Northern Great Plains; A potential isolation medium for radioactive waste. U.S. Geological Survey Open File Report 77-776, 27 p.

Smith, L.N., 1999. Structure contour map on the top of the Upper Cretaceous Pierre (Bearpaw) Shale, east-central Montana. Montana Bureau of Mines and Geology, Montana Ground-Water Assessment Open-File Report 13, Revision 1.1.

Sondhi, N. (2011). Petrophysical Characterization of Eagle Ford Shale, M.S. Thesis, University of Oklahoma.

Strapoc, D., Mastalerz, M., Schimmelmann, A., Drobniak, A., and Hassenmuller, N.R., 2010. Geochemical constraints on the origin and volume of gas in the New Albany Shale (Devonian-Mississippian), eastern Illinois Basin. American Association of Petroleum Geologists Bulletin Bulletin, v. 94 (11), 1713-1740.

Surles, M.A., Jr., 1987. Stratigraphy of the Eagle Ford Group (Upper Cretaceous) and its source-rock potential in the East Texas Basin. Baylor Geological Studies Bulletin No. 45, 57 p.

Sweetkind, D.S., Bova, S.C., Langenheim, V.E., Shumaker, L.E., and Scheirer, D.S., 2013. Digital tabulation of stratigraphic data from oil and gas wells in Cuyama Valley and surrounding areas, central California. U.S. Geological Survey Open-File Report 2013-1084, 44 p.

Sweetkind, D.S., Tennyson, M.E., Langenheim, V.E., and Shumaker, L.E., 2010. Digital tabulation of stratigraphic data from oil and gas wells in the Santa Maria Basin and surrounding areas, central California coast. U.S. Geological Survey Open-File Report 2010-1129, 11 p.

Swezey, C.S., 2008. Regional stratigraphy and petroleum systems of the Michigan Basin, North America. U.S. Geological Survey Scientific Investigations Map 2978, 1 sheet. http://pubs.usgs.gov/sim/2978/sim2978MichChart.pdf

Swezey, C.S., 2009. Regional stratigraphy and petroleum systems of the Illinois Basin, U.S.A. U.S. Geological Survey Scientific Investigations Map 3068, 1 sheet. http://pubs.usgs.gov/sim/3068/illinoisbasin.pdf

Thomas, L.K., Katz, D.L., Tek, M.R. (1968). Threshold Pressure Phenomena in Porous Media, Society of Petroleum Engineers Journal, Transactions, Vol. 243, pp. 174-184.

Thomas, W.A., 1988. The Black Warrior Basin. In: Sloss, L.L., ed., The Geology of North America, v. D-2, Sedimentary Cover-North American Craton: U.S.: Decade of North American Geology: Geological Society of America, pp. 471-492.

Tinjum, J.M., Benson, C.H., Blotz, L.R. (1997). Soil-Water Characteristic Curves for Compacted Clays, Journal of Geotechnical And Geoenvironmental Engineering, pp. 1060-1069.

Tosaya, C., Nur, A. (1982). Effects of Diagenesis and Clays on Compressional Velocities in Rocks, Geophysical Research Letters, Vol. 9, No. 1, pp. 5-8.

Tosaya, C.A. (1982). Acoustical Properties of Clay-Bearing Rocks, Ph.D. Dissertation, Stanford University.

USGS Southwestern Wyoming Province Assessment Team, 2005. The Southwestern Wyoming Province - Introduction to a geologic assessment of undiscovered oil and gas resources, U.S. Geological Survey Digital Data Series DDS-69-D, Chapter 2, 34 p. http://pubs.usgs.gov/dds/dds-069/dds-069-d/REPORTS/69_D_CH_2.pdf

USGS Uinta-Piceance Assessment Team, 2003. Petroleum systems and geologic assessment of oil and gas in the Uinta-Piceance Province, Utah and Colorado: U.S. Geological Survey Digital Data Series DDS-69-B, Ch. 2. http://pubs.usgs.gov/dds/dds-069/dds-069-b/REPORTS/Chapter_2.pdf

van Genuchten, M.T. (1980). A closed-form equation for predicting the hydraulic conductivity of unsaturated soils. Soil Science Society of America Journal, 44, 892-898.

Verma, S., Mutlu, O., Marfurt, K.J. (2013). Seismic modeling evaluation of fault illumination in the Woodford Shale, SEG Houston 2013 Annual Meeting.

Villar, M.V., Romero, F.J. (2012). Water Retention Curves of Opalinus Clay, Informes Técnicos Ciemat 1262, 33 p.

Waples, D.W., Tirsgaard, H. (2002). Changes in Matrix Thermal Conductivity of Clays and Claystones as a Function of Compaction, Petroleum Geoscience, Vol. 8 2002, pp. 365–370.

Waples, D.W., Waples, J.S. (2004). A Review and Evaluation of Specific Heat Capacities of Rocks, Minerals, and Subsurface Fluids. Part 1: Minerals and Nonporous Rocks, Natural Resources Research, Vol. 13, No. 2, pp. 97-122.

Wileveau, Y., Rothfuchs, T. (2007). THM Behaviour of Host Rock (HE-D) Experiment: Study of Thermal Effects on Opalinus Clay, Mont Terri Project, Technical Report 2006-01.

Williams, L.A., 1982. Lithology of the Monterey Formation (Miocene) in the San Joaquin Valley of California. In: Williams, L.A., and Graham, S.A., eds., Monterey Formation and associated coarse clastic rocks, central San Joaquin Basin, California. Pacific Section, Society of Economic Paleontologists and Mineralogists Annual Field Trip Guidebook, pp. 17-35.

Willman, H.B., Atherton, W., Buschbach, T.C., Collinson, C., Frye, J.C., Hopkins, M.E., and Lineback, J.A., 1975. Handbook of Illinois stratigraphy, Illinois Geological Survey Bulletin 95, 261 p.

Wylie, A.S., and Wood, J.R., 2005. Historical production trends suggest remaining upside for E&D in Michigan. Oil and Gas Journal, vol. 103, issue 23.

Wylie, A.S., Jr., and Wood, J.R., 2004. Map views of the producing formations in Michigan, the Michigan Basin, U.S. American Association of Petroleum Geologists Eastern Section Meeting, Columbus, OH, Oct. 3-6, 2004.

Yang, Y., Aplin, A.C. (2004). Definition and practical application of mudstone porosity–effective stress relationships, Petroleum Geoscience, Vol. 10, pp. 153–162.

Yang, Y., Aplin, A.C. (2010). A permeability–porosity relationship for mudstones, Marine and Petroleum Geology, 27, 1692–1697.

Zhao, H., Givens, N.B., and Curtis, B., 2007. Thermal maturity of the Barnett Shale determined from well-log analysis. American Association of Petroleum Geologists Bulletin, 94 (4), 535-549.